Investigation into the Mechanism of Human Carbonic Anhydrase II

Michael James Saunders

MSc by Research

2012

Investigation into the Mechanism of Human Carbonic Anhydrase II

Michael James Saunders

MSc by Research

University of York
Department of Chemistry
January 2012

Abstract

Human carbonic anhydrase II (HCAII) acts as a carbon dioxide sequestration catalyst, removing carbon dioxide from the blood stream and converting it into bicarbonate and a proton. The active site contains a tetrahedrally coordinated zinc atom coordinated by three facially-capping histidine residues. The fourth coordination site is occupied by a water molecule. The mechanism of its active site has been studied since the 1960s.[1] The majority of the mechanism is well understood, as it is comprised of two distinct stages. Firstly a zinc hydroxide is formed via deprotonation of the zinc-aqua species via a proton shuttle. This allows for an initial nucleophilic attack on the carbon dioxide from the hydroxide moiety, forming a coordinated bicarbonate species on the zinc centre. The bicarbonate species produced is then exchanged by a water molecule and a second reaction involving the transfer of a proton from the bound water molecule occurs to the surrounding solvent and regeneration of the zinc hydroxide takes place, ready for another cycle.

Disagreement arises as Lipscomb *et al.* believe that a proton is internally transferred from the original hydroxide group to an oxygen atom on the incoming carbon dioxide, whereas Lindskog *et al.* believe that there is an internal rotation of the oxygen atom bound directly to the zinc.[2] The two mechanisms also differentiate between each other by how the bicarbonate binds to the zinc centre. In the mechanism suggested by Lindskog *et al.* a bidentate bicarbonate is proposed, whereas Lipscomb *et al.* have suggested this is a unidentate bicarbonate. Several attempts have been made to understand in more detail which

of the two proposed mechanisms is correct.[3, 4] HCAII has been the focus of significant attention by the small molecule modelling community.[3-24] This is due to the further understanding of the mechanistic details, as well as finding a synthetic catalyst for the sequestration of carbon dioxide for a range of commercial opportunities of a complex. The aims of this project involved synthesising a suitable zinc hydroxide mimic complex and studying the reaction with carbon dioxide.

Initial challenges included design and synthesis of a suitable ligand system. Chapter 2 discusses the previous problems with ligands synthesised in the Walton group and how *cis,cis*-1,3,5-tris(3,5-ditertbutylphenylpropenylideneimino) cyclohexane, (3,5 ^{t}Bu TCT) looks to overcome them. Chapter 3 describes successful complexation of this ligand system to a zinc ion, with supporting NMR data. This complex can be reacted with carbon dioxide to give ^{13}C NMR and IR data. In addition, in several synthesise of these species, it was observed that a chloride-coordinated zinc complex was preferentially stable over the hydroxide as this was repeatedly observed in ESI and LIFDI MS. A crystal structure was successfully obtained for this species, along with that of a zinc-coordinated nitrate species. This is isoelectronic to the desired zinc bicarbonate species, allowing useful analysis of specific bond lengths in chapter 5.

Contents

Figures

Tables

Acknowledgements

I would firstly like to thanks my supervisor, Prof. Paul H. Walton, for his dedication to this research, as well as the funding to undertake it.

I would also like to thank Dr. Naser Jasim for his tireless efforts to get my project moving and for countless NMR experiments ran on my behalf, and his endless patience with me.

I must also thank Ed and Karl in mass spec, Dr. Adrian Whitwood for running the crystallography service and Mike and Steve in stores for keeping the department constantly stocked.

Finally I would like to thank Sharifa for her endless support throughout the year, for being a fantastic influence on my academic and personal life and for constantly looking out for my best interests, I will never be able to thank you enough.

Declaration

I declare that the work in this thesis was carried out in accordance with the regulations of the University of York. The work is original except where indicated by special reference in the text and no part of this thesis has been submitted for any other degree.

Any views expressed in this thesis are those of the author and in no way represent those of the University of York. This thesis has not been presented to any other university for examination, either in the United Kingdom or overseas.

Michael Saunders

3rd January 2012

Chapter 1: *Human carbonic anhydrase II and enzyme modelling*

Classically speaking *carbonic anhydrases* have been amongst the most studied proteins in scientific history.[1-10, 13, 19-72] For instance, on the Web of Knowledge (as of Oct 2011) 23,390 have been papers published concerning it, compared to the proteins *alcohol dehydrogenase* with 20,954 or even *haemoglobin* which has 15,022. Detailed work has been accomplished over the last 80 years resulting in the understanding of the structure and finer workings of the enzyme, as well as the many different forms of the enzyme present across different species and plants.

The initial discovery of *carbonic anhydrase* took place in Cambridge in 1932,[29] with the first recognised paper published in 1933 by Meldurm and Roughton.[25] The initial paper focused solely on its role as a carbon dioxide sequesterer, with a subsequent follow up in the same year noting its preparation.[26] Remarkably, a great deal of information was already known about its role by this point, and over the following decades scientists working simultaneously in a global effort came closer and closer to synthesising a catalytic mimic of the enzyme.[73]

1.1 Reaction and function

All *carbonic anhydrases* catalyse the same reaction with varying degrees of efficiency. *Human carbonic anhydrase* II or HCAII works as a carbon dioxide sequestration catalyst, removing carbon dioxide and water from the blood stream and converting it into a bicarbonate and a proton, see reaction 1 below.[36, 55, 60]

Reaction 1

$$CO_2 + H_2O \rightleftharpoons HCO_3^- + H^+$$

However *carbonic anhydrase* primarily functions as a means for increasing the solubility of carbon dioxide in the blood stream. This allows for quick diffusion from the alveoli in the lungs to the bloodstream, with the enzyme being ubiquitous to all tissue.[62] *Carbonic anhydrase* also helps to keep the body at a constant pH. It has been observed that HCAII has a turnover rate to be roughly in the order of 10^6 sec^{-1} at a pH of 9 and a temperature of 25°C.[57] The uncatalysed reaction on the other hand achieves a turnover rate of around 0.18 sec^{-1} at 37° C.

HCAII is the most efficient of the *carbonic anhydrases*, with HCAI for example having a turnover rate of around 2×10^5 sec^{-1}. This is of significant interest when considering that the only difference between HCAI and HCAII is one amino acid, Thr-200 → His-200. The efficiency of the enzyme suffers a whole change in magnitude, due to the different structure. This is helpful in elucidating important amino acids when comparing two similar enzymes together; this forms the basis of mutagenesis experiments. Other isozymes of *carbonic anhydrase* are not as efficient as HCAII, with HCAIII having a meagre turnover rate of 8×10^3 sec^{-1}, compared to HCAI with a turnover rate of 10^5 sec^{-1}.[55]

1.2 Structure

Specifically the protein family *carbonic anhydrase* is a class of enzymes which is divided into five subsets, these are all enzymes catalysing the same reaction but they are structurally exclusive of each other and they also all contain certain key features.[63] These different families are believed to be examples of convergent evolution.

In the *carbonic anhydrase* family the different orthologues are denoted α, β, γ with recent research discovering two more distinct but much less understood isozymes denoted δ and ε. These are generally found in different forms of life, with the α subset found primarily in mammals, and the β subset found in prokaryotes, whereas the ε form is found in archaebacteria.[54] These are again divided into different subsets or isozymes, with even less structural differences between them, i.e. as discussed earlier the α *carbonic anhydrases* I and II differ by one amino acid, Thr-200 →His-200.[49]

The structure of HCAII is somewhat standard for an enzyme of its size. HCAII is around 29300 Da with the active site lying at the bottom of a conical cavity which is 16 Å deep and 15 Å wide at the opening of the cone (see figure 1).[35, 39]

Figure 1, *A schematic diagram showing HCAII's active site cavity*

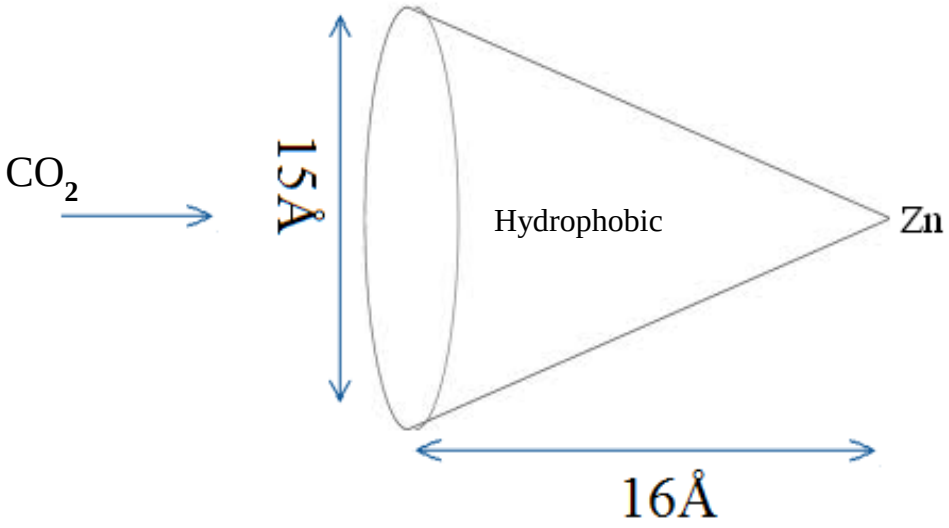

The inside of this cone is effectively hydrophobic and is divided into two separate chemical environments. This division of the active site is essential for orientation of the substrate entering the active site, and according to molecular dynamic studies it is believed the hydrophobic region directly orientates the carbon dioxide molecule into the active site. [70]

The enzyme itself contains an essential metallic element, zinc, and this in itself is one of the most widely used in nature. At least three hundred different enzymes contain a zinc centre, and over one thousand active sites utilise a zinc atom. [13, 15]

Zinc ions are difficult to study; they form colourless compounds, have virtually no redox properties and have no magnetic qualities. Zinc(II) complexes lack an associated crystal field stabilisation energy due to its $3d^{10}$ outer shell electron configuration. This means that zinc may adopt a four, five or six coordinate

geometry, although it prefers a tetrahedral geometry due to its vacant 4s and 4p orbitals.

The utilisation of zinc in the active site is interesting. Zinc complexes tend to have low thermodynamic stabilities as well as variable geometries allowing typically for low activation barriers. This makes the biological use of zinc almost essential for speed, versatility and availability as active site metals.[13]

One side of the zinc ion is located well within the active site that is comprised of hydrophobic amino acids, such as Val-121, Val-143, Leu-198, Thr-199-CH_3, Val-207 and Trp-209. [51] On the opposing side of the zinc to these hydrophobic amino acids is an area rich with hydrophilic amino acids. These lead away from the active site and contain the residues Tyr-7, Asn-62, His-64, Asn-67, Thr-199-$O_{\gamma 1}$, and Thr-200-$O_{\gamma 1}$, see figure 2 for an overview of this region.[2, 36]

The active site possesses a tetrahedrally coordinated zinc atom coordinated by three facially capping histidine residues (consisting of His-94, His-96 and His-119) via three imidazole groups. The fourth coordination site is occupied by a bound hydroxide ion; this is the catalytically active form of the enzyme. With low pH this hydroxide species may be converted to an aqua bound species, which may be easily regenerated into a hydroxide ion.[68] Alternatively at pH 8.5 this aqua species reverts back to the corresponding hydroxide.

Figure 2, *Electron density contour map of the HCAII active site with the hydrophobic regions residues highlighted in green, and the hydrophilic region in magenta, with the active site and its three histidine residues shown in purple. Also shown is a* carbon dioxide *molecule primed for activation by the hydroxide moiety of the zinc. The first diagram highlights the structure of the holo or active form of the enzyme, whilst the second shows the apo or inactive form of the enzyme.*[2]

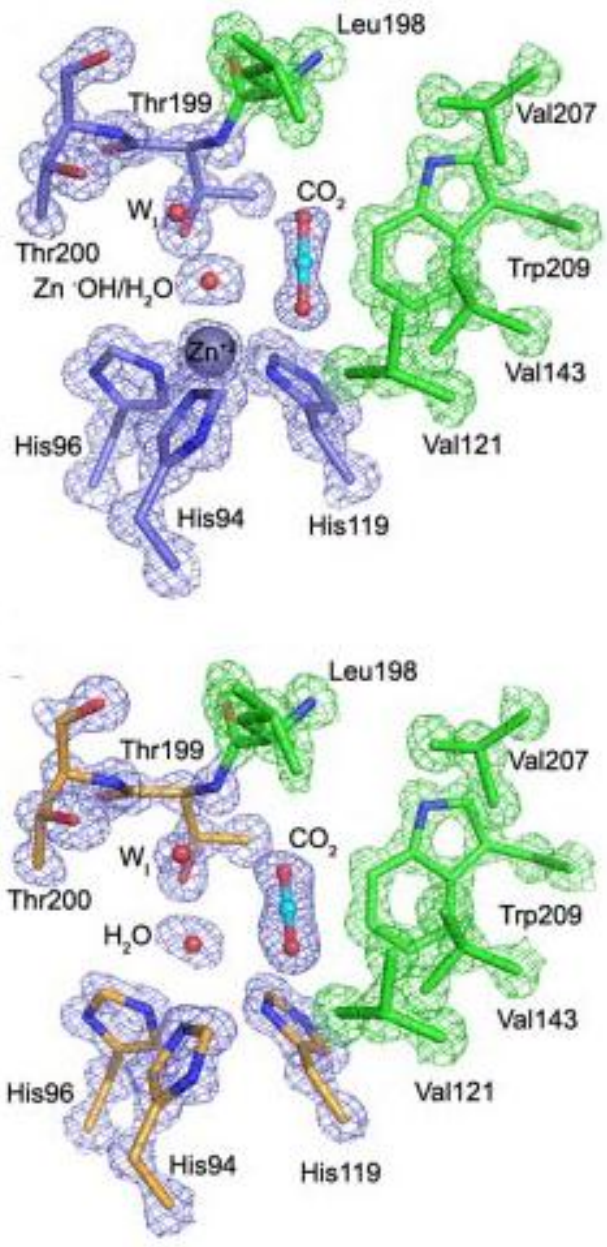

1.2.1 Significance of pK_a within the active site

The zinc-bound aqua species has a pK_a of 7.0,[31] whereas an unbound water species would have a pK_a of 15.7.[74] The reason for this low pK_a value is due to the low coordination number of the zinc increasing the Lewis acidity of the metal centre. This in turn increases the Brønsted acidity of the water by having a greater "pull" on the electrons in the water molecule. It must be noted however that low coordination number is not the only factor in the low pK_a, with the ligands themselves having a major influence.

By replacing one of the histidine residues coordinated to the zinc in the native enzyme with a negatively charged amino acid such as Asp or Glu, the pK_a of the coordinated water molecule is increased from 7.0 to 8.6.[75] The use of neutral histidine ligands and a low coordination number are not the only contributing factors. It is also understood that the secondary coordination sphere plays an important role in lowering pK_a. Hydrogen bonding interactions have also been shown to lower pK_a of bound aqua species.[75] This is because of the decrease in electron density on the hydrogen atoms and concentrating more electron density on the more electronegative atom. This provides an explanation as to why the pK_a of small molecule model complexes varies so much, even when utilising similar ligand systems.

The lowering of the pK_a of the zinc-bound water molecule is key to understanding how the enzyme performs its task so quickly. By lowering the pK_a of the water molecule, it means that it may be deprotonated at a lower pH than

that of a free water molecule. As the hydroxide is a much stronger nucleophile than the water species, it is paramount that the enzyme converts the aqua species quickly into a hydroxide. The enzyme utilises His-64 to shuttle protons away from the active site, to the surrounding milieu.

In *carbonic anhydrase*, the water molecules located around the active site also act as proton shuttles, efficiently removing protons created during the deprotonation of the aqua-bound zinc species back to the hydroxide bound form. This is accomplished by specifically taking advantage of a key amino acid close to the active site, His-64, a 0.75 nm away from the metal centre.[35] This histidine residue accepts a proton from the coordinated aqua species ligated to the zinc, leaving a zinc-bound hydroxide species.

A crystal structure of the active site and the key components of how the enzyme achieves its functionality is shown below (in figure 3). It should be pointed out that the water molecules shown are part of the extensive ordered water network found throughout the enzyme. This chain of water molecules helps to alleviate the build-up of protons within the active site via a proton shuttle mechanism.[37]

Figure 3, *Active site of HCAII with red dots indicating ordered water molecules and dashed lines referring to what is presumed to be hydrogen bonding between atoms in the region of 3Å around the zinc atom.*[37]

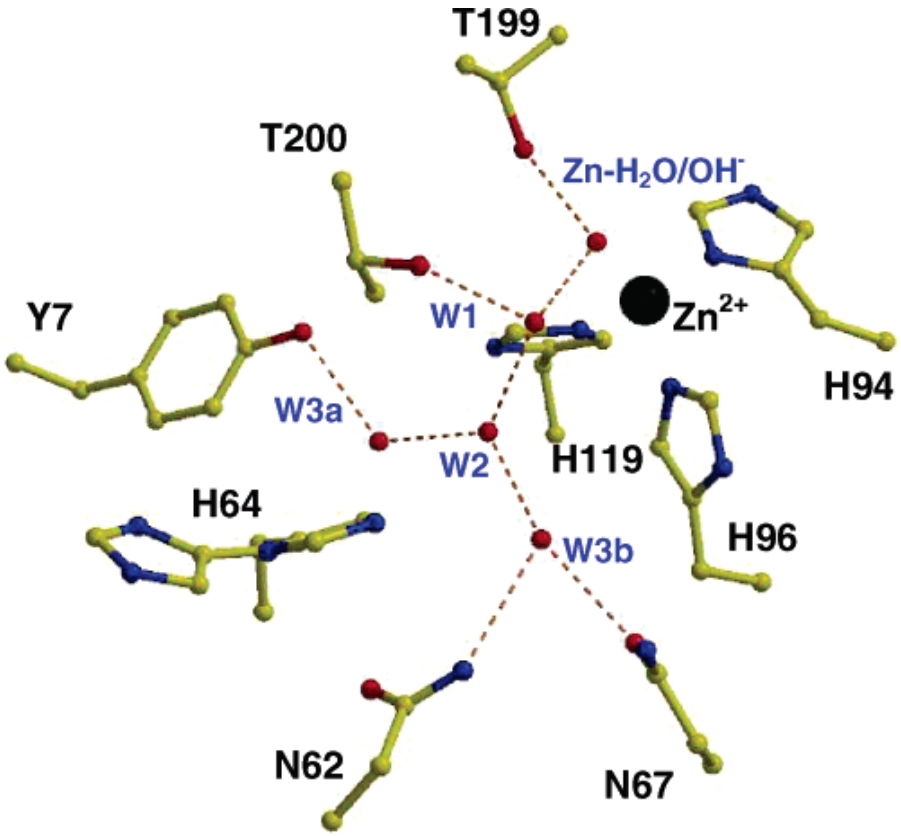

The facially capping tri-imidazole moiety binding the central zinc atom is of particular interest, with the extensive amount of hydrogen bonding around the active site apparent. As can be imagined this complicated network of hydrogen bonding is extended throughout the whole structure, with somewhere close to 258 amino acids and 486 water molecules comprising the body of the enzyme.[68] When considering the maximum diffusional rate of the substrates involved in the reaction the enzyme is almost perfect, it achieves near 100% efficiency. It

catalyses at a rate of K_M = 3 x 10^8 dm^3 mol^{-1} s^{-1}, which is one of the most efficient rates for a metal containing enzyme.[19]

Transmetallation studies have been performed on the native enzyme itself, with one method being to replace the zinc atom with another metal of choice for the study. However arguably more useful is the replacement of key amino acid residues to see what effect this has on the overall rate, or even if this introduced new properties to the enzyme, and thus how important the particular amino acid is overall. Mutagenesis studies focused on the replacement of Thr-199 with Ala, Glu-106 with Ala, Gln and Asp and finally Tyr-7 replaced with Phe have shown a number of interesting results.[50] The replacement of Thr-199 with Ala showed a 100-fold reduction in the rate of the catalysis achieved by the enzyme, whereas the replacement of Tyr-7 with Phe showed only a marginal difference in the activity.[50] Alternatively, replacing Glu-106 with Ala and Gln have shown a 1000-fold reduction in activity of the enzyme, a very large reduction considering the replacement of only one amino acid. Interestingly, replacing Glu-106 with Asp shows almost the same activity, hinting at the ability of the enzyme to recover from this change by exerting an equivalent influence which Glu-106 once had upon the structure. A macromolecular view of the enzyme is shown in figure 4.[65]

Figure 4, *Structural cartoons highlighting a simplified structural backbone model for HCAII and a surface rendered model respectively. Regions coloured in grey represent areas of almost no changes in H/D amide exchange rates, whereas yellow represents an exchange of between 5% and 9%, whilst orange indicates an exchange of between 10% and 20%.*[65]

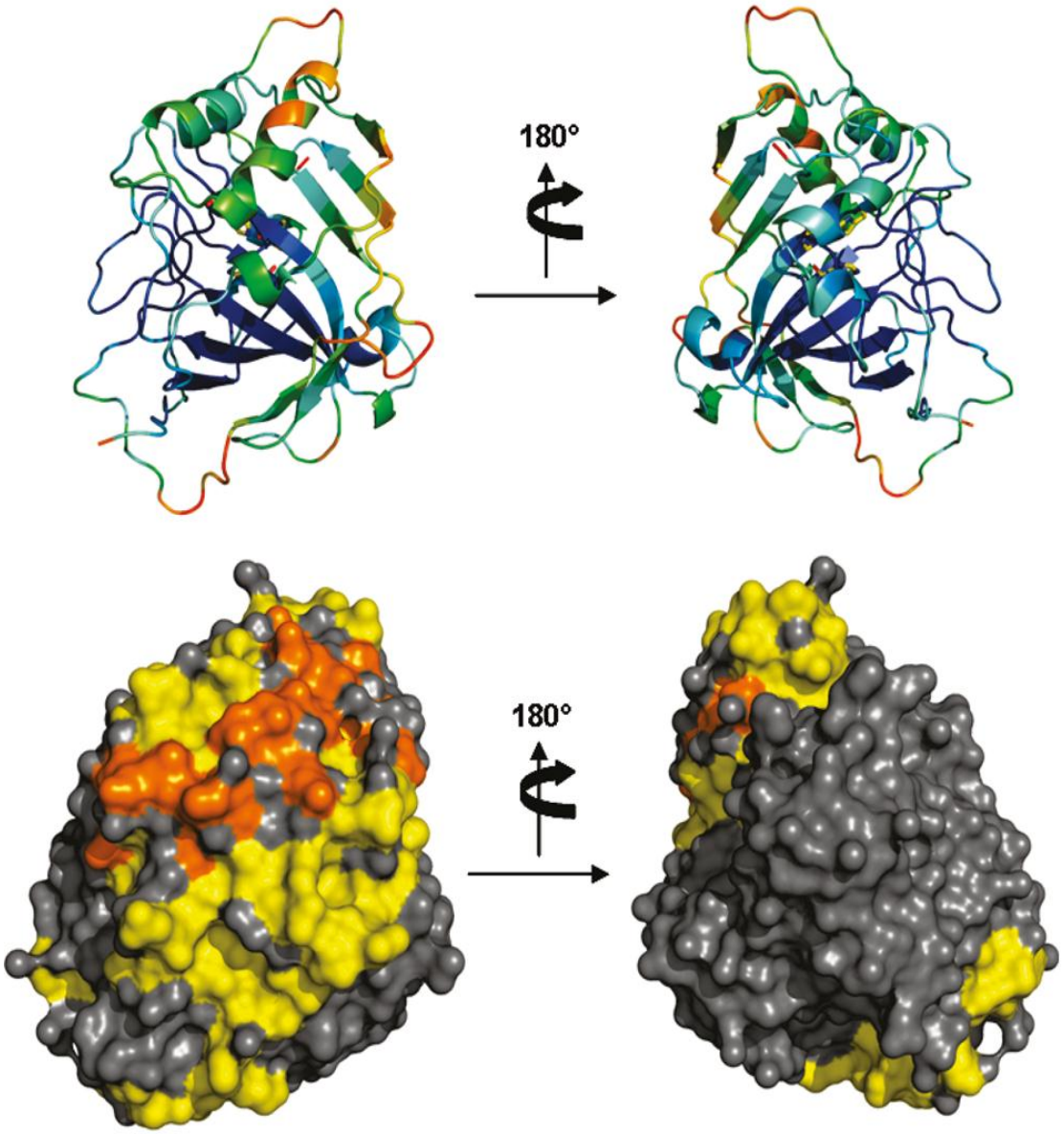

1.2.2 Deep water molecule and water network

There is another significant structural feature of the active site of *carbonic anhydrase.* A water molecule termed a "deep water" molecule or W_{DW} is significant for reactivity this is believed to be involved in substrate binding. This deep water stabilises substrates by hydrogen bonding to a nitrogen atom on the nearby Thr-199 residue. There is an extended hydrogen bonding network surrounding the inner coordination sphere, it is believed this allows the incoming carbon dioxide molecule to occupy the W_{DW} pocket.[40] The specific orientation of the pocket allows for maximum exposure to a lone pair of electrons on the oxygen of the hydroxide moiety. This results in a nucleophilic attack onto the carbon dioxide to form the bicarbonate intermediate species.

There also appears to be a secondary hydrogen bonding interaction to the zinc bound hydroxide or aqua species. It is understood that the W_{DW} molecule is most likely displaced within the binding pocket by a carbon dioxide molecule, before nucleophilic attack by the zinc bound hydroxide species.[41]

1.2.3 His-64 and the proton shuttle mechanism

The His-64 residue, found 6 Å away from the zinc centre well within the hydrophilic pocket in the active site, acts as a proton shuttle. [36] It is known that the extensive ordered water network seen throughout the entire macrostructure contributes to this mechanism. It involves the removal of protons from the active site, to generate the hydroxide species necessary for the beginning of catalysis

upon deprotonation of an zinc bound aqua species. This is significant because this step is believed to be rate limiting, and the proton transfer is suspected to be the slowest step of the mechanism.[66]

The His-64 residue has a conformational flexibility, which allows it to occupy two different positions. To accommodate more room in the active site, it can bend to an "in" and an "out" conformation. This conformational flexibility is believed to be directly involved in the proton shuttle mechanism. The conformational change may push or pull protons in the active site. To confirm the importance of the His-64 residue, a mutagenesis experiment involving the replacement of the His-64 with a more negative amino, acid Ala was undertaken. This one replacement caused the proton transfer step of the mechanism to have a 20 fold decrease in activity.

Kannan *et al.* have suggested a different proton shuttle mechanism to that of the more widely accepted His-64 route. The alternative pathway suggested still agrees with the mechanisms for the reaction set out by Lindskog *et al.* and Lipscomb *et al.*, but disagrees with the proton shuttle mechanism.[44] It is widely accepted that there must be removal of protons from the active site to facilitate the deprotonation of the aqua species to generate the hydroxide moiety. Kannan *et al.* have suggested that His-64 is not as essential as first thought, and instead a method involving Glu-106 and Thr-199 is used. However, this theory is doubted by an extensive molecular dynamic simulation, suggesting that a pK_a of around 7 is necessary for shuttling to commence. With Glu-106 having a pK_a of around 4.5, the plausibility of the mechanism is unlikely.[42] Figure 5 highlights the

extensive water network, with the zinc solvent distances highlighted and the large difference between the "in" and "out" conformations of the His-64 residue.

Figure 5, *Active site of the enzyme carbonic anhydrase, highlighting the essential parts of the proton shuttle mechanism.*[66]

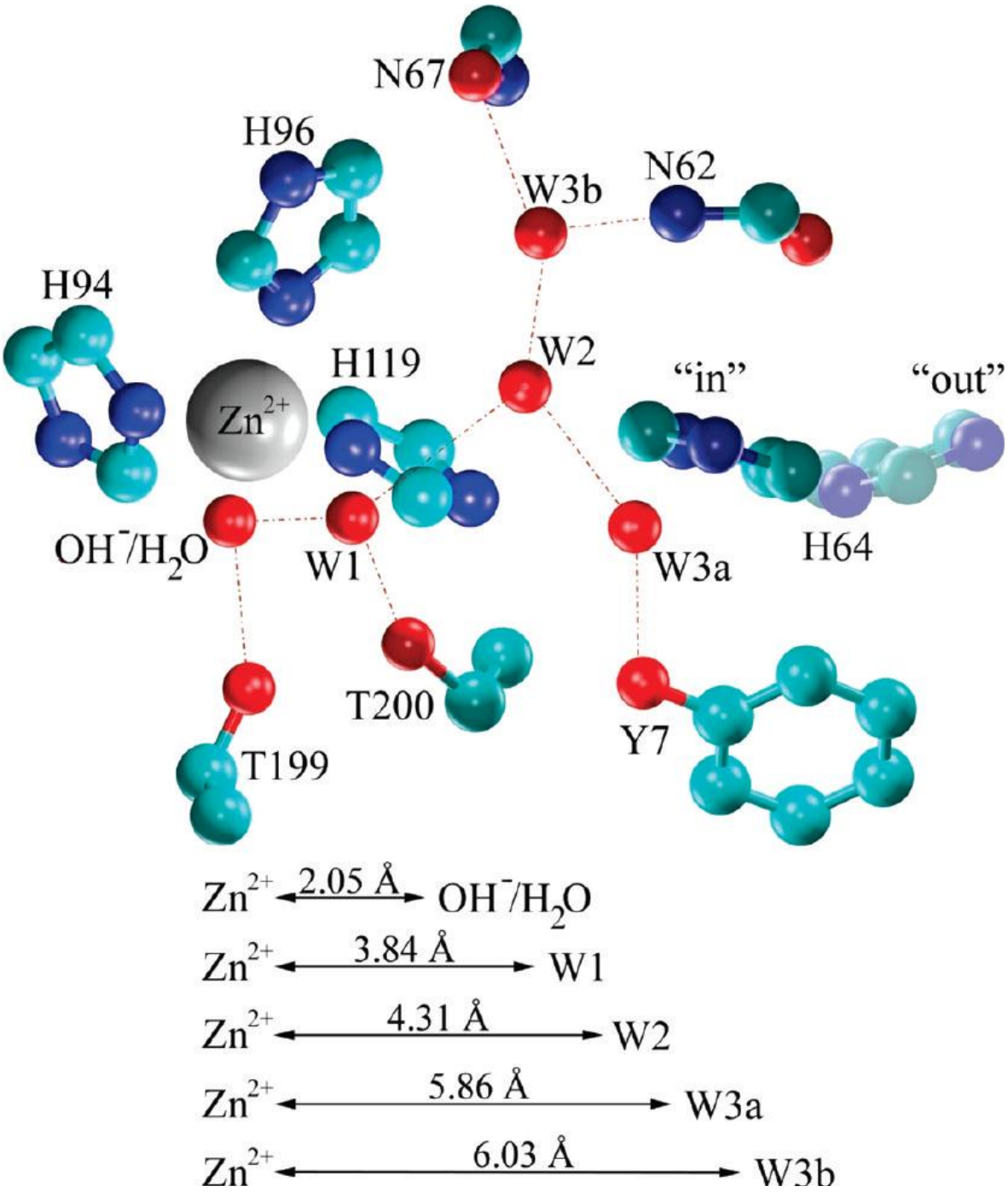

1.3 Mechanism of the active site

The mechanism of the active site has been studied since the 1960s,[1] with two eminent research groups emerging in the field by the 1980s. The first of these groups was led by the American physical inorganic chemist and Nobel Laureate William Lipscomb and the second group led by Swedish biochemist Sven Lindskog. Both research groups have suggested different mechanisms for the active site role of zinc. Although both pathways agree on the majority of the overall mechanism, they differ slightly in one key step, the fate of the zinc bound bicarbonate. Figure 6 below shows a summary of the mechanisms suggested, with the key step highlighted.[2]

Figure 6, *Summary of the two different mechanisms proposed by Lindskog et al. and Lipscomb et al., for the enzymatic reaction of HCAII with the relevant step highlighted in each case.*[2]

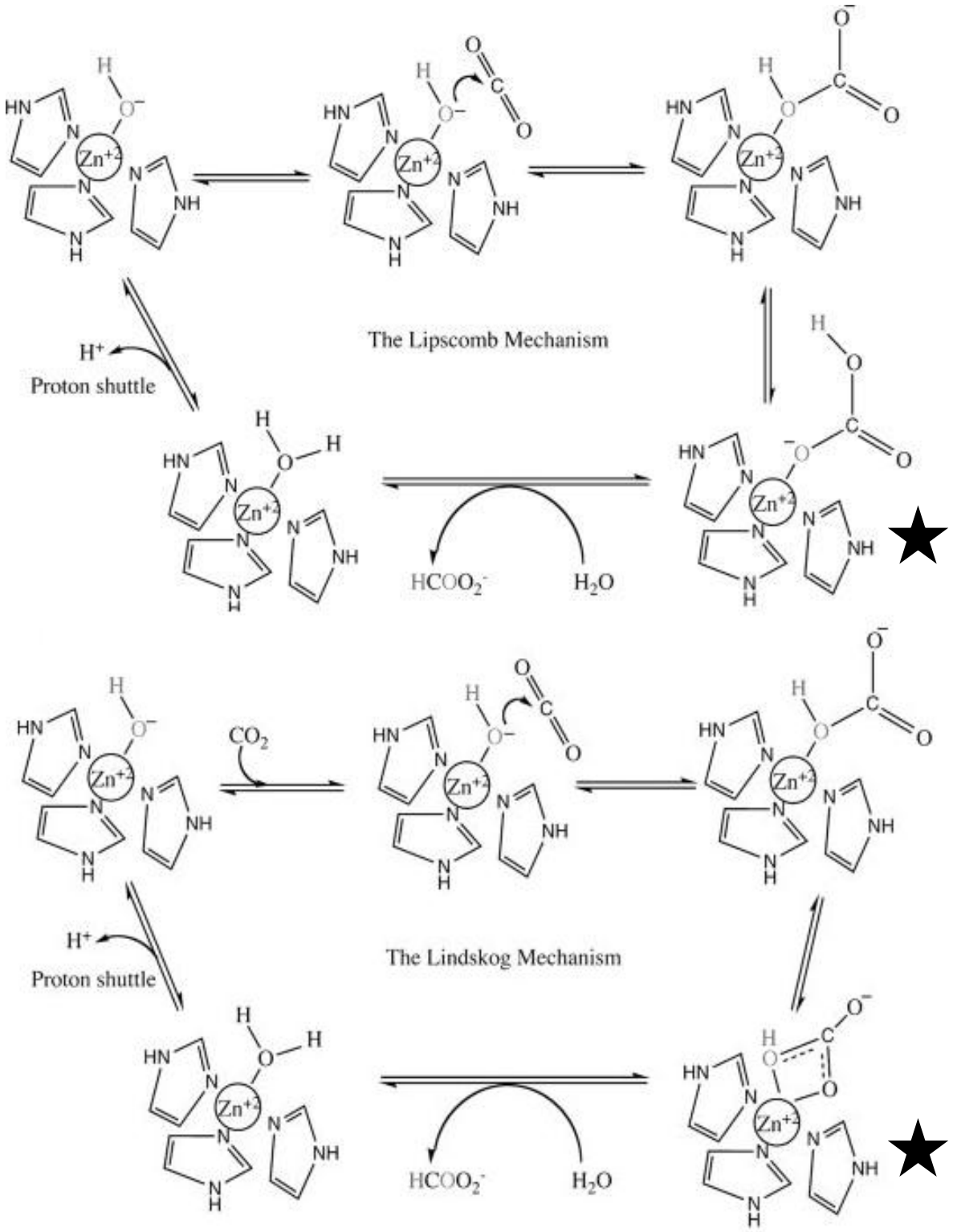

The pathways are two distinct stages, with the overall process being categorised as a “ping-pong” mechanism. Both mechanisms start with the zinc in its hydroxide form, with an initial nucleophilic attack on the carbon of the carbon dioxide from a lone pair of electrons on the hydroxide moiety, this creates a bicarbonate coordinated to the zinc centre.

The next step has caused controversy, on the one hand Lipscomb *et al.* believes that a proton is internally transferred from the original hydroxide group to an oxygen atom on the incoming carbon dioxide, whereas Lindskog *et al.* believe that there is an internal rotation of the oxygen atom bound directly to the zinc. The true step depends on whether the proton remains fixed to the original oxygen atom it was bound to, or whether it gets transferred.

The two mechanisms also differentiate between each other by how the bicarbonate binds to the zinc centre. In the mechanism suggested by Lindskog *et al.* a bidentate bicarbonate is suggested, whereas Lipscomb *et al.* have suggested this is a unidentate ligand. Figure 7 below highlights the differences between the two.

Figure 7, *Schematic diagrams showing the suggested intermediate bicarbonate binding modes by Lindskog et al. and Lipscomb et al., with the* κ^2 *Lindskog structure shown first and the structure shown second. For clarity sake, an* N_3 *facially capping environment has been shown to occupy the remaining coordination sites on the zinc atom and the histidine molecule is denoted as N(His).*[2]

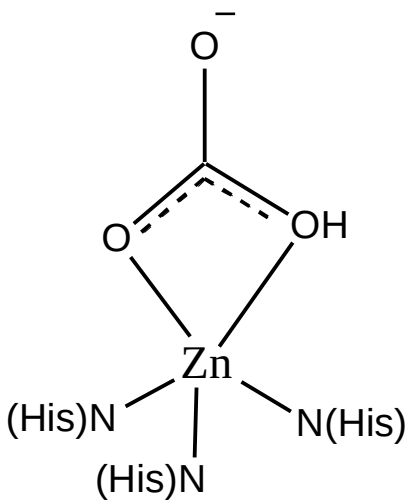

κ^2 binding mode by Lindskog *et al.*

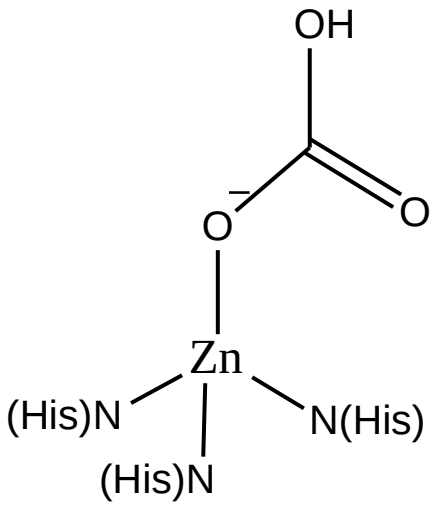

κ^1 binding mode by Lipscomb *et al.*

The bicarbonate produced is then exchanged by a water molecule. Finally, a second reaction involving the transfer of a proton from the water molecule bound to the zinc atom to the surrounding solvent occurs. With the release of the proton from the aqua species, regeneration of the hydroxide group coordinated to the zinc takes place, ready for another cycle, summarised above (see figure 6). The intramolecular proton transfer from the zinc bound aqua species to the His-64 residue is believed to be the rate limiting step of the reaction.[55 47]

His-64 promotes a proton shuttle mechanism between the metal bound water species and the surrounding ordered water network. In reaction 2 below, E is defined as the enzyme whereas in reaction 3, B is defined as a proton acceptor [36]. A summary of this mechanism is as follows, with all steps importantly being reversible;

Reaction 2

$$\mathbf{CO_2 + EZnOH^- \rightleftharpoons EZnHCO_3^- + H_2O \rightleftharpoons EZnH_2O + HCO_3^-}$$

Reaction 3

$$\mathbf{EZnH_2O + B \rightleftharpoons EZnOH^- + BH^+}$$

Evidentially speaking there has been several attempts at elucidating which of the two proposed mechanisms is correct. Firstly and arguably the most useful are the direct probing methods which would directly synthesise a zinc bicarbonate by

direct addition of carbon dioxide and isolating an enzymatic bicarbonate species.[2, 68] Another method utilised involves synthesis of small molecule mimics of the active site and attempting isolation of these smaller zinc bicarbonate complexes.[3, 4]

Both of these methods have their inherent disadvantages. The enzymatic reaction with carbon dioxide was believed to be unfeasible in generating a zinc bicarbonate via the HCAII route.[39] This is due to the complex process giving rise to the extremely high turnover rate of substrate, making it difficult to observe these short lived species by relatively slow spectroscopic methods.

Interestingly, in 2008 Silverman *et al.* managed to trap carbon dioxide within the enzyme and showed that the molecule binds to a hydrophobic cleft deep inside the active site, and also that the zinc atom does not play a critical role in either the orientation or binding of the carbon dioxide molecule, this has very important mechanistic implications because it means that the majority of the work is being done by the amino acid residues surrounding the active site.[76]

A crystal structure was obtained by using *cryo*-cooled crystals with carbon dioxide pumped into the enzyme at a low temperature (specifically cooled to liquid N_2 temperatures, 77 K), with the resulting active site crystal structure shown below in figure 8 and the macro crystal structure shown in figure 9.[76]

Figure 8, *Two forms of the active site of HCAII with the left diagram showing a superposition of unbound carbon dioxide and the HCO_3^- moiety, with the diagram on the left showing the unbound carbon dioxide and the resulting interactions with Trp209, inside the hydrophobic cleft (in green).*[76]

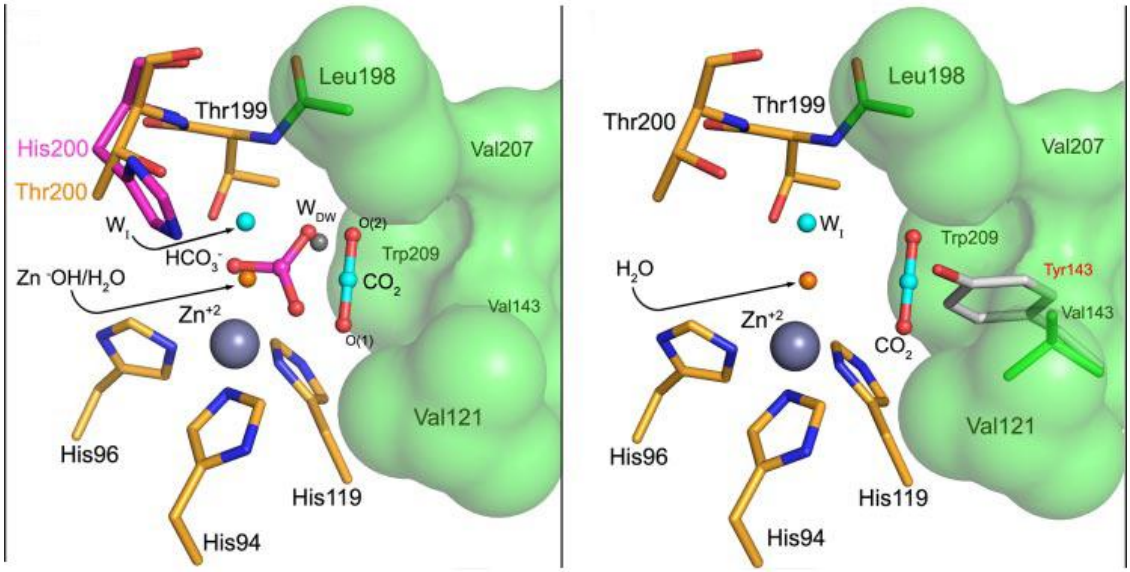

A second method that has been utilised for structural studies is that of transmetallation. This experiment involves replacement of the zinc centre with that of cobalt.[28, 32] This method has the specific aim of slowing the rate at which the substrate being turned over into the corresponding products to allow for observation.[28] Experiments using ^{13}C labelled HCO_3^- in ^{13}C NMR experiments have been attempted to characterise the bicarbonate, although again problems associated with the fast turnover rate of substrate have persisted.

Other attempts have focused on the removal of key amino acids, essential to the efficient recovery of the active site, or removal of residues which encourage carbon dioxide towards the active site. These methods decrease the rate of

reaction at the metal centre and thus overall decreasing the enzymes efficiency. This allows measurements to be taken on larger spectroscopic timescales. In NMR for instance, this could result in sharper peaks if the reaction is slower, allowing a more accurate glimpse at the processes governing the catalysis.

Mutagenesis experiments involving replacement of key amino acid residues appeared to give good insight into the approach and alignment of the carbon dioxide molecule into the active site.[1] For example, replacement of the Val-143 residue located in the hydrophobic pocket near the active site with a bulkier mutated amino acid reduced the activity of the enzyme to a figure of 0.02%. This shows just how large a factor that a small change can make upon the whole enzyme.[2] It was shown that this larger substitution blocks the carbon dioxide molecule from correctly aligning itself to the optimised orientation for a nucleophilic attack to take place via the hydroxide ion bound to zinc.

1.4 Structural mimics

At this stage it must be mentioned that the *carbonic anhydrase* enzymes are not limited to just utilising zinc in the active site. For instance, it has been shown by transmetallation studies that Mn^{2+}, Co^{2+}, Ni^{2+}, Hg^{2+} and Cu^{2+} can all bind to the tri histidine moiety within the active site.[60] This can show interesting activity for the new artificial enzyme. For instance, the manganese substituted *carbonic anhydrase* has been observed to enantioselectively catalyse olefins to epoxides. [61] Importantly, it is understood that *carbonic anhydrase* has a high affinity for the zinc ion compared to other transition metals.[77]

The native enzyme is not just limited to the use of zinc, as in nature it has been observed in areas of the ocean with lower concentrations of zinc ions that marine life had adapted the enzyme to allow it to take up cadmium in the active site. This removes the need for zinc, at the expense of a slower turnover rate.[64] This was until recently believed to be impossible due to the toxicity of cadmium(II), and is credited with being the first natural cadmium containing enzyme as of 2005.[64, 78] However attempts were made to synthesise a *carbonic anhydrase* with a cadmium centre. This was achieved in 1976 although it was discovered to be much less active than the native zinc containing *carbonic anhydrase*.[27]

1.4.1 Small molecule models of HCAII

HCAII has been the focus of significant attention by the small molecule modelling community.[3-24] The aim of the work has been twofold; firstly, the small molecule models synthesised aim to elucidate further the mechanism of the zinc catalysed carbon dioxide hydration reaction. Secondly, the molecule must act as a synthetic catalyst for the sequestration of carbon dioxide.

There has been a significant focus on trying to form a monomeric zinc bicarbonate complex for this purpose, with limited progress. This has proven to be very difficult; it was found that almost all models used formed a dimeric carbonate complex.

A bicarbonate species was reported by Parkin *et al.*, who in 1992 obtained IR data indicating potential stretches due to the bicarbonate at 1302 and 1675 cm^{-1} (see figure 12).[18] Although Parkin *et al.* had indeed reported IR data in 1992, there was no other supporting data, but on the basis of the seemingly validated results later by Ibrahim *et al.*, Parkin *et al.* could have been first to catch a glimpse of a zinc bicarbonate species. However, despite the lack of isolation of a monomeric bicarbonate structure, Parkin *et al*. have managed to isolate a dimeric carbonate solid, which has provided other spectroscopic data, focusing on binding modes (see figures 9 and 10).

There has been almost no data published concerning zinc bicarbonate complexes. However this was until very recently, with work by Ibrahim *et al.* in 2011

establishing one of the first reported footholds into the isolation of a zinc bicarbonate. The group reported some evidence to suggest they may have formed a zinc bicarbonate and isolated the species utilising a small ligand system.[71] They reported IR and ^{13}C NMR data which would correlate to the corresponding zinc bound bicarbonate. However a lack of ^{1}H NMR data as well as MS or even a crystal structure makes it difficult to validate this claim fully.

The approach by Ibrahim's group has been to produce a benzimidazole-based zinc aqua complex. They then deprotonated the aqua species in solution to the hydroxide form using triethylamine (Et_3N) as a base, whilst simultaneously bubbling carbon dioxide into the mixture to form a zinc bicarbonate complex. Their reported figures are a shift of 167 ppm in the ^{13}C NMR and IR stretches observed at 1440 and 1675 cm^{-1}. This IR data correlates well with the results published by Parkin *et al.*, although the model complexes synthesised contain different coordination numbers. Parkin *et al.* utilised a four coordinate model complex, whereas Ibrahim *et al.* has created five coordinate complexes. However even despite the promising data, all experiments were accomplished in solution, and no solid compound has yet been reported.

Figure 9, *Zinc hydroxide complex synthesised in situ by Ibrahim et al. utilising a benzimidazole Schiff base based ligand system.*[71]

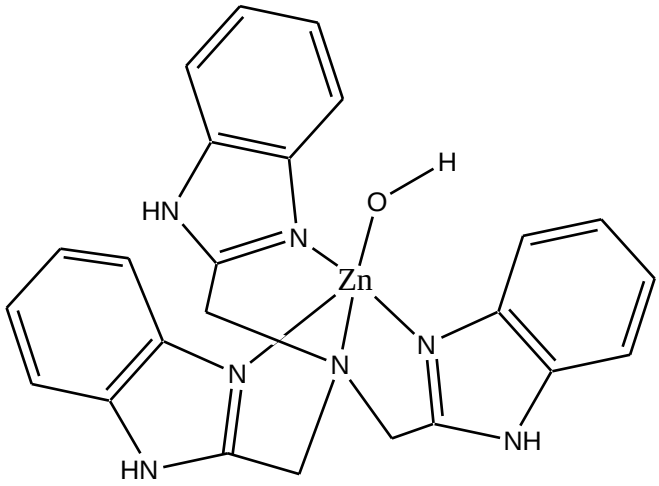

1.4.2 Zinc containing mimics

Studies in this area have focused on creating a structural mimic of the enzyme. The benefits of creating such a model become obvious considering the commercial opportunities of a complex which catalyses the hydrolysis of carbon dioxide. In particular, most attention has been focused on the active site encompassing the three histidine resides. Initial work recreated the corresponding imidazole functional groups, and the primary coordination sphere. Parkin *et al.* observed that upon reaction of carbon dioxide with their zinc hydroxide complexes, it was often seen that a bridged carbonate species was obtained.[45] A carbonate dimer effectively blocks the active site from catalysing any more reactions and thus rendering the mimic useless. These carbonate species are so stable that crystal structures have been elucidated of them (see figure 10). [9, 79]

Figure 10, *Structure of a dimeric zinc carbonate synthesised by Parkin et al.*[9]

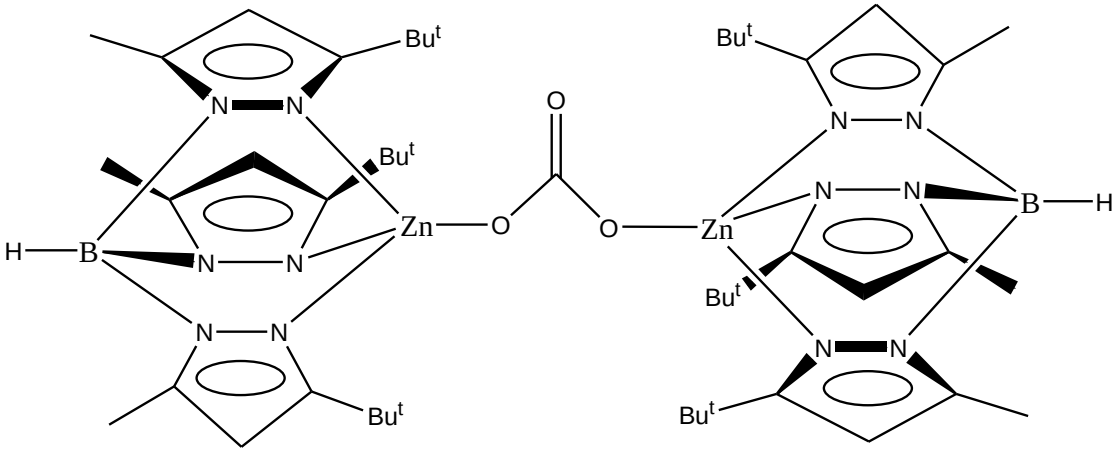

For example, Parkins' group created a carbonate dimer. This dimer complex appeared to reversibly decarboxylate once the carbon dioxide atmosphere was removed, allowing the reformation of the two separate zinc hydroxide complexes. This direct method of addition of carbon dioxide appears to be the only pathway to a zinc bicarbonate. A carbon dioxide atmosphere is necessary for the formation of either the carbonate or bicarbonate, due to the respective ligands labile nature preventing isolation.[9, 71]

To synthesise a structural mimic of the active site, it would seem sensible to start with using the basic amino acid residues to construct a suitable coordination environment. However, it is unlikely that the zinc will preferentially interact with the imidazole functional groups. The zinc may instead interact with the amine or carboxylic acid group on the end terminus of the histidine, with the structure of histidine shown in figure 11. In addition, the steric demands of these complexes

would not necessarily prevent carbonate or hydroxide bridged dimers or trimers etc., even if the electronic environment is assumed to be correct.

Figure 11, *Structure of the amino acid histidine, containing imidazole (A), amine (B) and carboxylic acid (C) functional groups.*

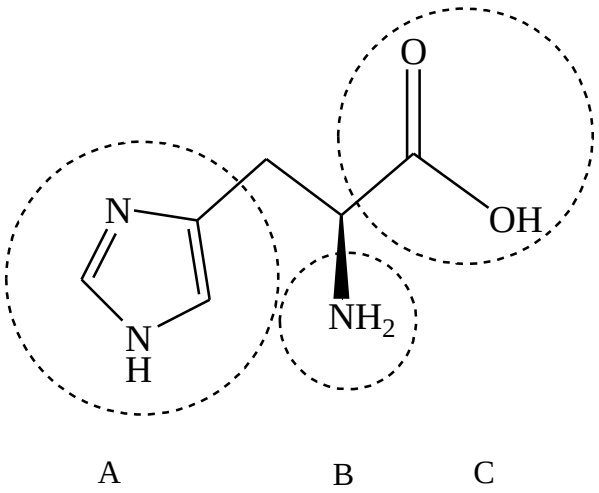

Initial attempts at creating an effective coordination environment of the active site focused on creating macrocyclic polyamines, with significant attention being shown to azamacrocyclic complexes. These model complexes utilised a derivatised azamacrocycle and reacted them with a Zinc(II) salt, in many cases this was a perchlorate, $[ClO_4]^-$ due to its non-coordinating anionic properties. However, the azamacrocycles have several drawbacks i.e. they struggle to maintain stability when a zinc hydroxide moiety is complexed to them, instead hydroxy bridged dimers are often seen.[18]

Significant attempts have been made particularly by Parkin *et al.*,[4, 9-11] with much research also undertaken by Vahrenkamp *et al.*[5, 15-18]with both utilising

similar tris(pyrazolyl)hydroborate ligands. Ibrahim *et al*. utilised a different ligand environment, achieving the strongest data yet, suggesting a bicarbonate complex was formed (see figure 12).[71, 80, 81] Parkins' and Vahrenkamps' groups have primarily focused on tris(pyrazolyl)hydroborate (see figures 13-17) zinc complexes, or pincer ligand synthesis, first discovered by Trofimenko in 1966 whilst working for DuPont.[82] There has been limited progress upon addition of carbon dioxide to these complexes. Ibrahim *et al.* have focused their attention to Schiff base based benzimidazole ligands.[71, 81]

Figure 12, *Structure of tris(pyrazolyl)hydroborate zinc bicarbonate complex.*[9]

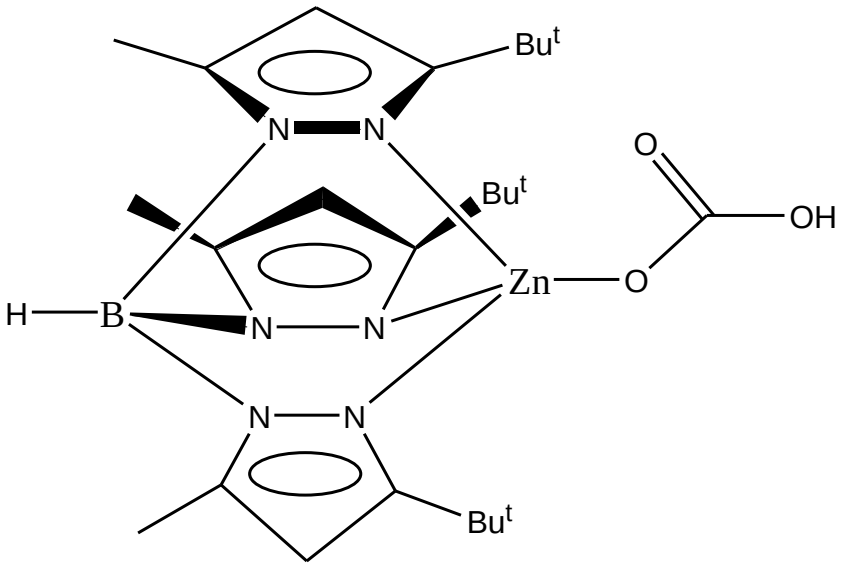

The pincer ligands are particularly useful for N_3 structural mimics, as they are easily synthesised from readily available starting materials and most importantly they are flexible to derivatisation. This means they can be fine-tuned sterically and electronically for a specific outcome. These pincer ligands are suited to this complexation, as they have become known as 'tetrahedral enforcers' due to their

ability to force many metals into a tetrahedral coordination, a key structural motif when considering the active site of *carbonic anhydrase*, and also of zincs structural versatility as a 4-, 5- and 6- coordinate species in the presence of certain counter anions.[15]

For the purposes of a *carbonic anhydrase* mimic, a four coordinate facially capping N_3 environment is essential for successfully recreating the active site. The fourth coordination site is typically bound to an aqua species depending on the pH of the media which the complex is in. The water-bound zinc must be deprotonated in order for the hydration of carbon dioxide to proceed. To accomplish this stage effectively, having a lower coordination number on the zinc allows for more electron density being "pulled" towards the metal centre from the bound oxygen, increasing the acidity of the protons in the $[N_3Zn(OH_2)]^+$ motif.

Attempts have been made to try and prevent the formation of the carbonate species. The most obvious route was to simply create enough steric bulk around the coordinated zinc atom, in order to avoid formation of the bridged carbonate dimers due to steric constraints.[6] The face which contains the hydroxide must have enough steric bulk to physically prevent the carbonate from being able to form a bimetallic dimer. Parkin *et al.* have often reported that the carbonate species will precipitate from solution immediately upon bubbling of carbon dioxide through a solution of a particular complex.[9] This allows for a quick visual inspection of the success or failure of the reaction when a precipitate is observed, indicating a carbonate species.

Parkin relied on IR and NMR measurements including the utilisation of ^{1}H and ^{17}O NMR techniques. However, it is stated that although ^{13}C NMR measurements were taken, no peak could be confidently assigned to the bicarbonate ligand. ^{1}H NMR data by Parkin assigned a hydroxide peak as a sharp singlet at -0.06 ppm.[9] This is verified by the work of Walton *et al.*, this suggests a hydroxide peak was observed as a singlet at -0.08 ppm.[20]

Parkin further showed that upon addition or removal of incremental amounts of carbon dioxide the ^{1}H NMR peak at -0.06 ppm due to the OH of hydroxide is either reduced in height or increased again respectively. This is to be expected if carbonate (or even bicarbonate) formation had occurred. Parkin *et al*. observed regeneration of the hydroxide moiety once the carbon dioxide atmosphere was removed.

Parkins' group used isotopically enriched samples to probe the bridging carbonate group, a peak was observed at 164 ppm in a ^{13}C NMR spectrum. However, efforts to elucidate the bicarbonate carbon atom in the spectra appeared inconclusive due to chemical exchange with the hydroxide in the absence of water. Taking advantage of isotopically labelled water (specifically $H_2{}^{17}O$) allowed for ^{17}O NMR analysis and exchange of the labelled ^{17}O atom with H_2O to carbon dioxide to take place. This confirmed the catalytic ability of their synthesised tris(pyrazolyl)hydroborate zinc complex, as rapid exchange takes place at room temperature in a matter of minutes. A sample was made up without the catalyst and the same reaction took days to go to completion,

highlighting the importance of the tris(pyrazolyl)hydroborate zinc complex and its role.

Parkin *et al.* also managed to achieve a clear IR spectrum of a zinc bicarbonate complex, strongly suggesting the presence of bicarbonate. Stretches seen at 1675 and 1302 cm^{-1} in a solution of $CDCl_3$ are indicative of a *ν*(CO) vibration.[9] Focusing on the bicarbonate, this would suggest a unidentate bound species (see figure 12), with direct comparisons drawn between already characterised palladium complexes which contain a bicarbonate with a known coordination mode.

1.4.3 Cadmium, Cobalt, Copper and Nickel structural mimics

Structural mimics with other metal centres existing with the same facially capping tetrahedral imidazole functional groups have also been studied. The native enzyme has a metal centre coordinated to three histidine residues, with models copying this

coordination. Different divalent metal ions inside the active site are studied to probe the changes certain metals make to the function of the enzyme. These changes look at either the specific hydrolysis of carbon dioxide as in the native enzyme, or new reactions undergoing catalysis such as esterase activity for instance, which has been observed in enzymes containing Co^{2+} and Mn^{2+} metal centres.[30, 61]

Spectroscopically speaking the zinc(II) centre is difficult to probe. Due to it being diamagnetic because of its d^{10} atomic configuration, it is inert to probing by any spectroscopic methods which promotes electrons or distorts its electronic structure. This effectively rules out UV-Vis spectroscopy (all zinc(II) complexes are colourless in appearance), but due to its diamagnetic nature also rules out ESR spectroscopy. One valid method that may be used is ^{67}Zn-NMR experiments. However, aside from probing how many different zinc environments are present in a sample, there is no direct structural information that could be used as evidence for the existence of a desired product.

Notably, an extensive amount of work has been undertaken with cobalt complexes, because it has a characteristic UV-Vis spectrum and provides a similar level of activity when compared to the native zinc enzyme and complexes. Cobalt however is paramagnetic and thus probing by NMR is extremely difficult. Arguably UV-Vis provides more valuable information for these structural studies, hence the lack of NMR is not a major issue.

Parkin *et al.* used a cobalt-substituted *carbonic anhydrase* for some of these electronic studies, specifically the coordination environment of the metal centre, as it proceeds through transitions of the mechanistic cycle[7]. It was deduced that the electronic spectra of the cobalt-substituted *carbonic anhydrase* was pH dependent, with the alkaline form elucidated as being a four coordinate tetrahedral structure, with acidic conditions the cobalt was observed as being in an equilibrium between four and five coordinate species. The evidence to support this included UV-Vis spectra, with a band at 553 nm seen at high pH, whereas at

low pH, a less intense peak was seen at 714-833 nm, with molar absorbtion coefficients of 300 M^{-1} cm^{-1} and 200-300 M^{-1} cm^{-1} seen respectively. It was concluded that the cobalt-bound nitrate complexes were clearly in an asymmetric mode of coordination. This was further denoted as being an intermediate between a symmetric bidentate and unidentate binding operation.

Similar studies were also undertaken with Ni(II) and Cu(II) substituted *carbonic anhydrases*. A surprising result was seen in the Ni(II) substituted *carbonic anhydrase,* showing a potential six-coordinate complex observed around neutral pH. At higher pH, a five-coordinate species was seen, with bands in a UV-VIS spectrum seen at 390 nm, 640 nm and a weak band observed at 1000 nm.[7] Contrary to the Ni(II) substituted enzyme, the Cu(II) substituted *carbonic anhydrase* has shown to have a pseudo-tetrahedral or five-coordinate geometry. It was concluded to be a pseudo tetrahedral or five coordinate geometry since square planar and six coordinate species absorb at much higher energies than that which was observed. In this case a single broad absorbance was observed at 760 nm.[7] Cadmium was also tested in an analogous way, with the cadmium derivative exhibiting a bidentate coordination mode.[10] Here the *carbonic anhydrase* enzyme substituted with cadmium was shown to exhibit substantially lower activity than the native enzyme.[27]

These studies were not just limited to substituted *carbonic anhydrases*, with focus on complexes synthesised utilising a *tris*(pyrazolyl)hydroborate ligand to elucidate potential binding modes of the bicarbonate in the active site by using the isoelectronic nitrate species as well as carbonate complexes. X ray diffraction

analysis of these complexes showed the nitrate ion was bound in a bidentate fashion, see figures 13-15. It was concluded that the preference of binding in a bidentate manner increased across the series Zn < Co < Cu < Ni as shown by Parkin *et al.*[7] The nickel-bound nitrate shows the most bidentate nature.

Figure 13, *Crystal structure of a tris(pyrazolyl)hydroborate Cobalt complex, with a metal bound nitrate. The M-O distances (Å) in the Cobalt complex are 2.001(3) and 2.339(3).* [7]

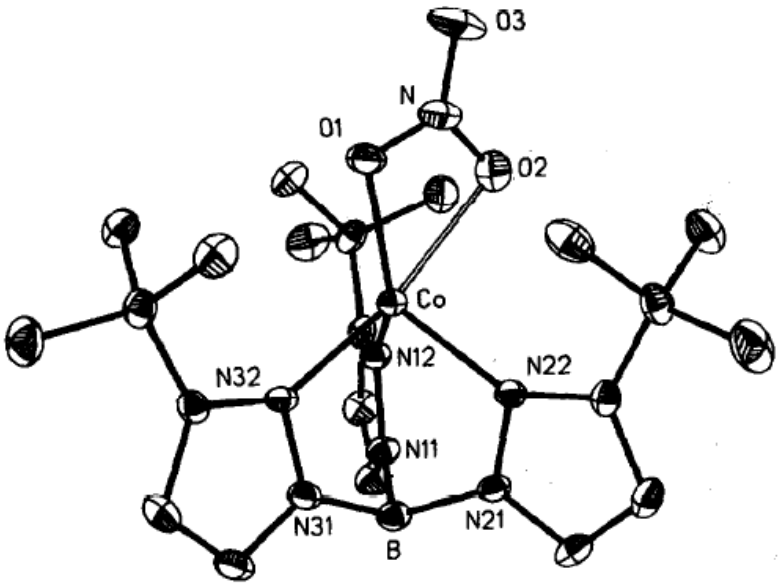

Figure 14, *Crystal structure of a tris(pyrazolyl)hydroborate Copper complex, with a metal bound nitrate. The M-O distances (Å) in the Copper complex are 2.042(3) and 2.266(4).* [7]

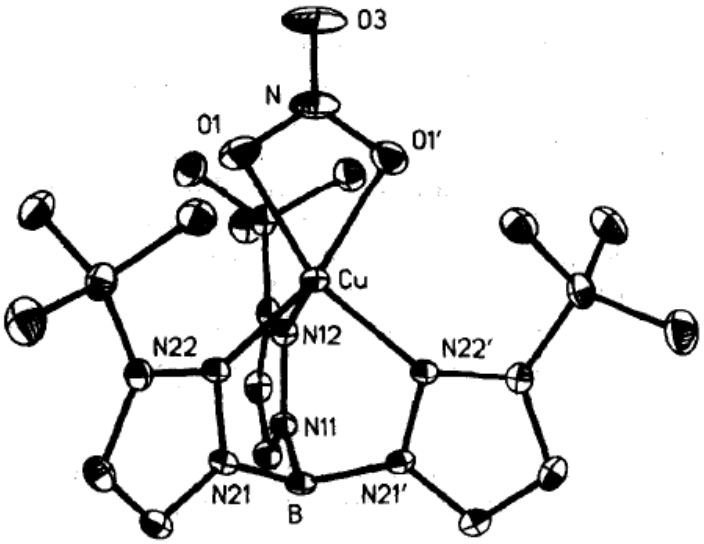

Figure 15, *Crystal structure of tris(pyrazolyl)hydroborate Nickel complex, with a metal bound nitrate. The M-O distances (Å) in the Nickel complex are 2.095(2) and 2.059(3).* [7]

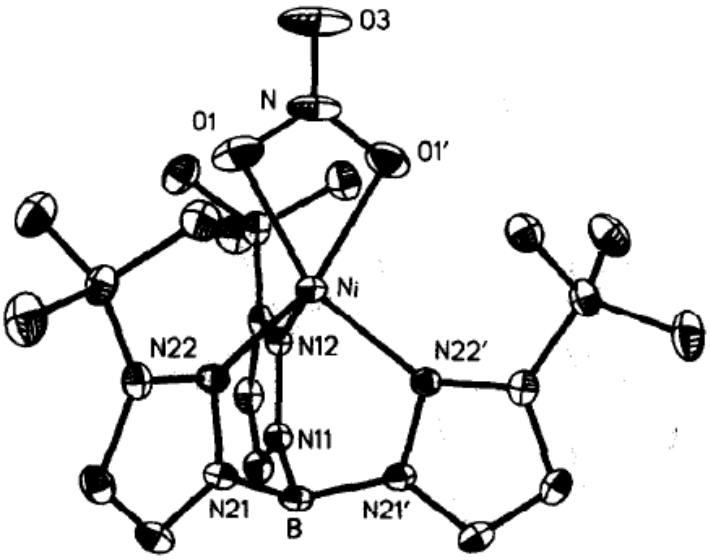

The bidentate nature of the nitrate is important for a number of reasons. Firstly, as the nitrate is isoelectronic to the bicarbonate ion and of a similar steric size, it provides essential information that is difficult to directly ascertain from the bicarbonate due to its high lability on the zinc atom in the native enzyme. Secondly, two competing *modus operandi* for the reaction have been proposed with the key step being a unidentate or bidentate bound bicarbonate in the mechanism itself, making elucidation of its binding mode essential to understanding how the native enzyme functions.

However, very interestingly a zinc nitrate with the same ligand system was also synthesised, and this was observed to be purely unidentate, with a primary Zn-O distance of 1.978(3) Å and a weak secondary interaction of 2.581(3) Å. This crystal structure of this complex is shown in figure 16 below. A carbonate dimer complex synthesised is shown in figure 17, it has a shorter Zn-O distance at 1.850 Å.[7] These zinc bridging carbonate dimers are unfortunately very different to their cobalt, copper and nickel counterparts, as only the zinc complex doesn't show bidentate coordination at both of its metal centres. This has also been confirmed by Katajima *et al.* who have observed asymmetry on the carbonate bridge in other *tris*(pyrazolyl)hydroborate complexes using the same metals as Parkins' group, as well as iron.[45] Evidence suggests the nickel and copper complexes show typical symmetric coordination modes whereas the cobalt and iron complexes have an asymmetric coordination mode.[45]

Figure 16, *Crystal structure of tris(pyrazolyl)hydroborate zinc complex with a unidentate bound nitrate to a Zn metal centre with a M-O distances (Å) of 1.978.*[7]

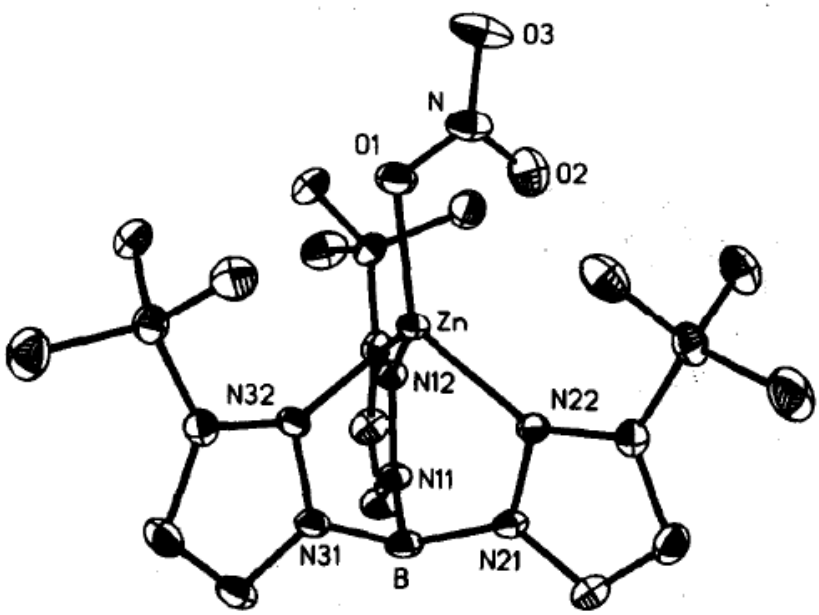

Figure 17, *Crystal structure of a dimeric tris(pyrazolyl)hydroborate zinc complex with a bridging carbonate ligand.*[7]

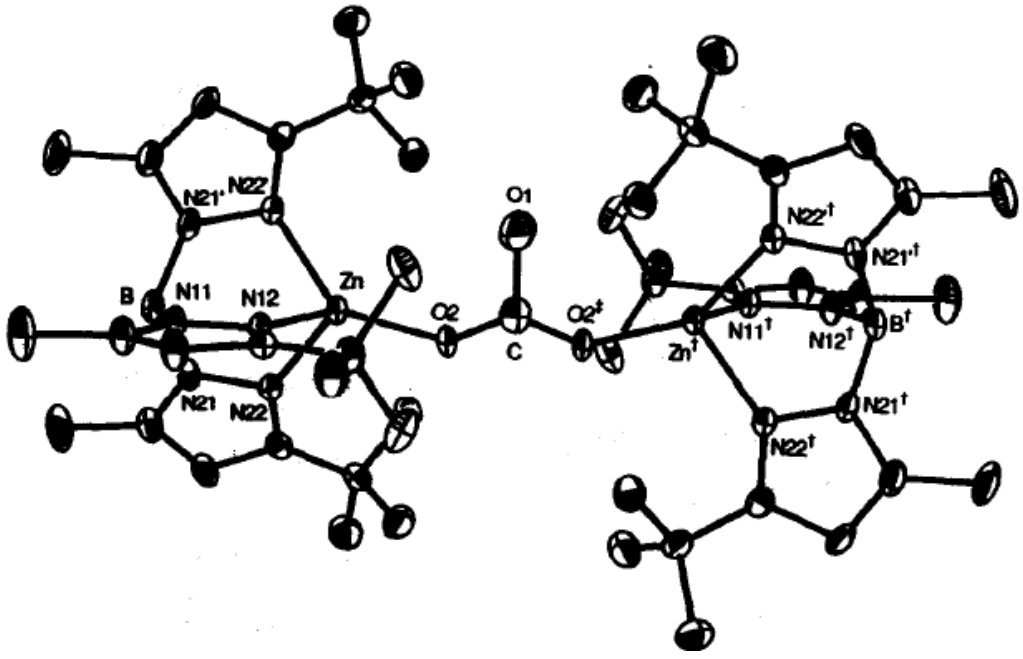

Kitajima *et al.* developed a method to synthesise dimers of bishydroxo complexes, with addition of carbon dioxide to create the bridging carbonate. They managed to observe a dimeric zinc complex with a carbonate bridge where one zinc centre was of unidentate coordination and the other bidentate (see figure 18). Preferential order of reactivity for their hydroxide complexes synthesised was also calculated; with Zn > Cu > Ni ≈ Co > Mn > Fe.[45] This was a surprise as this is not the same order for the respective metal-substituted enzymes, which is Zn > Co >> Ni ≈ Mn > Cu = 0. This discrepancy between the two different orders of reactivity is attributed to the degree of distortion that the carbonate ligand undergoes, Zn > Mn ≈ Fe ≈ Co > Ni ≈ Cu. It must be stressed that the zinc hydroxide complex synthesised was monomeric, whereas the use of the other divalent metals produced dimeric bishydroxo complexes, although care must be taken to note that a dimeric bridged carbonate complex was formed in each case.

Figure 18, *Kitajima et al. carbonate multi binding modes, with N_3 coordination environment representing tris(pyrazolyl hydroborate ligand system.*[45]

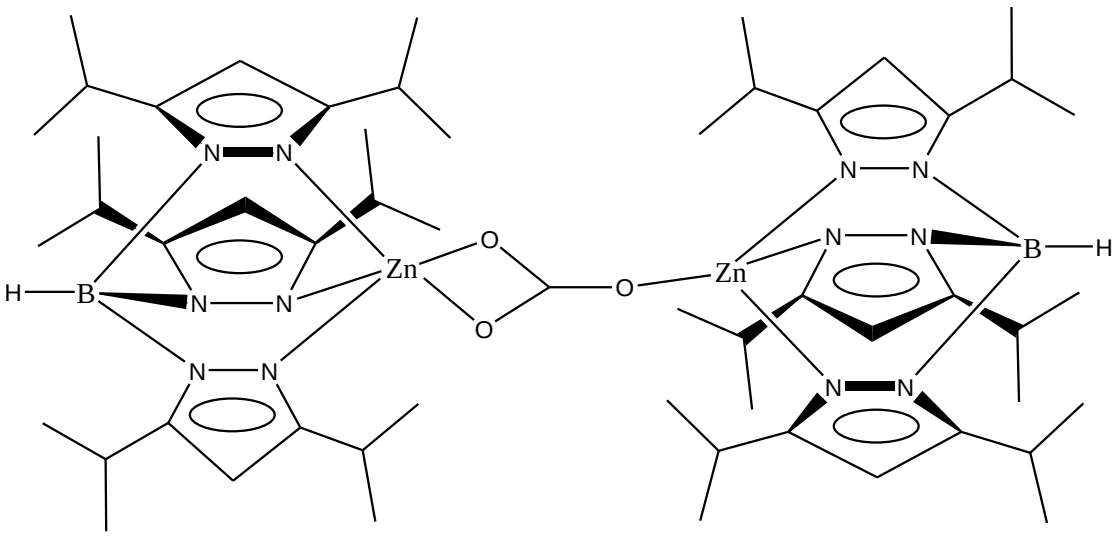

1.5 Designing a model for HCAII

There are three types of mimics of a protein; those being speculative, corroborative and functional modelling. [79] Speculative modelling examines the spectroscopic details of the protein in question, and attempts are made to synthesise a small molecule model complex that complies with the features of these spectra. Speculative modelling is undertaken when a crystal structure is unavailable, and not all details of a protein are known. This usually mimics the primary coordination sphere, where longer distance interactions exponentially increase the difficulty of modelling effectively.[83] Conversely, corroborative modelling utilises a known crystal structure of a protein. This approach focuses on the primary coordination sphere, but allows for more information to be garnered about the interactions around the active site of an enzyme. Finally, functional modelling mimics the catalytic function of an enzyme by matching key motifs. For example, this could include matching the coordination geometry, focusing on the secondary coordination sphere or matching conditions the enzyme operates in.

Generally these models do not allow for definitive answers about an enzyme. Replacement of the metal centre allows for direct comparison for two or more models containing the same ligands but different metal centres, or vice versa. This refinement process allows progressively more successful models to be synthesised, until ultimately a functioning model of the enzyme is synthesised.

Achieving the primary coordination sphere of an enzyme is key to initial mimic model design. In the case of HCAII, a crystal structure is already known, so a great deal of information can already be utilised when considering a model structures key motifs. Firstly, a zinc metal centre must be used, although cobalt-containing *carbonic anhydrases* also have significant catalytic ability. Table 1 below shows a list of the activity of HCAI I with different metal substitutions.[33, 55]

Table 1, *Relative catalytic activity of metal substituted HCAIIs*.[33, 55]

Metal Ion	**Activity of substituted HCAII relative to wild type HCAII towards CO_2 hydration / %**
Zinc(II)	100
Cobalt(II)	50
Manganese(II)	7
Cadmium(II)	2
Copper(II)	0
Mercury(II)	0

Secondly, the N_3 facially capping tri imidazole groups must be present for mimicking the coordination environment. The ligands used to provide this environment must also possess a similar electronic environment to the tri-histidine residues as seen in the native enzyme.

More detailed secondary features that have an effect on catalysis are also important, although not necessarily key for a catalytically active model. These

would include His-64 for its role as the proton shuttle key to overcoming the rate limiting step of proton diffusion. Another beneficial residue Thr-199, helps to facilitate release of the bicarbonate once it has formed as an intermediate or as well as Thr-200.[39, 49] It would also be worth considering the hydrophobic and hydrophilic portions of the active site, as these have been shown to be essential to the fast turnover rate of the enzyme. Final considerations could include solubility, ease of synthesis and stability of the complex to air and moisture.

Inhibition of the mimic upon formation of a dimer must be considered when designing a model complex. Dimerisation of a *carbonic anhydrase* model usually involves destruction of the hydroxide moiety and creation of a carbonate species. It has been shown that without enough steric bulk attatched to the primary coordination sphere of the zinc, these carbonate bridges easily form. [4, 7] These species can be a worry as the carbonate species is often more stable than the starting hydroxide complex. Some of these carbonate complexes have been isolated in the open atmosphere as crystals suitable for single crystal x-ray diffraction studies. However isolation of a single crystal suitable for x-ray diffraction analysis has not been accomplished with a zinc hydroxide model complex.

It is essential to consider what is classed as having an inhibitory effect upon not only the enzyme, but the N_3Zn environment utilised in the model complexes. By avoiding these inhibitors in the synthesis of a model complex it may be possible to isolate the species of interest. The nitrate and halogen anions, specifically iodine and chlorine are classed as inhibitory.[8] These may be useful in developing

inhibitors for the alleviation of symptoms of disease, such as the drugs acetazolamide, methazolamide, and dichlorphenamide developed to combat glaucoma and altitude sickness.[55, 59] Inhibition of *carbonic anhydrase* is also believed to have a diuretic effect on the body.

These inhibitors are important because their coordinative effect must be considered further down the field when a route to the labile hydroxide is accomplished. Drugs such as acetazolamide add to the coordination sphere, forcing the zinc to adopt a pentacoordinate geometry, see figure 19.[69] This reduction in conformational flexibility by the binding of a drug effectively renders the enzyme ineffective until the inhibitor unbinds. What is interesting to note is that the inhibitor not only binds to the zinc motif as would be expected, but actually forms favourable hydrogen bonding interactions with no fewer than four residues around the active site. This inhibitor completely blocks the active site, and it is understandable why the acetazolamide class inhibitors are so effective at inhibition.

Figure 19, *A schematic representation of HCAII interacting with an adamantyl analogue of the topical inhibitor acetazolamide, with hydrophobic interactions shown by orange hashed lines, H-bonds and lengths in Å are shown.*[69]

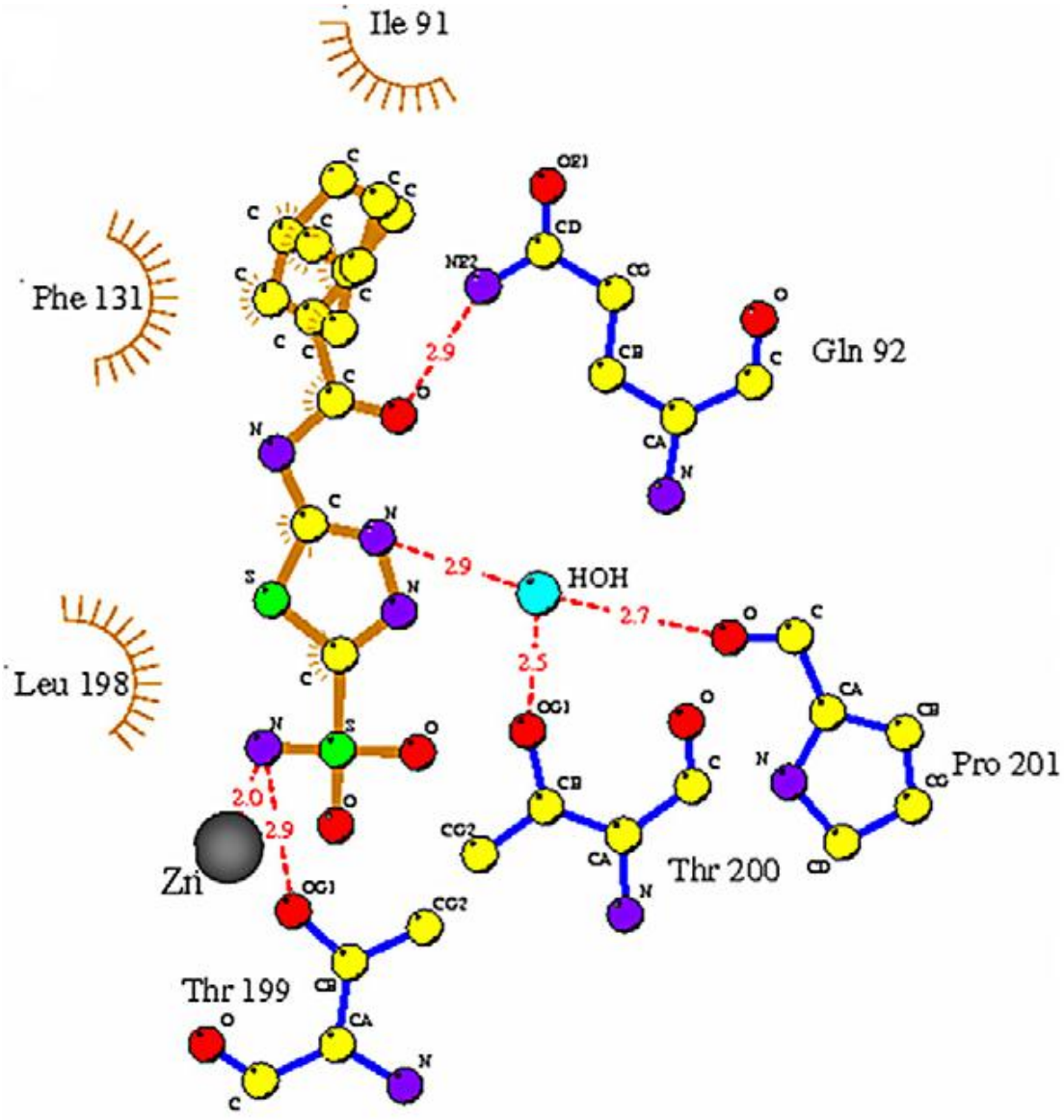

1.6 Project aims

The aims of the project involved synthesising a zinc hydroxide complex. This is known to be a key intermediate in the enzymatic reaction of HCAII after deprotonation via a proton shuttling mechanism. Once this is achieved, studies could focus on the reaction with carbon dioxide in hope of producing a zinc bicarbonate complex, another key intermediate from the mechanism studied. Isolation of the resulting complex would allow further understanding of the binding mode of the bicarbonate. Initial challenges of this project would be designing a suitable ligand system to mimic the HCAII enzyme, with the design of this ligand based on previous work by the Walton group.[21-24, 53]

The reasons behind isolation are two fold; firstly, understanding the binding mode of the zinc bicarbonate is key to providing evidence to the mechanistic aspects of *carbonic anhydrase*. A unidentate binding mode would support the Lipscomb mechanism, whereas a bidentate zinc bicarbonate would suggest the Lindskog mechanism is the preferred pathway. Isolation of this zinc bicarbonate complex would be a remarkable achievement. Since there is limited evidence to suggest it has been observed in previous attempts, with the only indication of a zinc bicarbonate complex being observed being IR and ^{13}C data.[9, 71]

The isolation of a zinc bicarbonate complex would benefit future work hoping to synthesise a structural mimic of the enzyme *carbonic anhydrase*. The stabilisation of such a labile ligand could aid other studies looking to understand the mechanistic aspects of other enzymes with similar coordination

environments. For instance, with the highly tuneable ligand system utilised, it could be possible to introduce aspects of the secondary coordination sphere, which could potentially aid catalysis by the metal centre. This has been attempted in the past, with Walton *et al.* attempting to incorporate a hydrogen bond associated with Thr-199 in the native enzyme into the ligand system.[23]

Secondary investigations would focus on deermining the catalytic ability of the synthesised complex. Previous work has been done on similar tach-based ligand systems by Walton *et al.*, with limited progress achieved in isolation of a zinc bicarbonate species. [19-24, 53] The ligand system used, 3,5 ^{t}Bu(TCT) was believed to provide enough steric bulk to prevent dimerization. A 3,5 dimethyl-substituted ligand proved unsuccessful in analogous studies, with no crystal structure of a zinc bicarbonate complex ever obtained. The methyl substituted ligand highlighted the need for additional steric bulk, with Figure 20 below showing the ligand system utilised for this project.

Figure 20, *The free 3,5 ^{t}Bu (TCT) ligand system utilised for the project.*

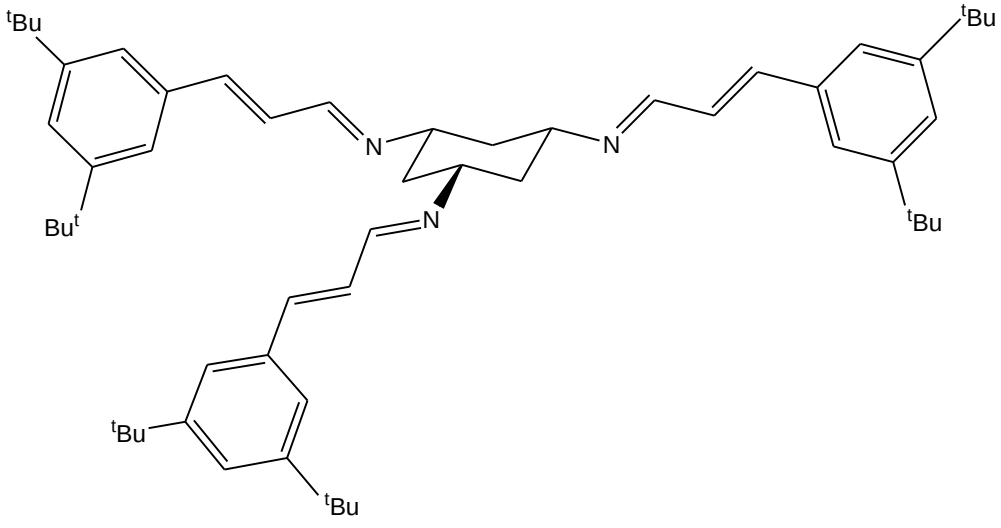

Chapter 2: *Synthesis of 3,5 ^{t}BuTCT ligand system*

2.1 Introduction

In order to synthesise a zinc bicarbonate complex, a new ligand system has been produced which has been designed to be bulkier than previous ligand systems. The binding mode of the bicarbonate ligand in this complex is key to providing further information on the mechanism of *carbonic anhydrase*. It is essential to provide an environment which is as similar to the native enzyme as possible. Previous ligand systems have not been able to isolate a monomeric zinc bicarbonate complex due to the formation of bridging carbonate complexes. A key feature of the ligands used in earlier studies is a facially capping N_3 environment.[9, 10, 22-24, 52, 53, 84, 85] This must also be stereochemically rigid, as if there is too much flexibility dimerization may still take place. An effective ligand system must also to be able to form a zinc bound water species and have a pK_a of ca. 7 to mimic the active site.

Utilising tach-based ligands has proven useful in previous studies modelling HCAII due to their N_3 facially capping binding, ease of derivitisation and in providing a structurally rigid cavity upon complexation.[20, 56, 86-89] Figure 20 shows the ligand system utilised by this project, the bulky ^{t}Bu groups are hoped to prevent dimerization occurring.

One of the first studies using tach to mimic HCAII was undertaken by Itoh *et al.*[90] A zinc aqua complex was synthesised, and the pK_a of the aqua species was

shown to be 7.95, figure 21 shows this complex. The aqua species in HCAII has a pK_a of ca.7, and it was realised that tach provided a good mimic of the primary coordination sphere. [31] It is interesting to note that upon complexation with a metal, the tach molecule undergoes a 'ring flip'. This conformational transition sees the amine groups go from an equatorial to an axial conformation, providing a facially capping coordination for the metal.

Figure 21, *Structure of Itoh et al. zinc(II) tach complex*[90]

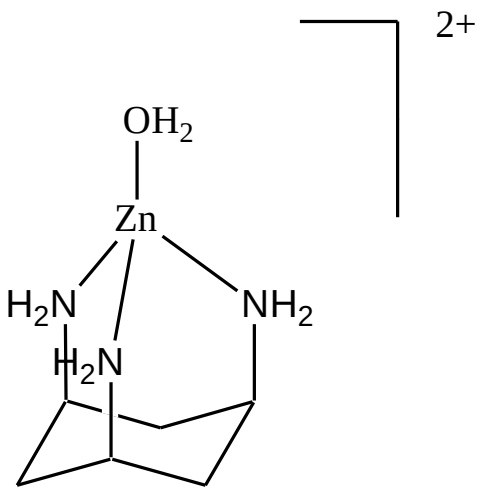

Walton *et al.* realised that a tach-based Schiff base ligand could be synthesised and highly derivatised. It was realised that the aldehydes used for these ligands were able to incorporate important structural features such as steric bulk or favourable hydrogen bonding. [21, 23, 24, 53]

Walton *et al.* realised that to effectively mimic the active site cavity of HCAII, the side arms which were used to create the Schiff bases would have to create a

deep enough pocket. One of the first generation of tach-based complexes utilised benzaldehyde to react with the amine, with the new ligand nicknamed TBT (*cis*, *cis*– 1,3,5-*tris*[(E,E)-benzylideneamino]cyclohexane, see figure 22). However, it was concluded that unfavourable steric bulk caused hydrolysis upon complexation, with the benzylidene groups twisting upon coordination of the ligand with a metal.[23, 52, 86] This saw two of the side chains hydrolysed, with one remaining benzylidene group left on the ligand.

Figure 22, *Structure of TBT designed by Walton et al., showing attached steric bulk*[91]

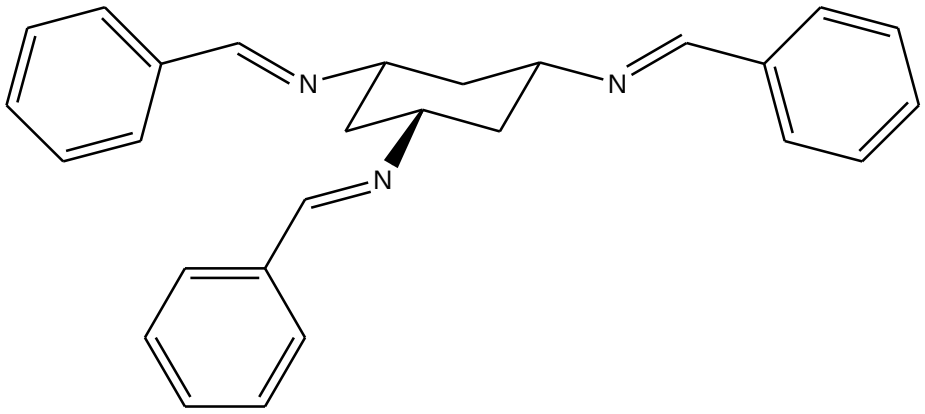

The next generation of ligand systems developed by Walton *et al.* utilised cinnamaldehydes groups. These cinnamaldehyde moieties were believed to provide enough distance between the bulky aryl groups to help prevent hydrolysis. The complexes created using this ligand system denoted TCT (*cis*, *cis*-1,3,5-*tris*[(E,E)- phenylpropylideneamino]cyclohexane, see figure 23) were investigated to determine any activity towards hydration of carbon dioxide. A monomeric cobalt complex, $[Co(TCT)OH]^{+}$ was synthesised and reacted with

carbon dioxide. This formed a dimeric carbonate species, and prevented the reversible reaction between the hydroxide moiety and the carbon dioxide. [88]

Figure 23, *Structure of TCT designed by Walton et al., showing attached steric bulk* [88]

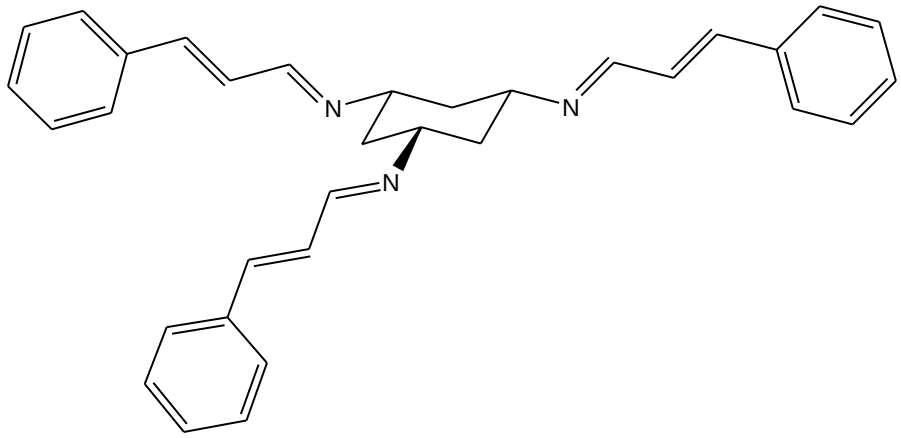

2.2 Synthetic route to tach

Cis, cis -1,3,5 – triaminocyclohexane (tach) has been used extensively by Walton *et al.* as a way of modelling the facially capping N_3 environment in *carbonic anhydrase* (see figure 24).[19-21, 23, 24, 52, 53, 56, 84, 86-89, 91, 92] Tach is particularly useful for providing a stereochemically rigid N_3 array which will coordinate to a metal centre via derivatisation of the amines with stereochemically rigid aldehydes to give the corresponding imine.

Figure 24, *Structure of tach*

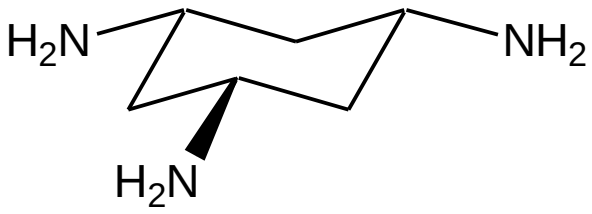

The tach used was prepared by the method of Bowen *et al.*[93] By starting with *cis*, *cis*-1,3,5-cyclohexanetricarboxylic acid as a precursor, diphenylphosphoryl azide is added and heated to reflux in benzene for 2 hours. This produced *cis*, *cis* 1, 3, 5-cyclohexanetricarboxylic acid in a 25% yield. This was then deprotected using HBr in acetic acid, which produced *Cis*, *Cis* 1, 3, 5 triaminocyclohexane. 3HBr (35.5%). The HBr salt was removed from the tach by using an anion exchange column, and it was then sublimed. The removal of the HBr is key to minimise bromide contamination of the later complexes produced. Figure 25 below highlights the key reaction steps. Figure 22 shows an NMR of the tach after sublimation.

Figure 25, *Synthetic route to cis, cis-1,3,5-triaminocyclohexane.3HBr described by Bowen et al.*[93]

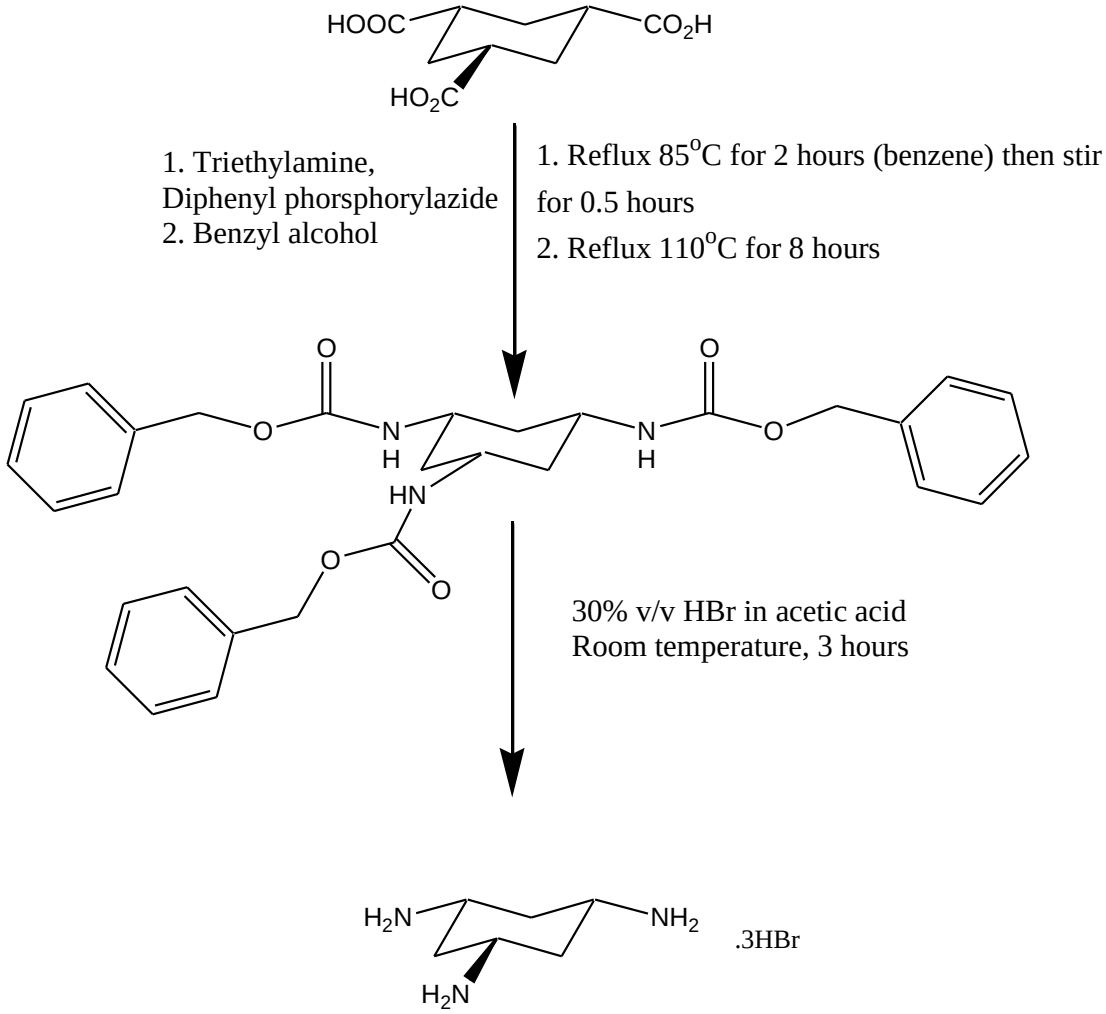

Figure 26, *^{1}H NMR spectrum of cis, cis-1,3,5-triaminocyclohexane (partial)*

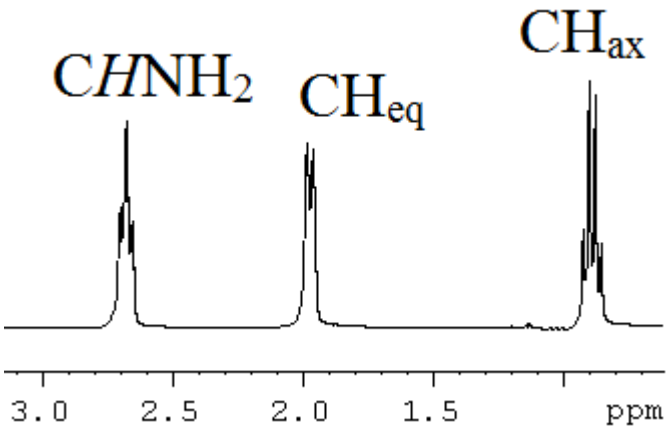

This method of synthesising tach has the advantage of high selectivity, as the *cis, cis-1,3,5-* tricarboxylic acid precursor is of high isomeric purity. Figure 26 highlights the purity which can be achieved after sublimation, and also the conformation which the protons adopt, which changes upon complexation as discussed in Chapter 3.

2.3 Synthesis of sterically bulky ligands

The synthesis of bulky ligands is the focus of this project. After studies showed that the unsubstituted TCT ligand was unable to produce a monomeric zinc bicarbonate complex, extra steric bulk was generated by utilising a 3,5-di methoxy substituted cinnamaldehyde. A ^{t}Bu-substituted cinnamaldehyde was also synthesised.[56] Figure 27 shows these two ligand systems developed by Walton *et al.*, although neither were able to form a monomeric zinc bicarbonate species.

Figure 27, *Structure of 3,5 - dimethoxy TCT and 4 - ^{t}Bu TCT respectively*[24, 56]

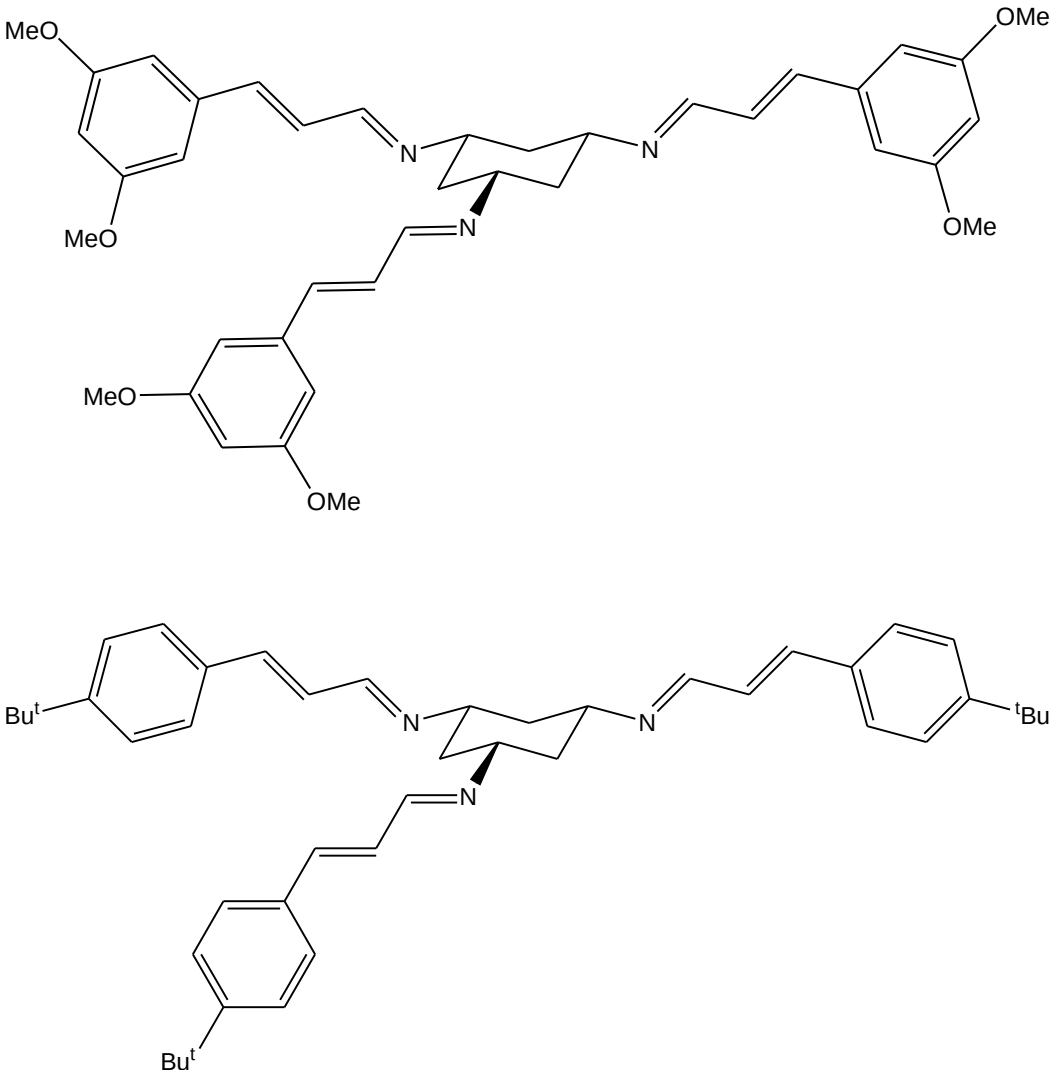

The 3,5 ^{t}Bu cinnamaldehyde used can be prepared by a Heck type cross coupling one pot reaction adapted by Battistuzzi *et al.* to produce cinnamaldehydes.[94] This adapted method utilised a substituted aryl halide which undergoes a Heck type cross coupling reaction with acrolein diethyl acetate to afford the cinnamaldehyde in the presence of palladium acetate as a catalyst. Figure 28 below shows the schematic route used. Figure 29 shows an NMR spectrum of the aldehyde, although some impurities are present due to minor products

synthesised during the reaction. By ^{1}H NMR the cinnamaldehyde is ca. 70% pure, when a ratio is taken of the major : minor products. The cinnamaldehyde was also characterised by mass spectrometry, with a peak seen at m/z = 242.24.

Figure 28, *Schematic route of the synthesis to 3,5 di ^{t}Bu cinnamaldehyde.*[94]

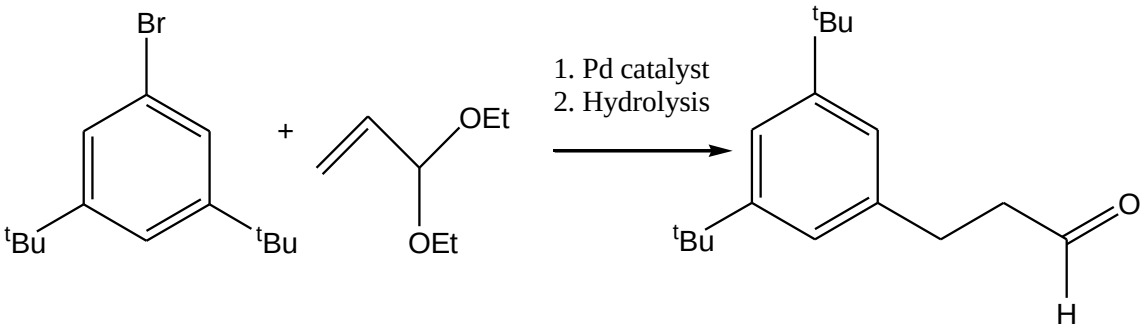

Figure 29, *NMR spectrum of 3,5 di ^{t}Bu cinnamaldehyde in $CDCl_3$*

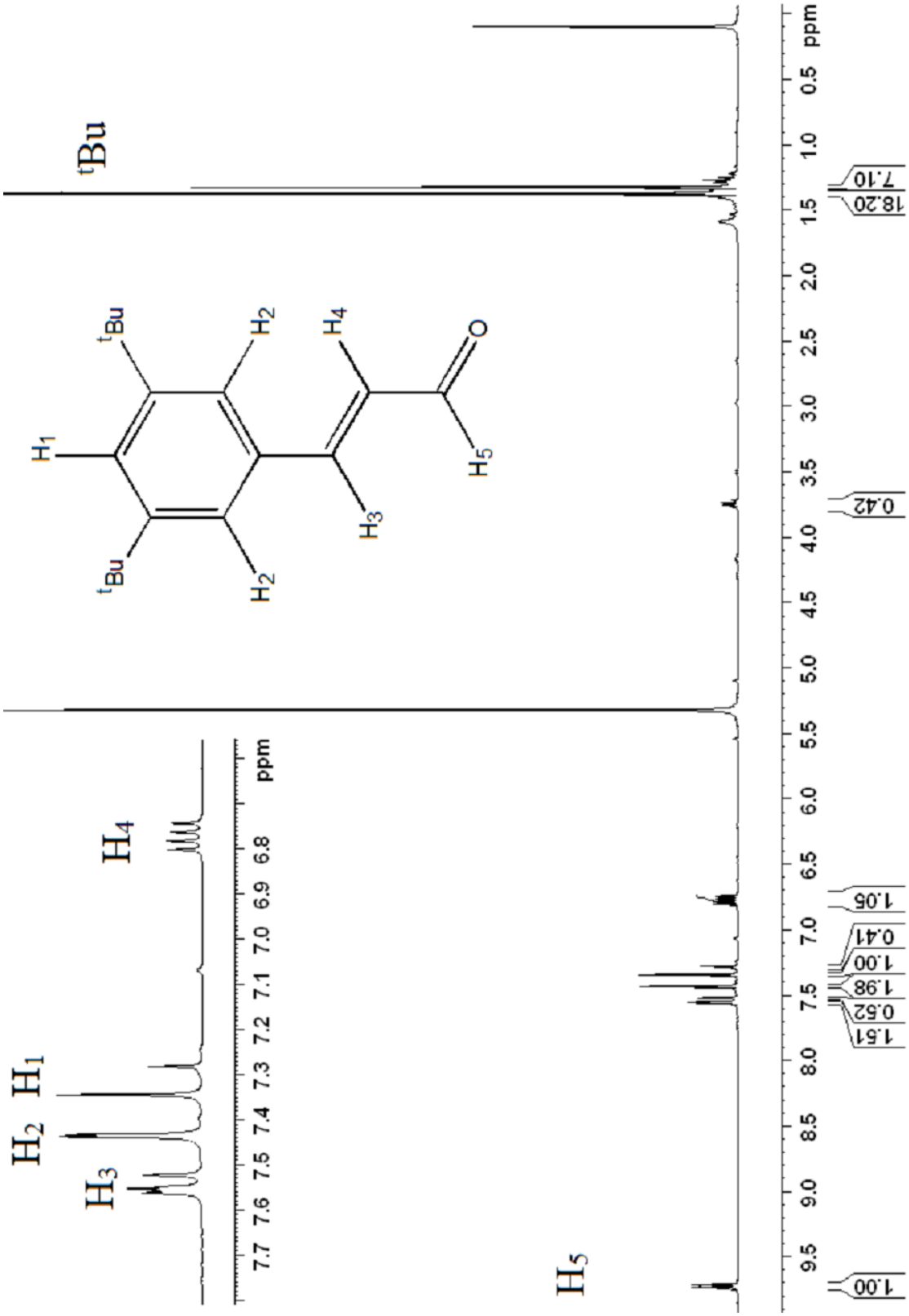

2.4 Synthetic route to 3,5 ^{t}Bu TCT

The focus of this project was to design a new ligand system based on the previous designs of Walton *et als*, with the hope of overcoming the steric issues discussed previously. Using CPK modelling kits and 3D computer modelling, Walton *et al.* concluded that by using bulkier tert-butyl groups substituted onto the aryl ring, dimerization could be prevented. It was hoped that the ligand would be rigid enough to prevent the side arms from changing conformation. In the complex, the side arms stay fixed in an axial position relative to the cyclohexane ring, and in the free ligand they sit in an equatorial position. It was unknown just how much flexibility these side arms could have, and whether upon introduction of carbon dioxide these side arms would strain toward the equatorial position and ultimately dimerise two zinc hydroxide complexes.

It was hoped that with enough steric bulk this strain would be minimised by introducing more intermolecular clashing between two different complexes, and making dimer formation more thermodynamically unfavourable. This new ligand system would use 3,5 ^{t}Bu cinnamaldehyde to create the Schiff base, with this being the most sterically encumbered ligand. Figure 30 below shows the new cinnamaldehyde that was prepared for the ligand and the ligand system *Cis,cis*-1,3,5 –tris(3,5-ditertbutylphenylpropenylideneimino) cyclohexane shown directly underneath it.

Figure 30, *Structure of 3,5- di ^{t}Bu cinnamaldehyde and 3,5 ^{t}Bu TCT respectively*

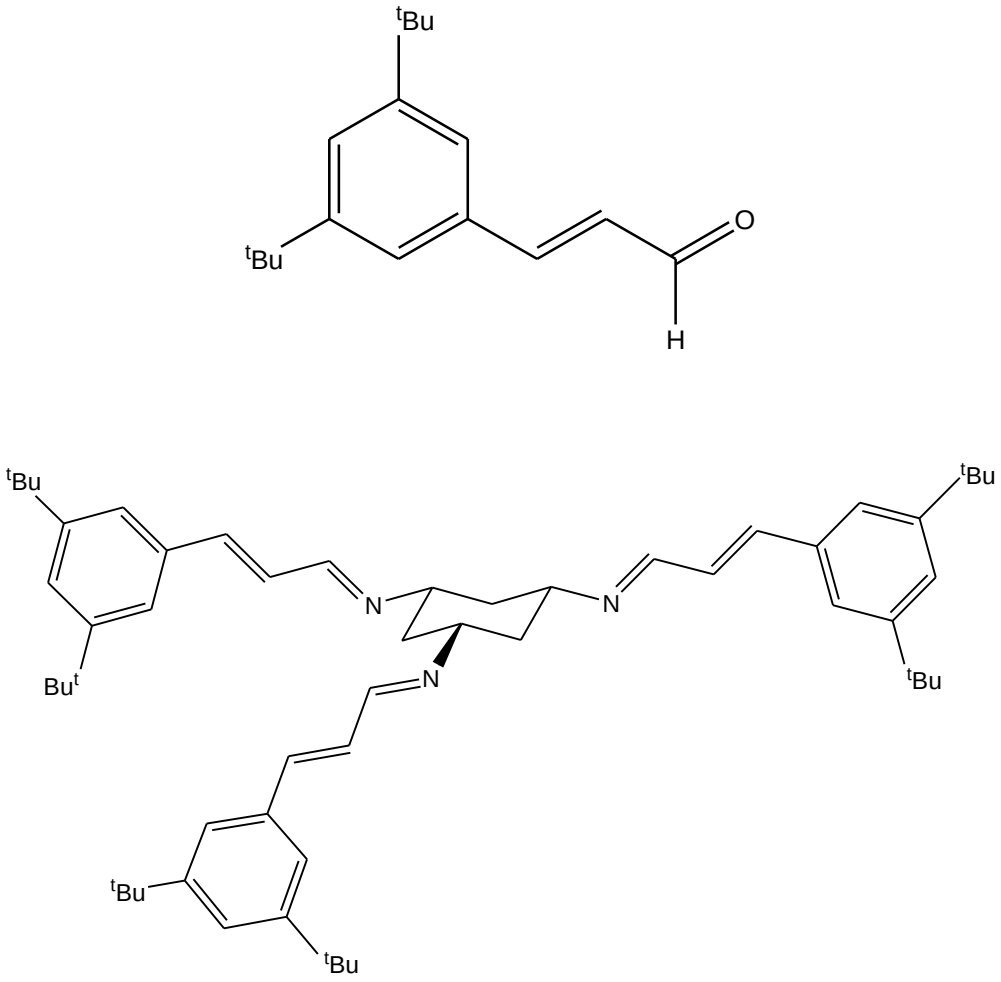

The ligand was prepared by a condensation reaction by adding 3 moles of cinnamaldehyde to 1 mole of tach suspended in dry degassed methanol. The reaction mixture was stirred over activated 3 Å molecular sieves and heated at reflux for 3 hours producing the 3,5 ^{t}Bu TCT ligand. Characterisation of the product was done by ^{1}H NMR and mass spectrometry, with a peak seen at m/z = 808.65. Figure 31 shows the ^{1}H NMR of the resulting product.

Figure 31, *NMR spectrum of 3,5 ^{t}Bu TCT in CD_2Cl_2*

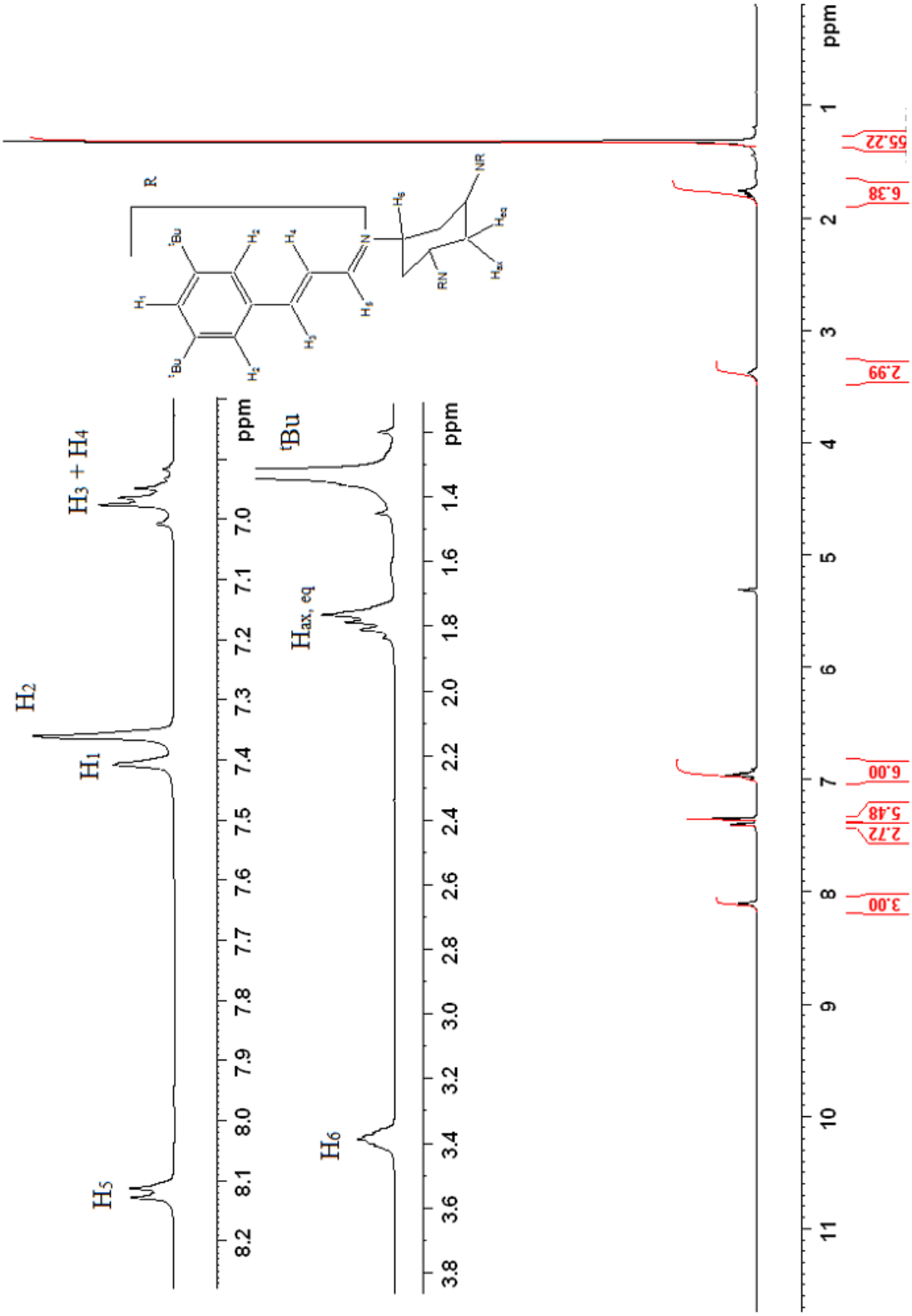

The most significant difference between the NMR spectra of the free tach and the free ligand is the change in position of the tach protons. We see three distinct peaks in the ^{1}H NMR of free tach, with a distinction between the CH_2's axial and equatorial protons, whereas this appears as one peak in the free ligand shown in figure 30. Observation of this peak in the ^{1}H NMR is a good indication as to whether the ligand has complexed or not, as in the complex this peak becomes two once again upon the axial ring flip conformational change. These take the appearance of two roofed doublets, as shown in figure 33.

As shown in figure 31, the ^{1}H NMR spectra also shows two singlets at around 7.4 ppm representing the protons on the aromatic ring. We also see a multiplet at around 7.0 ppm corresponding to the protons H_3 and H_4 and finally a doublet at around 8.1 ppm denoting proton H_5.

This chapter has seen the method development for the ligand system utilised in the project, as well as key spectroscopic details which distinguish free tach, the free ligand, and the zinc complexes. Key to understanding this is the conformational change from equatorial to axial from the free ligand to the zinc complex, and the effect seen in the ^{1}H NMR on the tach protons.

Chapter 3: *Preparation and characterisation of $[Zn^{II} X\ 3,5\ ^{t}BuTCT]^{+}\ [BPh_4]^{-}$ complexes*

By utilising a ligand which provides a facially capping N_3 environment, it was hoped that an effective model of the active site of HCAII could be synthesised. A zinc hydroxide complex was to be synthesised and carbon dioxide would be introduced to hopefully create a zinc bicarbonate complex. This zinc hydroxide species is a key step in the intermediate of *carbonic anhydrase* as discussed in chapter 1, and is believed to be a pre requisite necessary for the formation of a zinc bicarbonate complex.[9]

A zinc hydroxide complex was synthesised and characterised by NMR, which had carbon dioxide added to it to create a zinc bicarbonate complex. The peak corresponding to the zinc bound hydroxide in a ^{1}H NMR spectrum was observed to decrease in its integrated value upon addition of carbon dioxide, suggesting formation of another species. This was confirmed by ^{13}C NMR after observation of two possible peaks which could correspond do a zinc bound bicarbonate. These two peaks agreed well with published data by Ibrahim *et al.* IR data was also taken and possible observation of a bicarbonate species has been seen, again correlating well with pre-existing data published by Parkin *et al.* and Ibrahim *et al.*[9, 71]

3.1 Method development of synthesis for $[Zn^{II}(OH)\ 3,5\ ^{t}BuTCT]^{+}\ [BPh_4]^{-}$

Several attempts for the synthesis of the zinc hydroxide complex were trialled before a successful synthetic route was found. All reactions attempted were under air sensitive conditions and carried out at room temperature. Figure 32 below shows the structure of the desired zinc hydroxide complex.

Figure 32, structure of $[Zn^{II}(OH)\ 3,5\ ^{t}BuTCT]^{+}\ [BPh_4]^{-}$

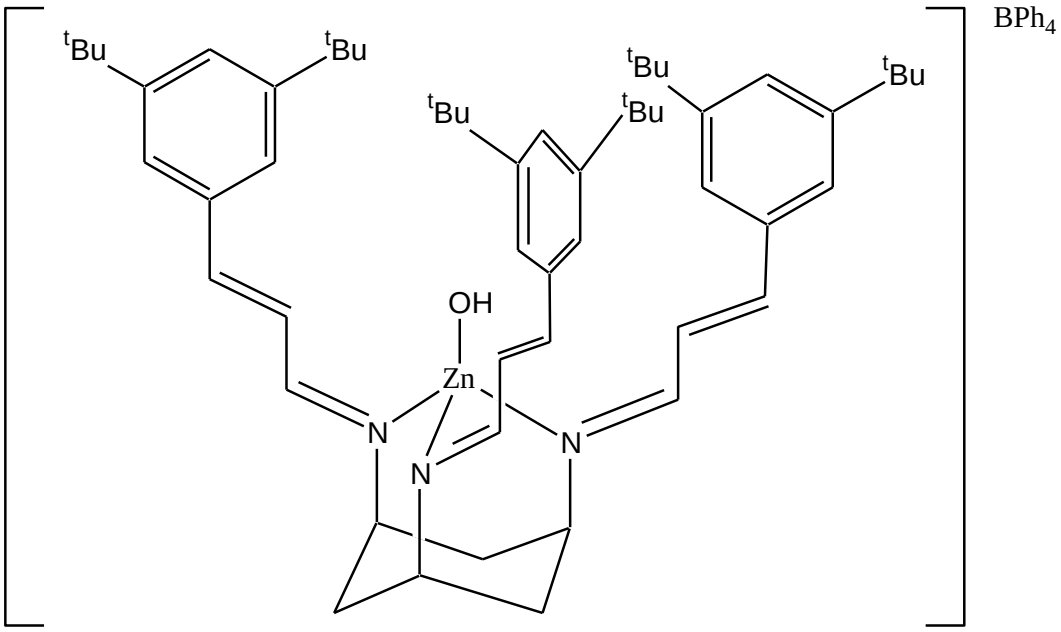

The first synthetic route which was tested utilised Zinc(II) trifluoromethane sulfonate, $Zn(CF_3SO_3)_2$. This was reacted with a stoichiometric amount of the 3,5 ^{t}Bu(TCT) ligand in tetrahydrofuran solvent system for a period of 1 hour. A pellet of sodium hydroxide (NaOH) was ground, added to the solution and then stirred for thirty minutes. This was followed by a cannulae filtration to remove

any undissolved sodium hydroxide. The solvent was then removed in vacuo, and the products were isolated as a white solid.

The products could not be characterised by any spectroscopic method, although the free ligand was seen in mass spectrometry, with no peaks of heavier mass observed to indicate a zinc complex were seen. The most likely explanation is that the zinc(II) triflate is too stable to react under these conditions. The reaction was also repeated in acetonitrile but the outcomes were the same as above.

The second method employed, followed the same conditions but used sodium tetraphenylborate ($NaBPh_4$) as a precipitating agent. This reaction also failed, with no precipitation of a solid taking place. NMR and mass spectrometry showed the uncoordinated free ligand, but no evidence for the zinc hydroxide complex.

The successful method involved using zinc(II) dinitrate hexahydrate, this was reacted with a stoichiometric amount of the ligand in methanol and toluene. This was stirred for 90 minutes at which point tetra-n-butylammonium hydroxide was added. This was then allowed to stir for 30 minutes, and then $NaBPh_4$ was used to precipitate the complex out of solution. Finally the product underwent a cannulae filtration and was dried using nitrogen to afford a white solid. Figure 33 below shows the ^1H NMR of the zinc hydroxide complex with the ligand underneath for comparison.

Figure 33, *^{1}H NMR of $[Zn^{II}(OH)$ 3,5 $^{t}BuTCT]^{+}$ $[BPh_4]^{-}$ and the free ligand 3,5 ^{t}Bu TCT, with characterisation in chapter 5.*

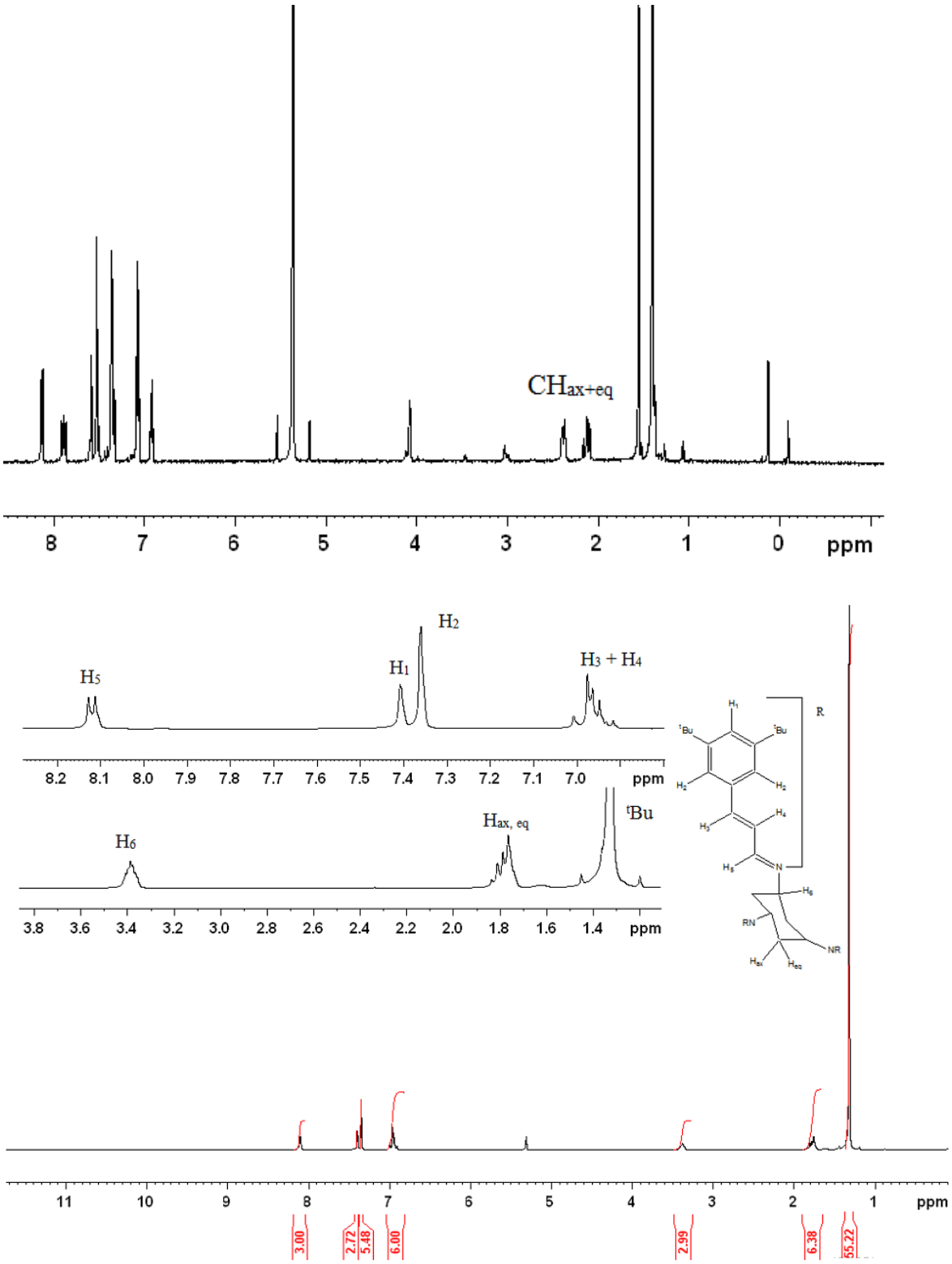

There are several shifts observed in the ^{1}H NMR spectrum of the zinc hydroxide complex when compared to free tach or the free ligand. For instance the CH_{ax} and CH_{eq} peaks seen in the ^{1}H NMR of tach in figure 26 are shifted to 2.23 ppm and 1.95 ppm in the complex, taking the appearance of two doublet peaks. These two peaks are roofed due to the cyclohexane ring undergoing an equatorial to axial ring flip upon complexation. This is in comparison to the multiplet seen in the free ligand ^{1}H NMR spectrum at 1.77 ppm. We also see a shift in the C*H*N peak, which shifts from 3.39 to 4.05 ppm, due to deshielding due to electron donation from the three nitrogen atoms to the zinc metal centre decreasing electron density around the C*H*N proton. Finally we see the ArC*HCH* become two peaks seen at 7.81 ppm and 7.25, whereas in the free ligand these protons are seen as one peak at 6.97 ppm in the ^{1}H NMR spectrum.

3.2 Synthetic route to $[Zn^{II}(OH)$ 3,5 ^{t}BuTCT$]^{+}$ $[BPh_4]^{-}$ and synthetic problems

The synthetic route to the zinc hydroxide complex has proved very difficult, with a number of problems. Several problems seemed to persist with the different synthetic routes.

Firstly, the chosen NMR solvent, d^2-DCM can be prone to forming acids when left in sunlight, and it was observed that the longer the complex was left in solution the smaller the hydroxide peak would appear in a ^{1}H NMR. This is primarily due to the formation of a zinc chloride complex. The zinc chloride complex appears to be the most favourable complex to form. It was consistently

seen in every single mass spectrometry analysis, even when d^2-DCM is kept away from the complex. This is because of residual chloride anions from inside the instrument itself, which have reacted with the complex to form the zinc chloride complex. The zinc chloride complex was observed as a peak in ESI and LIFDI mass spectrometry, with m/z = 908.91. This complex was stable enough to be crystallised and is discussed in chapter 4.

The NMR solvent was important for another reason as well, as exchange between the proton on the zinc bound hydroxide with a deuteron from the solvent could lead to the hydroxide peak disappearing from the spectrum. Some solvents were also prone to exchanging with the labile hydroxide moiety in its entirety. For example, d^4-MeOD was prone to producing the zinc methoxide complex. $CDCl_3$ experiences a similar problem with production of acids in sunlight, where the deuteron on DCl could exchange once in solution with the proton on the hydroxide, rendering it invisible in ^{1}H NMR.

Formation of the chloride complex was also found to be problematic, as evident in almost all mass spectrometry analysis. When crystallisation attempts of the bicarbonate and hydroxide were carried out, synthesis of a zinc chloride complex happened due to its preferred stability. For instance, almost all crystallisation media included d^2-DCM layered with hexane, pentane, toluene or benzene. The d^2-DCM was also substituted with a number of other solvents which dissolved the product including $CDCl_3$, d^6-acetone, THF and ethanol for the zinc ethoxide. However crystals almost never formed, and when they did the form was always

needles. These crystals diffracted poorly and also turned out to be inorganic salts (usually n-tetrabutylammonium salts).

As discussed in the next chapter, the two crystal structures of zinc complexes that were observed were the zinc chloride complex and the zinc nitrate complex. These two structures were obtained from block type crystals. These crystals diffracted without any problems other than disordered solvent molecules in the unit cell. Problems with halogens persisted with some of the IR data, as some spectra were taken with the complex pressed into KBr disks. This saw the bromine intercalating into the complex and removal of the hydroxide or other ligand of interest and replacing it with a bromine atom. This zinc bromide complex was observed by ESI and LIFDI mass spectrometry as a peak at m/z = 952.60.

All complexes were insoluble in short chained hydrocarbons including pentane and hexane, as well as aromatic solvents such a benzene and toluene, ruling out the latters use as NMR solvents. The zinc hydroxide and zinc ethoxide complexes were both soluble in d^6 - acetone, although the hydroxide was not observed in this solvent, even though full characterisation of the rest of the complex was achieved. One suggestion for this could be due to acetones inherent problem of being hygroscopic, and doesn't easily give up small amounts of water due to strong hydrogen bonding between one water molecule and two acetone molecules. This would allow for exchange taking place, and thus line broadening in the NMR, abolishing the observable hydroxide peak.

For similar reasons as the acetone, D_2O was not used due to potential exchange with the hydroxide, thus rendering the peak unobservable in ^1H NMR spectra. Water would also hydrolyse the imine bonds of the ligand system used. In the case of the complex, the carbon-nitrogen double bond is weakened substantially by the inclusion of the zinc, complexed to three quaternary nitrogen atoms.

Figure 34, *^1H NMR of $Zn(tach)_2$ $[BPh_4]_2$ and ^1H NMR of free tach*

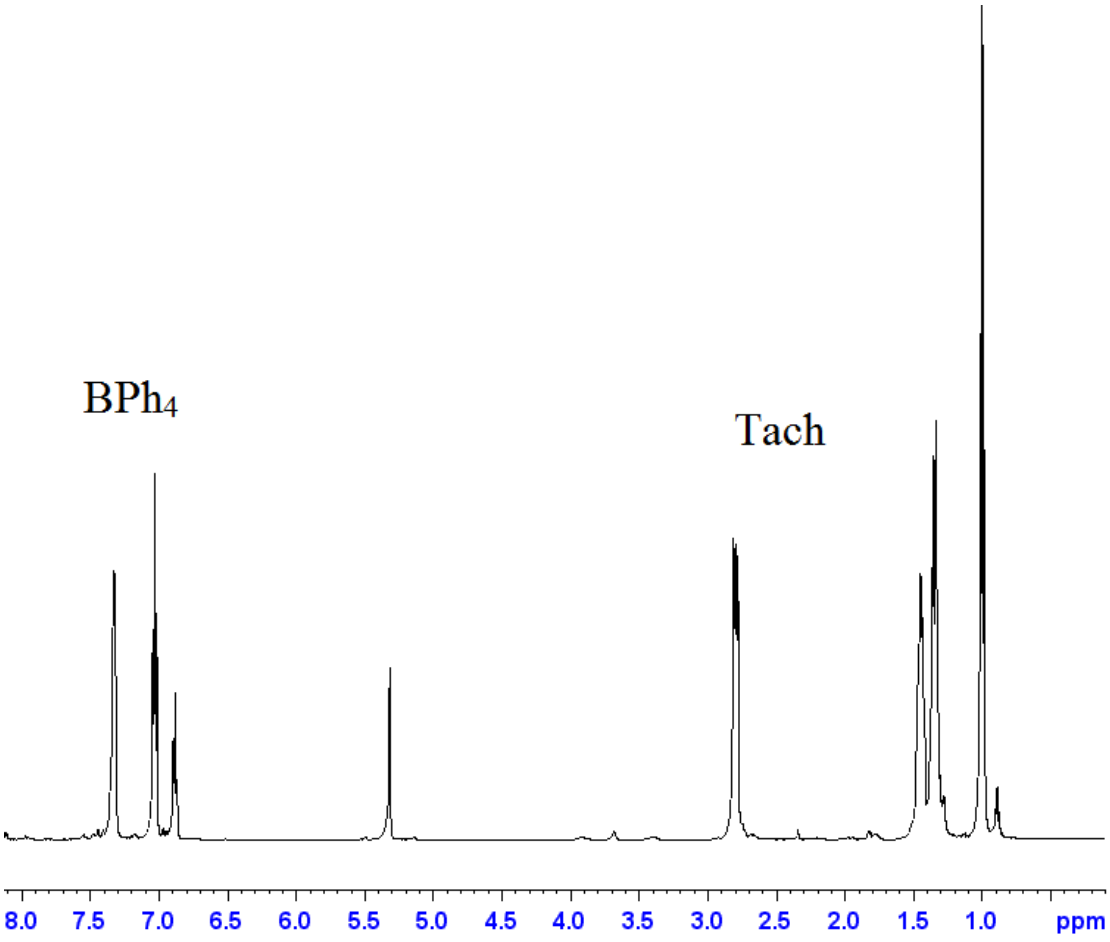

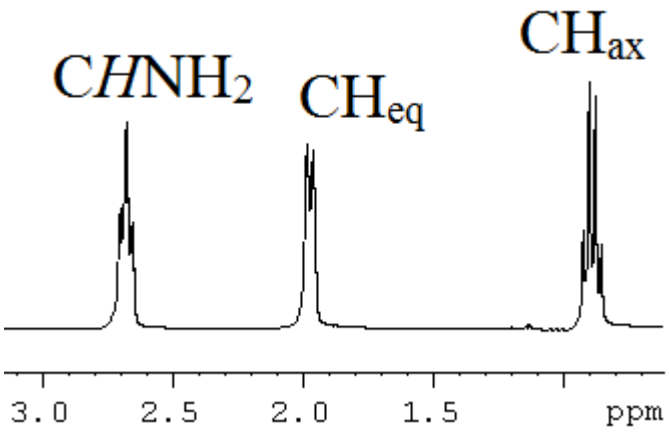

The complex has in some reactions undergone hydrolysis due to the inclusion of water in the reaction. This broke the imine bonds and split the Schiff base back into its constituent parts, the tach and the 3,5^{t}Bu cinnamaldehyde. Analysis by NMR showed the solid contained the BPh_4 species, with none of the peaks associated with the side arms such as any of the aromatic protons, the large ^{t}Bu peak (with an integration of 54) or the propylidene peak. It is believed that a dimeric $Zn(tach)_2$ species formed in these cases, although no further evidence to suggest this was found. No crystals could be obtained which would diffract and it was not observed by mass spectrometry.

Figure 34 shows a ^{1}H NMR of this dimeric tach species, with the only peaks present being the tach protons and the protons on the BPh_4 species. The integrals of the tach and $NaBPh_4$ species are 1:1 to each species, although this does not conclusively show that a dimer has formed or a monomer has formed. Below this is a ^{1}H NMR spectra of free tach, of which it is useful to point out the shift in peaks which would indicate complexation. Upon complexation the C*H*NH_2 peak changes in multiplicity due to the new conformation, with the C*H*NH_2 adopting an axial position in free tach, and an equatorial position in bound tach. This is a good indication as to whether the tach has complexed or not.

One interesting aspect of all ^{1}H NMR data that was taken was that the hydroxide peak never integrated to a stoichiometric ratio compared to protons on the rest of the complex. A more likely explanation for this observation is the proton on the hydroxide may be undergoing rapid dynamic exchange either with the deuterated solvent. This would shield the group from being NMR active in both cases, with the former being entirely NMR invisible if the hydroxide has now formed the deuteroxide moiety.

Mass spectrometry data showed that almost every sample submitted had unreacted starting material present, some zinc nitrate complex and some of the zinc chloride complex. These peaks were observed both in LIFDI and ESI mass spectrometry. The free ligand was observed at m/z = 808.65, the zinc nitrate complex was observed at 932.56 and the zinc chloride complex was observed at m/z = 908.53. A peak was observed in almost every mass spectrometry analysis at m/z = 897.57, with this possibly being the a sodium zinc oxide (Zn-O-Na) complex.

3.3 Observation of $[Zn^{II}(OD)$ 3,5 ^{t}Bu TCT$]^{+}$ $[BPh_4]^{-}$ by IR

The zinc hydroxide complex described above in figure 32 was isolated by evaporation and analysed for any potential O-H stretches present in its IR spectrum.

Figure 35, *ATR-IR spectrum of the* $[Zn^{II}(OH)$ *3,5* ^{t}*BuTCT*$]^{+}$ $[BPh_4]^{-}$ *species, with broad water band highlighted at ca. 3650* cm^{-1}

It had proved difficult to definitively observe a peak corresponding to the zinc hydroxide complex by IR spectroscopy. A synthesis of the deuteroxide was attempted in an effort to observe any shift in the broad band at 3650 cm^{-1} indicative of water. It was believed that a stretch relating to the hydroxide was unobservable due to the intensity of this band. TBAH was stirred with d^4-MeOD

for a period of ca. 6 hours to produce a deuterated hydroxide. This was used for the attempted synthesis, see chapter 5 for the method.

It was not possible to characterise the $[Zn^{II}(OD)\ 3,5\ ^{t}BuTCT]^{+}\ [BPh_4]^{-}$ species by NMR due to the now invisible deuterated hydroxide (OD) group, so an ATR-IR was taken as shown in figure 35. Unfortunately, no shift of the broad band was observed, indicating no deuterated product was present.

3.4 Synthetic route to $[Zn^{II}(HCO_3)\ 3,5\ ^{t}BuTCT]^{+}\ [BPh_4]^{-}$

The first synthetic route was attempted in air and used stoichiometric amounts of the ligand, 18-crown-6 and potassium bicarbonate suspended in ca. 2 ml of toluene. A few drops of water were added for a phase transfer reaction to take place. It was expected that the crown ether would chelate the potassium ion and remain in the organic layer. The water present in the reaction was believed to contain the bicarbonate species. More water was added to separate the reaction into layers, and this was left to stir overnight.

This reaction was repeated using the zinc(II) triflate salt, $Zn(CF_3SO_3)_2$ as well as the zinc(II) nitrate salt, $Zn(NO_3)_2$ as starting reagents. The zinc salt was added to 3,5 ^{t}Bu(TCT) and stirred for 1 hour in a solution of toluene and methanol. The aqueous solution containing the bicarbonate was added and the solution was left to stir for a period of ca. 2 hours. Finally, sodium tetraphenyl borate ($NaBPh_4$) was used to precipitate the product out of solution. No precipitate was seen in either reaction, and no product could be characterised. Mass spectrometry and ^{1}H

NMR showed uncoordinated ligand again. It was concluded the complex had not been achieved with any of the synthetic routes described above.

3.4.1 Observation of $[Zn^{II}(HCO_3)$ 3,5 $^tBuTCT]^+$ $[BPh_4]^-$ in ^1H and ^{13}C NMR

The synthesised zinc hydroxide complex was exposed to carbon dioxide to prepare a zinc bicarbonate complex, with analysis by NMR proving more useful than IR. The direct addition method of carbon dioxide is method employed by Ibrahim *et al.* and Parkin *et al.*[9, 71]

Figure 36, *^{13}C NMR spectrum showing a solution of the zinc hydroxide complex exposed to carbon dioxide. The zinc hydroxide complex before addition of carbon dioxide is shown in blue and the zinc hydroxide complex upon addition of carbon dioxide shown in red. Spectrum recorded in d^2-DCM.*

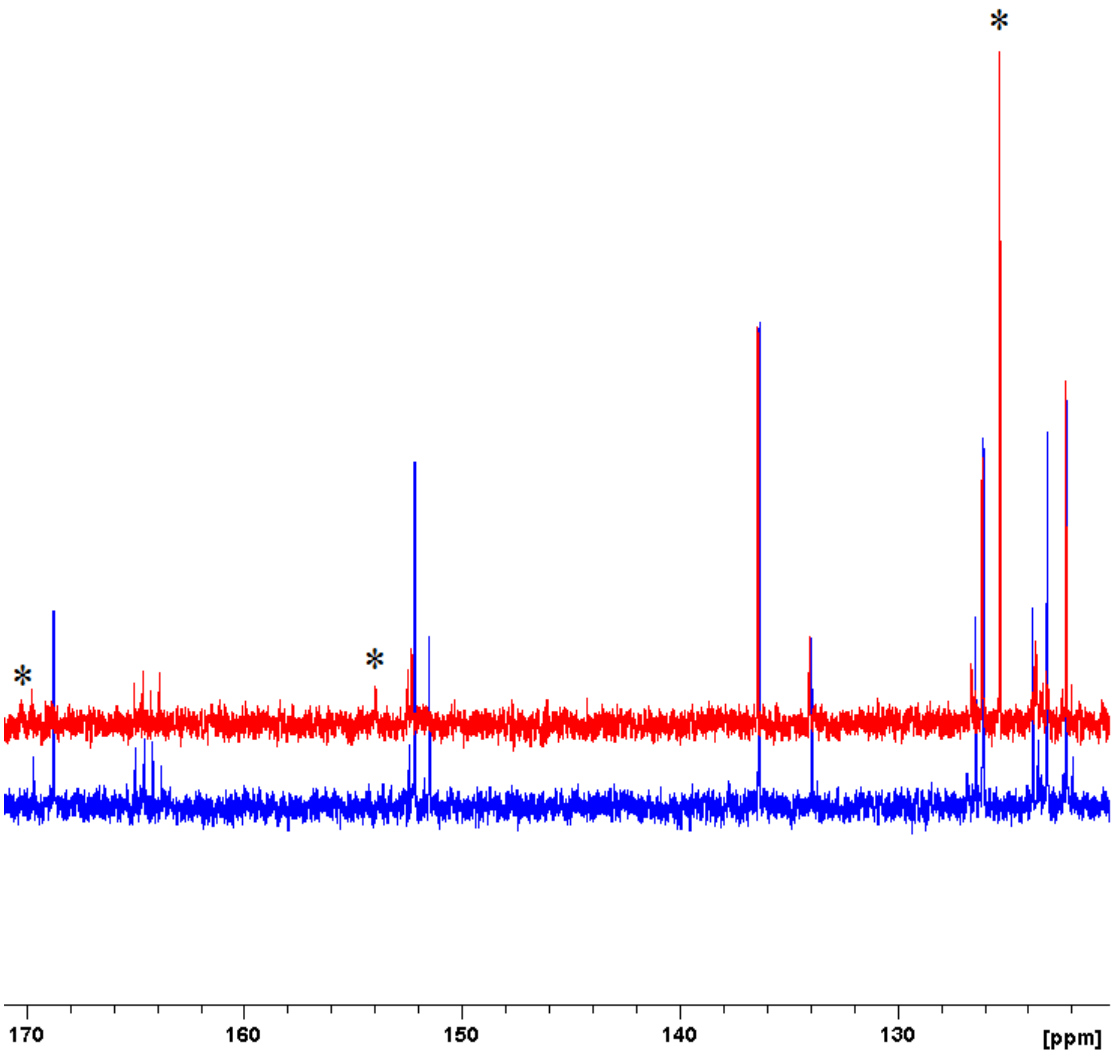

The zinc bicarbonate complex was prepared by dissolving ca. 5mg of the synthesised zinc hydroxide complex with dry and degassed d^2-DCM in an NMR tube fitted with a J. Youngs PTFE seal. This was then exposed to carbon dioxide and the solution was shaken for a period of 10 seconds. This was repeated a further two times, to increase the saturation of carbon dioxide in the solution.

Upon inspection by ^{13}C NMR spectroscopy, carbon dioxide was observed to be dissolved in the solution, with a peak seen at 125.3 ppm. A further peak was observed when compared to a spectrum obtained before carbon dioxide saturation at 154 ppm, as shown in figure 36. [30]

There are two peaks of significant interest in the spectrum; firstly, a peak was observed at 171 ppm, although it is not as intense as the peak observed at 154ppm. The peak observed at 154 ppm was the best evidence seen in the spectrum for characterisation of the carbon atom of the bicarbonate. As of 2011, only Ibrahim *et al.* has published ^{13}C NMR data on a zinc bicarbonate model complex, which was observed at 167 ppm. As no other zinc bicarbonate data has been published, for a comparison sodium bicarbonate ($NaHCO_3$), has been observed at 161.08 ppm in a ^{13}C NMR spectrum.[95]

Figure 37, *^{1}H NMR spectrum showing a solution of the zinc hydroxide complex exposed to carbon dioxide. The zinc hydroxide complex before addition of carbon dioxide is shown in red and the zinc hydroxide complex upon addition of carbon dioxide is shown in blue. Spectrum recorded in d^2-DCM*

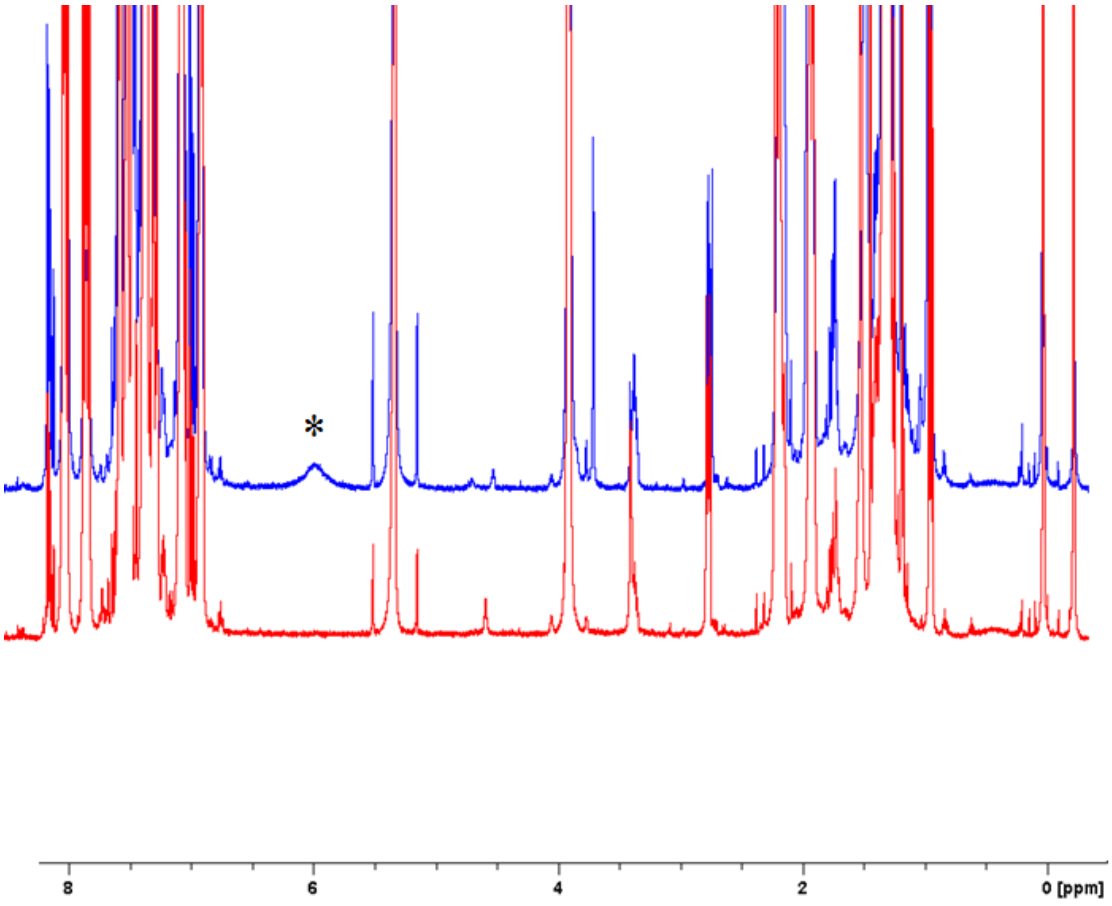

The other data collected for the zinc bicarbonate complex consisted of a ^{1}H NMR spectrum, with again a comparison drawn between pre- and post-carbon dioxide saturated solutions of the zinc hydroxide complex dissolved in d^2-DCM. Figure 37 shows an observed peak at 5.97 ppm with an integration of 0.18. With no other reported ^{1}H NMR data for a zinc bicarbonate, there is nothing to use to reference this peak to. There are two probable explanations for this peak, with the first being a zinc bicarbonate complex. The second, less likely explanation, is

that small amounts of residual water molecules left over could have reacted to form a bicarbonate and a proton. This is less likely considering the very low rate at which this reaction takes place, 0.18 s^{-1} at 37°C.[57] This would also mean a decrease in integration of the residual water peak, which is not seen in the spectrum. The water peak is located in the spectrum at 1.52 ppm.[96]

In all experiments which tried to produce a zinc bicarbonate complex, two further observations were made. Firstly, as expected, the hydroxide peaks were always observed to either decrease in intensity or completely disappear. Secondly, the propylidene peak which faces into the cavity created by the ligand upon complexation, diminished completely. One possible explanation for this is because of the inclusion of the new bicarbonate moiety, distorting the electrons around this proton so much that it broadens its ^{1}H NMR peak and drops into the baseline. This could also be as a result of dynamic exchange taking place.

Figure 38, *^{1}H NMR spectrum showing a solution of the zinc hydroxide complex in blue. A spectrum showing the same solution after exposure to CO_2 is shown in red, and the spectrum in green shows the same solution after removal of the CO_2 atmosphere. Spectrum recorded in d^2-DCM.*

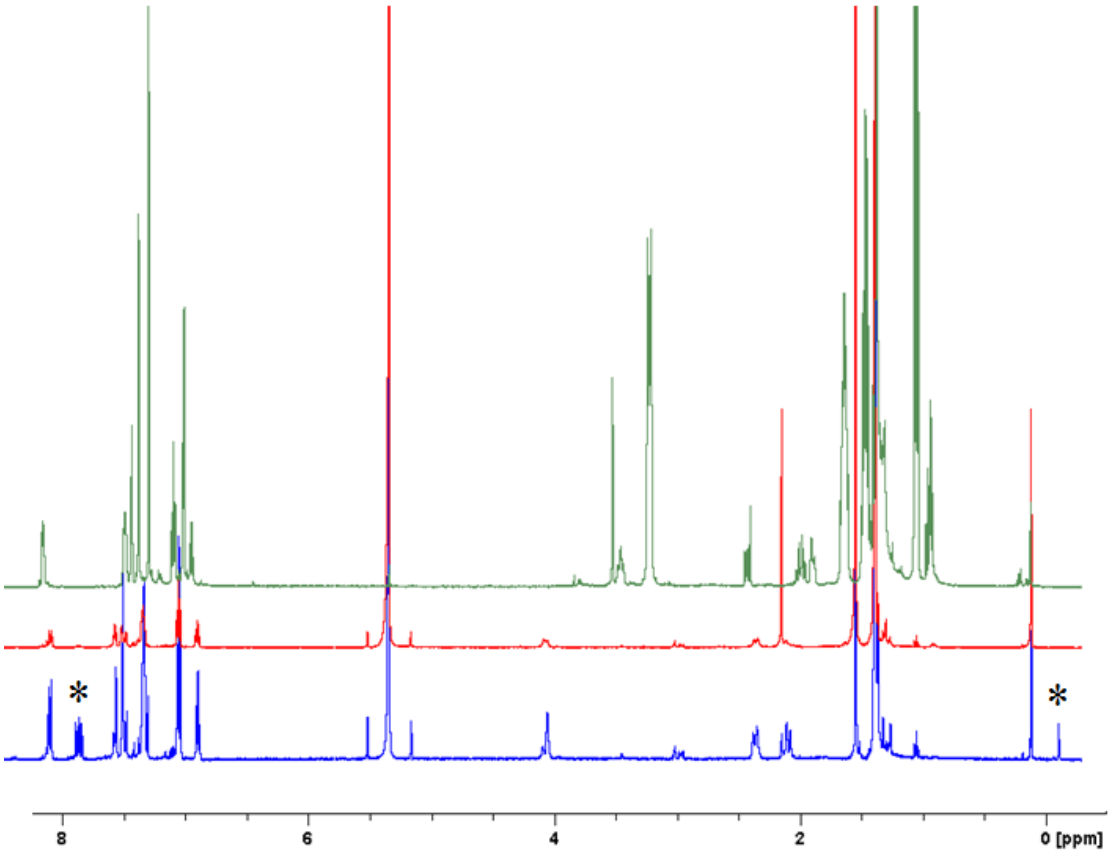

Upon removal of the CO_2 atmosphere, it was expected that the hydroxide moiety would be regenerated. However, this was not the case and several new peaks which could not be assigned were observed. Figure 38 shows three overlaid ^{1}H NMR spectrums showing before addition, during addition and removal of CO_2 atmosphere on the complex. As the propylidene peak at 7.85 ppm does not

increase in its integration value after the removal of CO_2, this suggests that a species is blocking the fourth coordination site of the zinc.

The zinc could have likely formed either the nitrate or chloride species, although it appears that there is now a mix of different species. Firstly, the ligand appears to remain intact, indicated by the fact that a peak corresponding to the hydrolysed cinnamaldehyde at 9.73 ppm (C*H*O) is not observed in the spectra. However, the tach protons have been shifted and this would indicate that the conformation of the ligand system has changed. This could indicate that some of the complex has uncoordinated, with the formation of a more stable zinc salt such as a zinc chloride complex, being the driving force of this.

3.4.2 Observation of $[Zn^{II}(HCO_3)$ 3,5 ^{t}BuTCT$]^{+}$ $[BPh_4]^{-}$ by IR spectroscopy

Figure 39, *Solution cell IR Spectrum of* $[Zn^{II}(HCO_3)$ *3,5* ^{t}*BuTCT*$]^{+}$ $[BPh_4]^{-}$ *in* CD_2Cl, *with the stretching frequencies reported in* cm^{-1}.

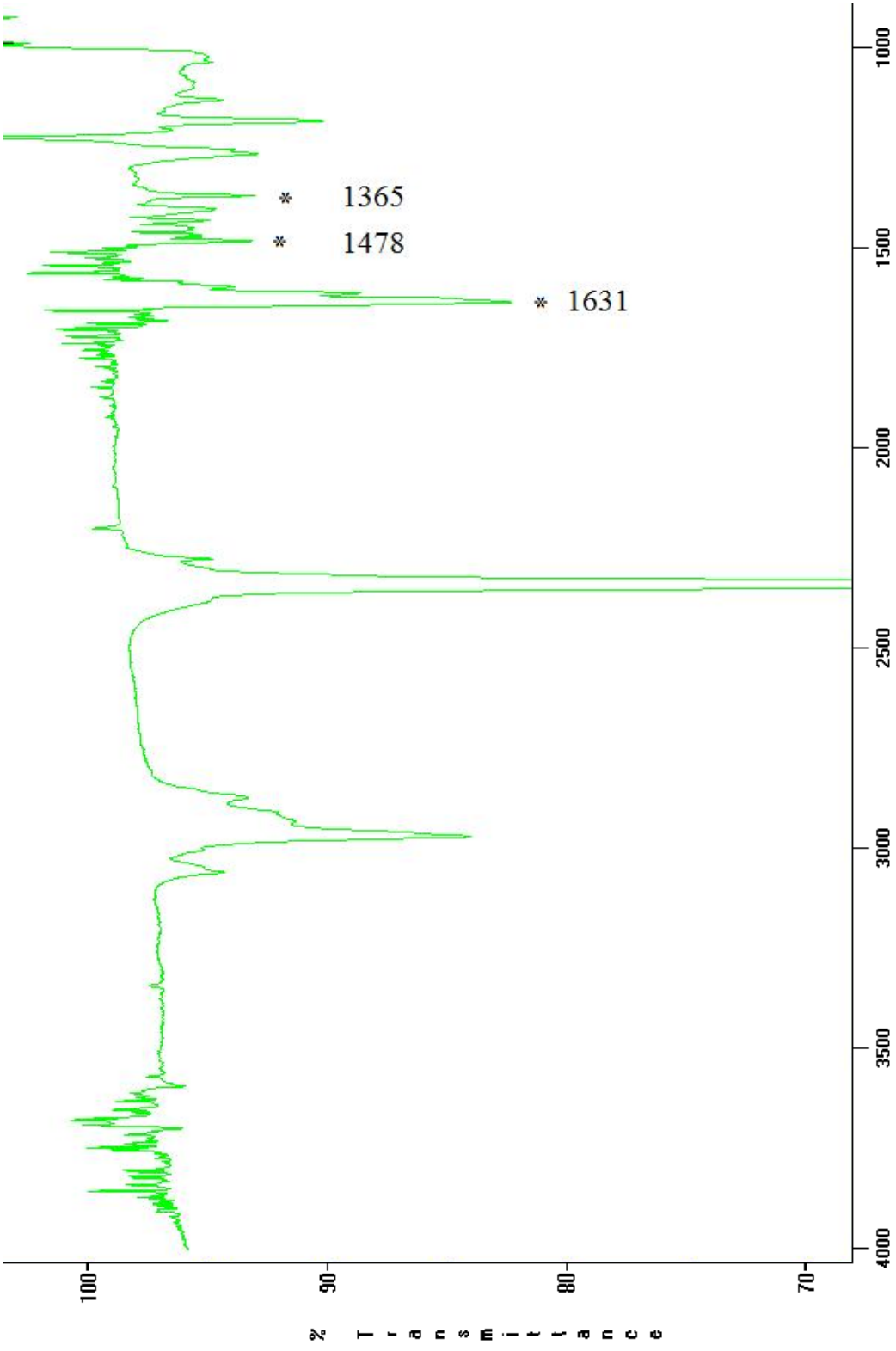

Two different types of experiments were carried out in an attempt to observe a zinc bicarbonate species; solid state ATR-IR and solution cell IR. Firstly, a measurement was taken before addition of carbon dioxide, and then after in d^2-DCM. Figure 39 shows the result of this, with the significant peaks appearing at 1631 cm^{-1}, 1478 cm^{-1} and 1365 cm^{-1}. Table 2 shows a comparison between these results and the peaks observed by Parkin *et al* and Ibrahim *et al.*[9, 18, 71]

Table 2, *Comparison of v(CO) stretches observed in solution IR by Parkin et al and Ibrahim et al for monomeric zinc bicarbonate complexes and the stretches observed for* $[Zn^{II}(HCO_3)\ 3,5\ ^tBuTCT]^+\ [BPh_4]^-$ [9, 18, 71]

Data	**Stretches (cm^{-1})**
Parkin et al	1302 and 1675
Ibrahim et al	1440 and 1675
$[Zn^{II}(HCO_3)\ 3,5\ ^tBuTCT]^+\ [BPh_4]^-$	1365, 1478 and 1631

The data would suggest that a bicarbonate could have been formed in the solution, with the peaks correlating well with observations made by Parkin *et al.* and Ibrahim *et al.* Parkin *et al*. has reported that their data suggests a unidentate bound bicarbonate. [9]

However, it is not impossible to definitively assign the binding mode of the bicarbonate. It has been suggested that using the same principles to distinguish between different binding modes of carboxylate (RCOO) ligands, it may be possible to hypothesise a binding mode for the bicarbonate.[9] For monomeric

carboxylate species, a transition between bidentate to unidentate coordination sees an increase in separation between the symmetric and antisymmetric CO_2 stretches.[97] It has been observed that if $\Delta\nu$(CO) is greater than 200 $cm^{=1}$, the species is likely unidentate, and if less than 200 cm^{-1} bidentate. By taking Δv(CO), in this case being (1631 – 1365 cm^{-1}) 266 cm^{-1}, it could be concluded that if a bicarbonate species is present it may be unidentate.

ATR IR was used to obtain a spectrum of the hydroxide species, as well as another solution cell spectrum of the same species. This highlights the loss of the broad stretch at ca. 3600 cm^{-1} which was believed to be free water. However as was hypothesised, it could indicate that this was masking the hydroxide species. Parkin *et al.* observed a hydroxide peak at 3668 cm^{-1} for the tris(pyrazolyl) borate zinc hydroxide complex.[9] Figure 40 below shows the loss of this peak upon addition of carbon dioxide to a solution of the zinc hydroxide complex. This is exciting evidence that the zinc hydroxide complex was potentially synthesised (3450 cm^{-1}, OH stretch), and reacted further with carbon dioxide to form the bicarbonate species (with loss of the 3450 cm^{-1} stretch observed).

Figure 40, *ATR IR and solution spectra (acquired in d^2DCM) of the for [Zn^{II}(OH) 3,5 ^{t}BuTCT]$^+$ [BPh_4]$^-$ and for the [Zn^{II}(HCO_3) 3,5 ^{t}BuTCT]$^+$ [BPh_4]$^-$ complexes respectively.*

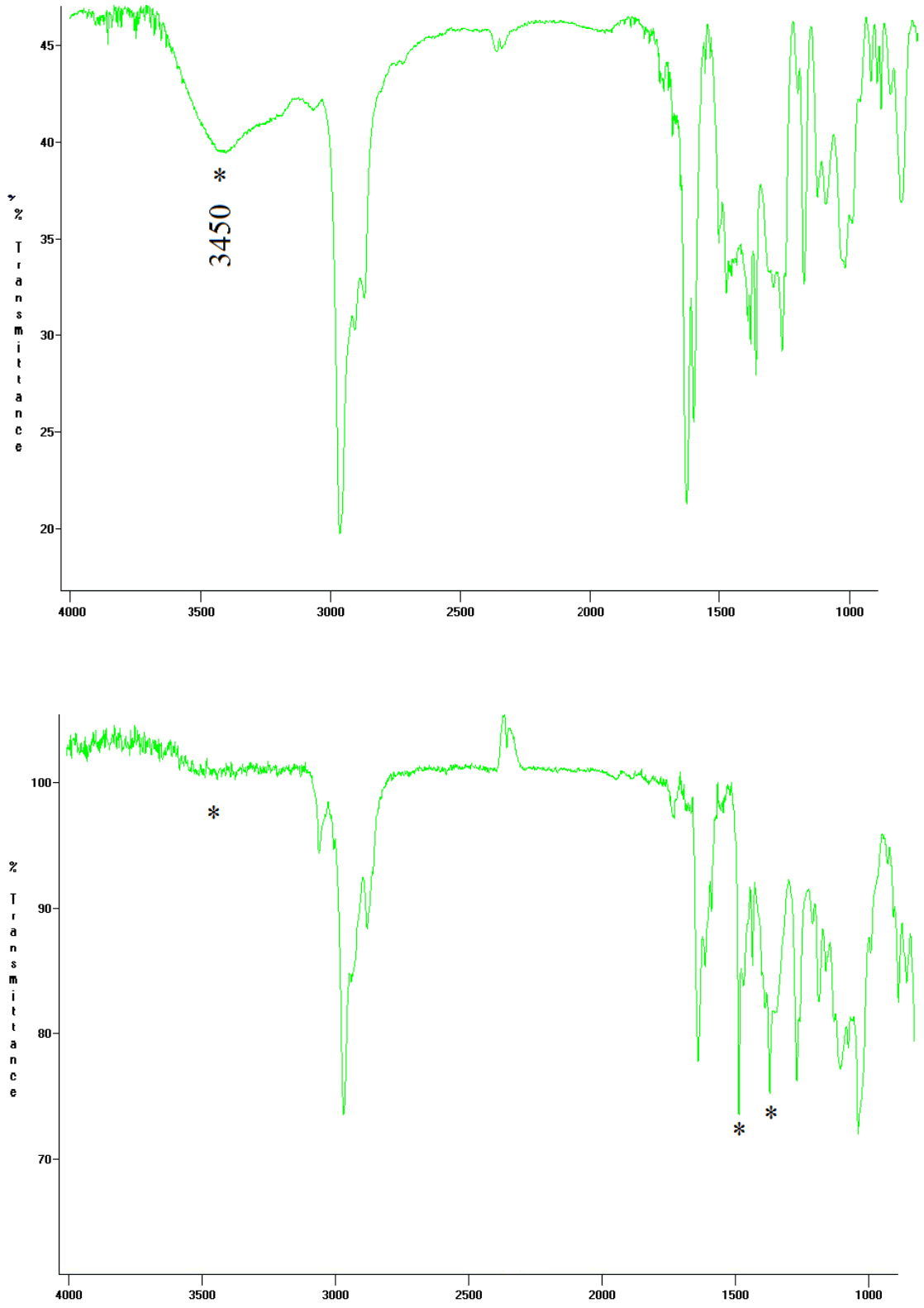

Chapter 4: *Structural characterisation of [Zn^{II} X 3,5 ^{t}BuTCT]$^{+}$ [BPh_4]$^{-}$ complexes*

Crystal Structure Data and Refinement

Single crystal X-Ray crystallography has proved a valuable technique at determining whether the synthesised complexes are accurate structural models of the active site environment of HCAII.[4, 19, 45, 52, 72, 75, 87, 88, 92, 98, 99] With this technique it gives useful information when comparing significant bond lengths and angles to pre-existing crystallographic data.

4.1 [Zn^{II}(Cl) 3,5 ^{t}BuTCT]$^{+}$ [BPh_4]$^{-}$

To obtain the zinc chloride complex, [Zn^{II}(Cl) 3,5 ^{t}BuTCT]$^{+}$ [BPh_4]$^{-}$, the zinc hydroxide complex was taken, and using a d^2-DCM / THF / pentane solvent system allowed colourless block-type crystals to be grown over a period of ca 1 week. Figure 41 shows a stick diagram of the complex. The resulting crystals were analysed by X-Ray diffraction. It is interesting to note the new rigid cavity that has been created upon complexation, with the chloride anion sat at the bottom bonded to the zinc.

Figure 41, *Stick diagram of* $[Zn^{II}(Cl)\ 3,5\ ^{t}BuTCT]^{+}\ [BPh_4]^{-}$

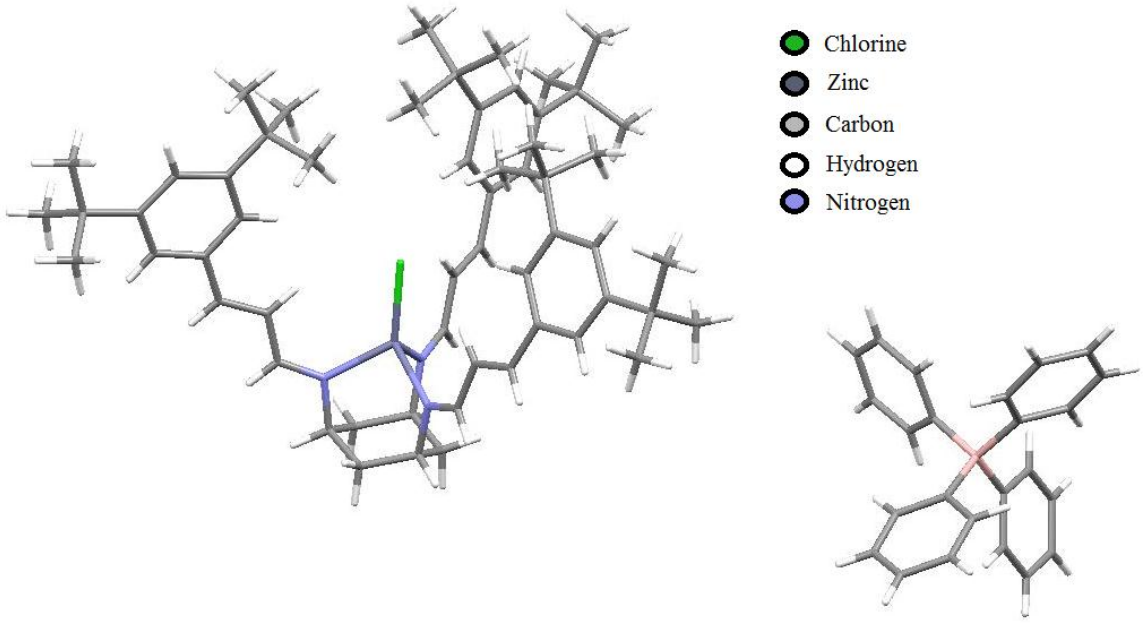

Selected bond lengths (/Å) and angles (/°): Zn(1)-Cl(1) 2.219(1), Zn(1)-N(1) 2.044(3), Zn(1)-N(0AA) 2.040(3), Zn(1)-N(1AA) 2.049(2), Cl(1)-Zn(1)-N(1) 121.17(8), Cl(1)-Zn(1)-N(0AA) 123.14(8), Cl(1)-Zn(1)-N(1AA) 121.64(8), N(1)-Zn(1)-N(0AA) 94.5(1), N(1)-Zn(1)-N(1AA) 94.3(1), N(0AA)-Zn(1)-N(1AA) 94.8(1), Zn(1)-N(1)-C(9) 112.4(2), Zn(1)-N(1)-C(13) 130.1(2), C(9)-N(1)-C(13) 117.5(3), Zn(1)-N(0AA)-C(24) 129.0(2), Zn(1)-N(0AA)-C(29) 112.9(2), C(24)-N(0AA)-C(29) 118.0(3), Zn(1)-N(1AA)-C(21) 112.6(2), Zn(1)-N(1AA)-C(38) 130.1(2).

The crystal structure of the zinc chloride complex shows that the zinc(II) centre has an approximately tetrahedral coordination geometry. The primary coordination sphere around the zinc(II) ion is characterised approximately as $\mathbf{C}_{3v}$. The ligand system is shown to bind in the expected N_3 facially capping manner,

with the ligand forming a stereochemically rigid cavity around the zinc centre. The bulky tert-butyl substituents point into the cavity, with the second meta substituent pointing in the opposite direction. This forces the steric bulk to sit right over the metal centre, as shown in figure 42. The cavity depth is 5.96 Å, this is calculated by creating a plane using the quarternary carbon atoms of the tert-butyl substituents facing into the cavity, and measuring the distance to the zinc atom. This distance is much shorter than the cavity distance seen in the native enzyme of around 15 Å.

Figure 42, *stick diagram of* $[Zn^{II}(Cl)\ 3,5\ ^{t}BuTCT]^{+}\ [BPh_4]^{-}$ *with hydrogen atoms omitted for clarity.*

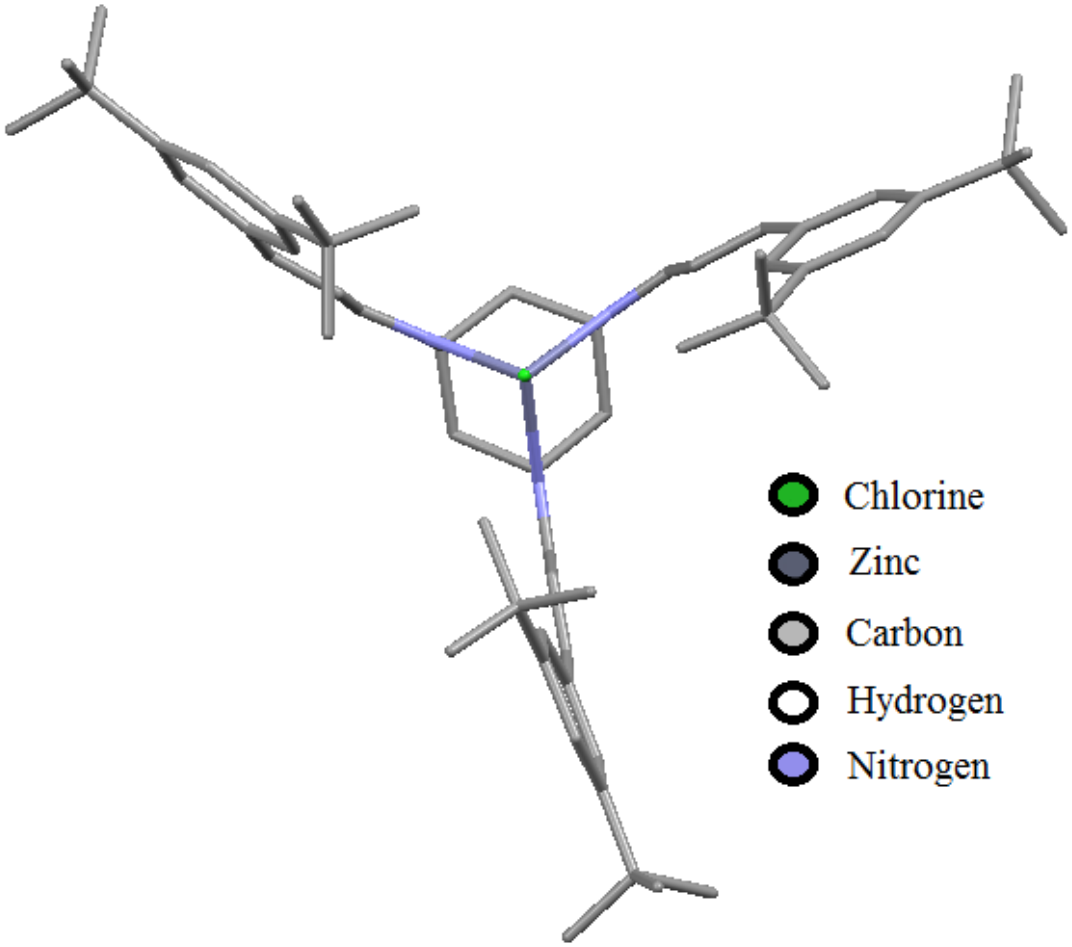

The average bond angle for N-Zn(1)-Cl(1) is 121.99(13)°, the N-Zn(1)-N average bond angle is 94.54(3)° and the average N-Zn bond length is 2.044(6) Å. These figures are comparable to the TCT ligand system, as seen in figure 25. Table 3 below compares the structures of $[Zn^{II}(Cl)\ 3,5\ ^{t}BuTCT]^{+}\ [BPh_4]^{-}$ to $[Zn^{II}(Cl)\ TCT]^{+}\ [BPh_4]^{-}$ and HCAII with bound bicarbonate. It is useful to compare the zinc chloride complex with the native enzyme bound to a bicarbonate because this crystal structure is also four-coordinate.[67, 88]

Table 3, *Significant bond lengths (/Å) and bond angles (/°) for the complexes* $[Zn^{II}(Cl)\ 3,5\ ^{t}BuTCT]^{+}\ [BPh_4]$, $[Zn^{II}(Cl)\ TCT]^{+}\ [BPh_4]^{-}$ *and HCAII with bound bicarbonate.*[67, 88] *NB: No ESD data has been published for the HCAII with bound bicarbonate.*

	$[Zn^{II}(Cl)\ 3,5\ ^{t}BuTCT]^{+}\ [BPh_4]^{-}$	$[Zn^{II}(Cl)\ TCT]^{+}[BPh_4]^{-}$	HCAII with bound bicarbonate
N-M(1)-Cl(1) average angle	121.99(8)	121.74(16)	-
M-N average bond length	2.044(3)	2.036(5)	2.019
M-Cl bond length	2.219(1)	2.188(2)	-

It is interesting to note that in the less bulky ligand, unsubstituted TCT, the bond lengths are smaller than in the substituted 3,5 ^{t}Bu TCT ligand. On the basis of metal-nitrogen bond length, the TCT ligand appears to be a closer fit to the native enzyme. One possible explanation for this could be the extra electron density now in the phenyl rings due to the tert-butyl groups, these provide a +I inductive effect into the aryl ring. The aryl ring thus has less of a -I effect on the propylidene side arms, which means less electron density is "pulled" towards it when compared to the unsubstituted rings. Thus, as electron density is not being "pulled" as much toward the phenyl rings, the electrons on the nitrogen groups do not get as disturbed. This in turn means there is less pull on the electrons on the zinc(II) atoms, resulting in a slightly longer bond length.

4.2 $[Zn^{II}(NO_3)\ 3,5\ ^tBuTCT]^+\ [BPh_4]^-$

A crystal structure for the zinc nitrate complex, $[Zn^{II}(NO_3)\ 3,5\ ^tBuTCT]^+\ [BPh_4]^-$ was also obtained from an unsuccessful zinc hydroxide complex reaction, as detailed in Chapter 6. Colourless block-type crystals were grown from a THF / pentane solvent system. Figure 43 below shows a stick diagram of the crystal structure.

Figure 43, *Stick diagram of* $[Zn^{II}(NO_3)(THF)\ 3,5\ ^tBuTCT]^+\ [BPh_4]^-$

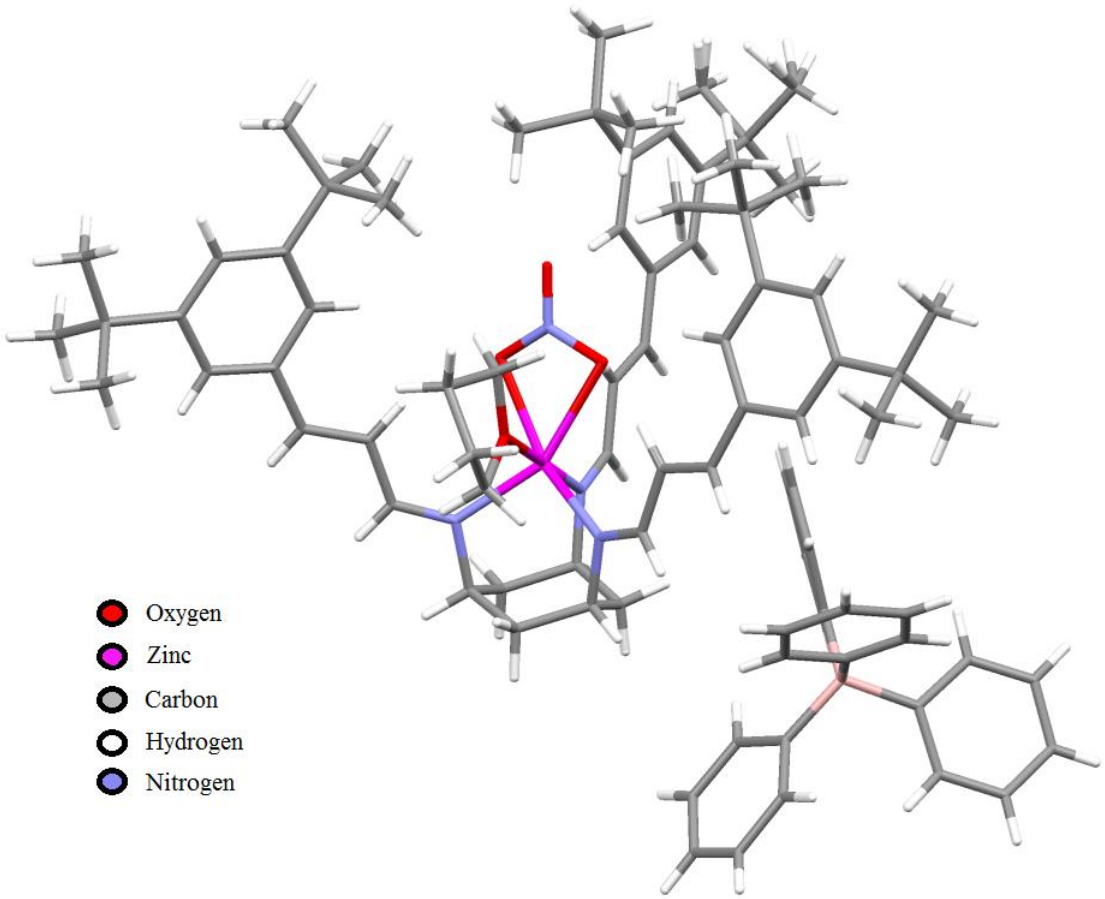

Selected bond lengths (/Å) and angles (/°): Zn(1)-O(1) 2.367(5), Zn(1)-O(2) 2.148(6), Zn(1)-O(6) 2.534(4), Zn(1)-N(1) 2.043(1), Zn(1)-N(2) 2.089(3), Zn(1)-N(3) 2.061(3), N(4)-O(1) 1.25(1), N(4)-O(2) 1.31(1), N(4)-O(3) 1.21(8), N(1)-Zn(1)-N(2) 92.8(1), N(1)-Zn(1)-N(3) 96.3(1), N(2)-Zn(1)-N(3) 93.6(1), N(1)-Zn(1)-O(1) 102.8(1), N(1)-Zn(1)-O(2) 155.0(2), N(1)-Zn(1)-O(4) 82.7(1), O(1)-Zn(1)-O(2) 56.6(2), O(1)-Zn(1)-O(4) 77.9(1), O(2)-Zn(1)-O(4) 79.2(1), O(1)-N(4)-O(2) 114.4(8), O(1)-N(4)-O(3) 123.7(8), O(2)-N(4)-O(3) 121.8(8)

In the zinc nitrate complex, it is interesting to see that the zinc appears to be six coordinate. We observe the expected N_3 facially capping mode present bound to the zinc, but included in this primary coordination sphere is a bidentate bound nitrate anion, and a THF solvent molecule creating a third zinc-oxygen bond. As seen in figure 41 with the chloride complex, the tert-butyl substituents sit above the metal centre.

This binding mode for the nitrate is interesting as it contradicts results published by Parkin *et al.* who observed a unidentate nitrate using the tris(pyrazolyl)hydroborate ligand system as seen in figure 16. However, in Parkin's crystal structure, they do not have a solvent molecule present in the primary coordination sphere of the zinc. This makes a direct comparison between the two different coordination modes difficult. Parkin describes empirical conditions which would indicate either unidentate or bidentate binding modes. By taking the difference in the two metal-oxygen lengths (l_2-l_1) Parkin has suggested that this parameter can be used to assign the coordination modes in metal nitrates as shown in table 4.[58]

Table 4, *Parkins' suggested coordination modes for the parameter* $(l_2\text{-}l_1)$[58]

Coordination mode	$(l_2\text{-}l_1)$ / Å
Symmetrically bidentate	< 0.3
Unsymmetrically bidentate	0.3-0.6
Unidentate	> 0.6

Using this system, it could be deduced that the $(l_2\text{-}l_1)$ value for the nitrate complex is 0.219 Å, which would therefore make it symmetrically bidentate. With the isoelectronic nature of the nitrate to the bicarbonate, it could be further hypothesised that the bicarbonate could also exist as a symmetrically bidentate anion when bound to the zinc centre. This would support Lindskog's hypothesised mechanism of a bidentate bicarbonate intermediate if correct, although the zinc atom in both the Lindskog and Lipscomb mechanisms is without a solvent molecule. They are also either 4 or 5 coordinate species respectively, and not 6 coordinate as the zinc nitrate crystal structure is. A crystal structure of a mutated HCAII with Thr-200 to His, was solved with bound bicarbonate anion and was shown to be pseudo-bidentate.[49]

However, in a solved structure of the native enzyme with a four coordinate zinc bound bicarbonate, we see a unidentate bicarbonate, with the geometry shown in figure 44.[67] In a cobalt-substituted HCAII with bound bicarbonate, a bidentate bicarbonate was observed. This cobalt-substituted enzyme was also 6 coordinate, with the sixth coordination site occupied by a zinc bound aqua species. This would make for a better comparison to the nitrate complex due to the similarities

in coordination number, but also in binding mode. Table 5 below highlights the significant bond lengths in the crystal structure of the native enzyme and cobalt substituted enzyme with bound bicarbonate compared to those in the zinc nitrate complex. [43]

Figure 44, *Image constructed using Mercury software to highlight the geometry of the zinc bound bicarbonate solved for the HCAII native enzyme. The bottom image shows the cobalt substituted HCAII enzyme with bidentate bound bicarbonate and bound water molecule, with bond lengths in Å.*[43, 67]

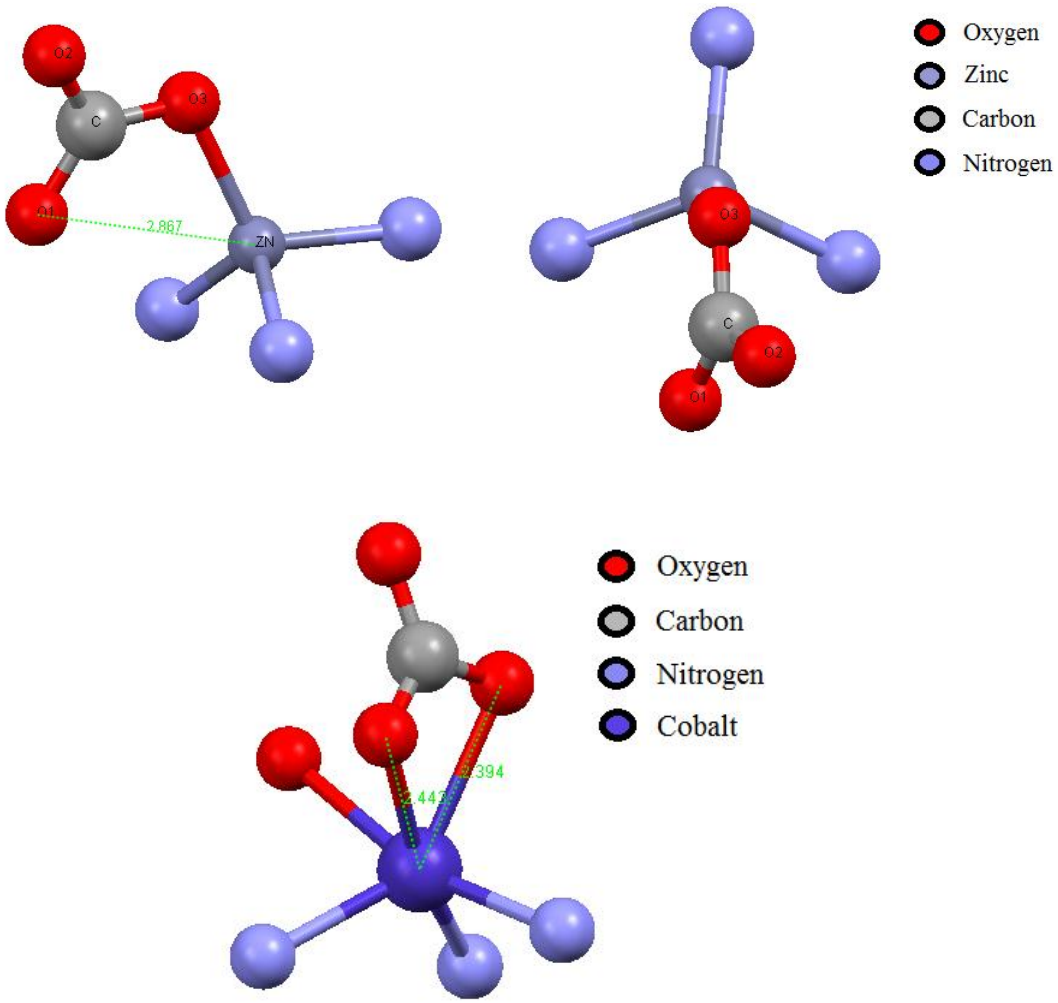

Table 5, *Significant bond lengths (/Å) for the complex* $[Zn^{II}(NO_3)$ *3,5* ^{t}*BuTCT]*$^{+}$ $[BPh_4]^{-}$ *as well as those in the cobalt substituted and native HCAII enzyme with metal bound bicarbonate.*[43, 67] *NB: No ESD data has been published for the HCAII with bound bicarbonate.*

	HCAII with bound bicarbonate	**Cobalt substituted HCAII with bound bicarbonate**	**$[Zn^{II}(NO_3)$ 3,5 ^{t}BuTCT]$^{+}$ $[BPh_4]^{-}$**
Average M-N bond	2.019	2.167	2.064(3)
M-O bond length in bicarbonate or nitrate	2.0293	2.394, 2.443	2.367(5), 2.148(6)
C-O and N-O average bond length	1.259	1.275	1.26(3)

There is a major discrepancy in the binding mode between the three species. The HCAII bound bicarbonate is unidentate whereas the bicarbonate on the cobalt HCAII and nitrate on the zinc complex exist as bidentate. The average zinc-nitrogen distance is very similar, with the N_3 environment provided by the ligand system appearing to be a good mimic of the native enzymes tri histidine residues. The cobalt HCAII metal-nitrogen distance is also close to the zinc nitrate complex. Despite the difference in binding mode between the two species, the

nitrate is shown here to be a good approximation to the bicarbonate with its bond lengths almost matching those of the bicarbonate.

There is some correlation seen between the two bidentate bound ligands, with one bond being similar, 2.394 Å for a M-O in the bicarbonate, and 2.367(5) Å for a M-O bond in the nitrate. However the second M-O distance varies between the two much more, with a M-O distance in the bicarbonate observed to be 2.443 Å compared to a M-O in the nitrate at 2.148(6) Å. This highlights that despite the isoelectronic nature of the two species, the metal centre plays a bigger role in binding than first thought. It could be concluded that the cobalt centre perhaps prefers to bind in a bidentate fashion more than a zinc centre. This was the same conclusion that Parkin *et al.* reached, with the preference for bidentate binding increasing across the series Zn < Co < Cu < Ni.[7]

Although the zinc nitrate complex does show bidentate nature, it may not be concluded that HCAII exhibits the same properties. The reason being that in the native enzyme, zinc is either in a four or five coordinate geometry, depending on the suggested mechanism.

Chapter 5: *Conclusion and future work*

5.1 Conclusions

A tach based ligand was synthesised which incorporated a degree of steric bulk in an attempt to model several stages of the hypothesised mechanism of HCAII. This ligand system was then used to isolate a zinc bicarbonate complex. Although the ligand system proved unsuccessful in isolating a crystal structure of the zinc bicarbonate complex, useful data has been discovered. These include a bidentate six coordinate zinc nitrate complex which is analogous to a six coordinate zinc bicarbonate complex due to its isoelectronic nature. ^{1}H NMR data has also shown that a monomeric zinc hydroxide complex is converted to another species upon addition of carbon dioxide, believed to be the zinc bicarbonate complex. IR data has shown the same result. Finally ^{13}C data has shown the formation of two new species, at 171 ppm and 154 ppm, which correlate well to data published by Ibrahim *et al*. at 167 ppm perhaps validating the result seen in this project.

5.2 Possible future experiments

It had proved difficult to grow any single crystals which would diffract well of the zinc hydroxide complex, although the two linked structures of the zinc chloride and nitrate complexes have proved useful. It would prove very helpful to grow a crystal of the zinc hydroxide and zinc bicarbonate complexes, to further understand the binding mode of the bicarbonate in the native enzyme. A

time lapse experiment using ^{1}H and ^{13}C NMR would be very useful in showing whether the bicarbonate peaks observed change upon addition of carbon dioxide and removal of it. The synthesis could be carried out in an aprotic ionic liquid, which are easily prepared at room temperature and can contain low amounts of water, as well as having the obvious advantage of being non-coordinating.[100] With the development of new weakly coordinating anions, it would also prove useful to evaluate the use of an anion such as $[B(C_6F_5)_4]^-$ in the synthesis. An alternative to this would be the carborane class of weakly coordinating anions, such as$[CB_{11}H_6Cl_6]^-$.[101]

Chapter 6: *Experimental*

6.1 Experimental details

All solid and liquid reagents were procured from either the Sigma-Aldrich Corporation or Lancaster Chemicals Ltd, and used without further purification unless otherwise stated. Gasses including N_2 and carbon dioxide were supplied by B.O.C. Ltd, and were not purified or dried any further.

All synthesised complexes in this report were air and moisture sensitive. They were all handled using Schlenk line techniques under N_2 gas, or inside a glove box under argon gas, both gases were oxygen free. The reactions were carried out in Schlenk tubes for the air sensitive reactions, and round bottom flasks for the synthesis of the ligand. All glassware was washed with deionised water prior to placing in an oven at 80°C overnight. Prior to use, the glassware was removed from the oven and immediately placed under vacuum and purged with oxygen free nitrogen gas, this vacuum and purge cycle was repeated three times. Reagents were added to the reactions vessels through a rubber septum using a nitrogen purged syringe, or under positive pressure of the nitrogen gas with no rubber septum.

All solid reagents were stored in a dessicator prior to use, and all liquid reagents were dried, distilled and stored under nitrogen in a glass ampuole with a J. Young tap. The d-chloroform ($CDCl_3$) and d^2-dichloromethane (CD_2Cl_2) were dried for 24 hours using calcium hydride (CaH_2) and then degassed before

storage. Solvents were gathered from a solvent purification system, with the exception of methanol (MeOH) which was dried under argon using I_2 and magnesium.

Infrared (IR) spectroscopy was run on the Thermo-Nicolet Avator 370 FTIR spectrometer or the unicam RS 10000-E spectrophotometer. All IR spectra were obtained using ATR-IR, with the exception of a solution study which bubbled CO_2 through a solution of the zinc hydroxide complex. NMR spectra (both ^{1}H and ^{13}C) were run on a Jeol EXC400 or a Bruker AVANCE 500, with NMR spectra referenced to internal solvent peaks.

Single crystal X-ray diffraction quality crystals were grown under a argon or nitrogen atmosphere, and were removed from the mother liquor under nitrogen and run on a Bruker Smart Apex diffractometer. This was equipped with a 3-circle goniometer, a 2kW Mo X-Ray source and SMART CCD camera recorded the results. Samples were run at 110 K using liquid nitrogen to cool the system.

Electronspray ionisation mass spectrometry analysis was performed on an Esquire 6000 instrument, with the samples made up in dry solvents including d^2-DCM, DCM, acetonitrile, or acetone. LIFDI was performed on a Waters GCT Premier MS.

6.2 Preparation of organic precursors

6.2.1 Synthesis of *Cis, Cis* 1, 3, 5 triaminocyclohexane (*cis*-tach)

Cis, cis 1, 3, 5-cyclohexanetricarboxylic acid

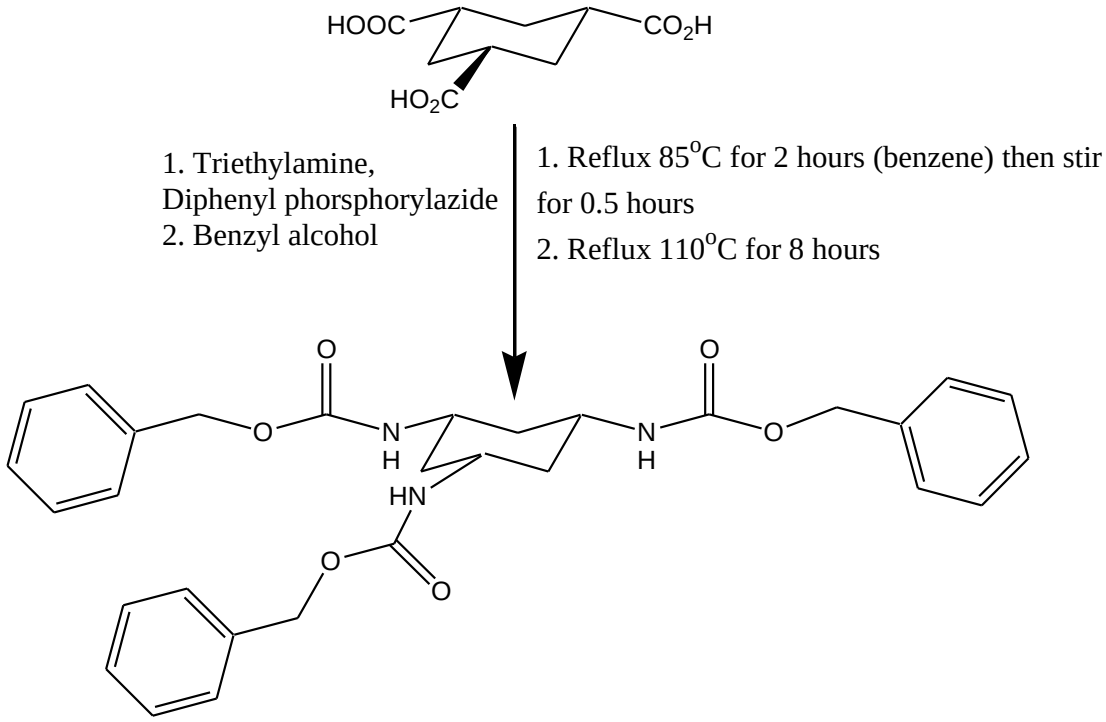

Benzene (85 cm^3) was added to *cis, cis* 1,3,5-cyclohexanetricarboxylic acid (2.5051 g, 11.6 mmol) with stirring and then heated at reflux at 85 °C for 2 hours. Triethylamine (4.8 cm^3, 34.4 mmol) and diphenyl phosphorylazide (7.5 cm^3, 34.8 mmol) was then added to the mixture before stirring for a further 30 minutes. To this colourless solution benzyl alcohol (7.9 cm^3, 35.1 mmol) was added, and the whole mixture was heated overnight (for 18 hours) at 110°C. The mixture was then left to cool and then filtered off under vacuum to yield *cis, cis* 1, 3, 5-cyclohexanetricarboxylic acid as a white solid (1.5452 g, 25.1%).

6.2.2 *Cis, Cis* 1, 3, 5 triaminocyclohexane. 3HBr

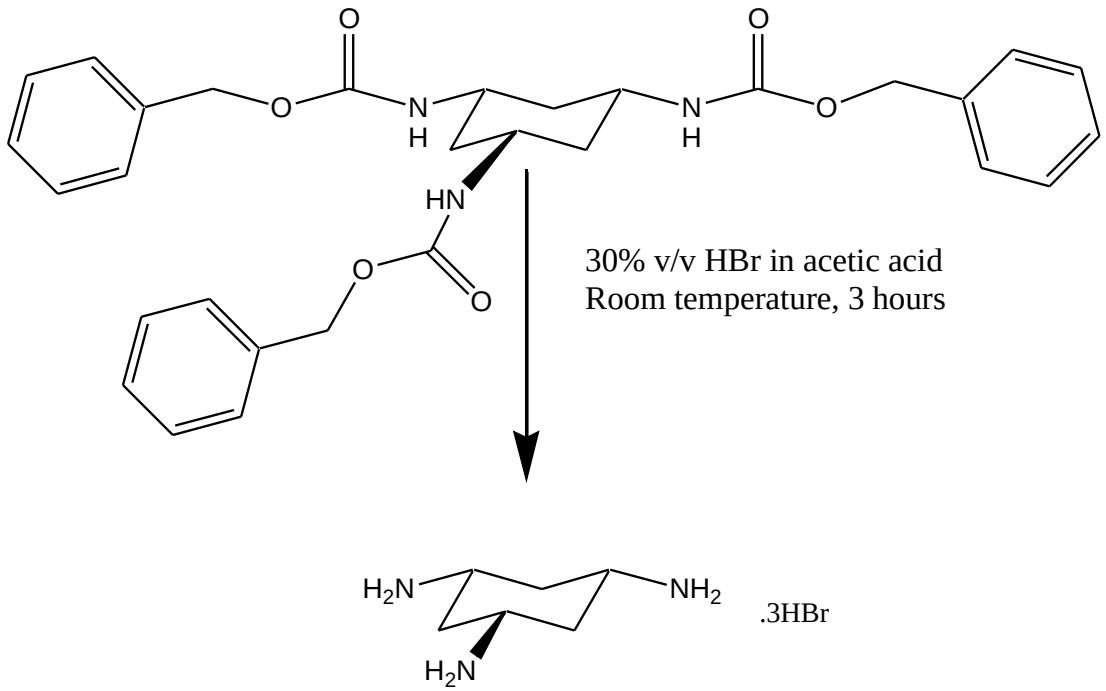

30% v/w hydrogen bromide in acetic acid (50 cm^3) was added to *cis, cis*-1,3,5-cyclohexanetribenzylcarbamate (1.5258 g, 7.06 mmol). This was then stirred for a period of 24 hours, during which the effervescence of carbon dioxide was observed. To this was added ethanol (50 cm^3) which was stirred for a further 24 hours, after which a white precipitate was observed and removed by filtration under vacuum and washed with chilled ethanol. This yielded *cis, cis*-1,3,5-Triaminocyclohexane.3HBr (0.9325 g, 2.51 mmol, 35.5%).

^{1}H NMR 400 MHz (D_2O): δ_H, 3.38 (dt, 3H, $^3J_{HH}$ 8.1 Hz, C*H*N), 2.34 (d, 3H, $^3J_{HH}$ 8.1 Hz, CH_{eq}), 1.53 (q, 3H, $^3J_{HH}$ 8.1 Hz, $CH_{ax)}$

IR (cm^{-1}), 2893 CH, 1586 NH, 1209 CN

6.2.3 *Cis, Cis* 1, 3, 5 triaminocyclohexane (*cis*-tach)

Using an anion exchange column with Dowex 1X4-50 beads fitted, large amounts of deionised water were used to wash the resin beads, before being washed with 1M HCl and then 1M NaOH. The column was washed until the eluent stream coming from the column was neutral. The *Cis, Cis* 1, 3, 5 triaminocyclohexane. 3HBr was then dissolved in a minimum amount of water and sent through the column. The basic fractions were taken and combined, and then the water was removed. The product was finally sublimed under reduced pressure using a cold finger.

^{1}H NMR 400 MHz (CD_2Cl_2): δ_H, 2.73 (dt, 3H, $^{3}J_{HH}$ 17.8 Hz, C*H*N), 1.94 (d, 3H, $^{3}J_{HH}$ 17.8 Hz, CH_{eq}), 1.10 (s, 6H, N*H*$_2$) 0.82 (q, 3H, $^{3}J_{HH}$ 17.8 Hz, CH_{ax}).

^{13}C NMR 400 MHz (CD_2Cl_2): δ 48.5 (*C*H_2), 47.5 (*C*H)

6.3 Synthesis of trans-cinnamaldehyde

3,5 ditertbutyl *trans* cinnamaldehyde

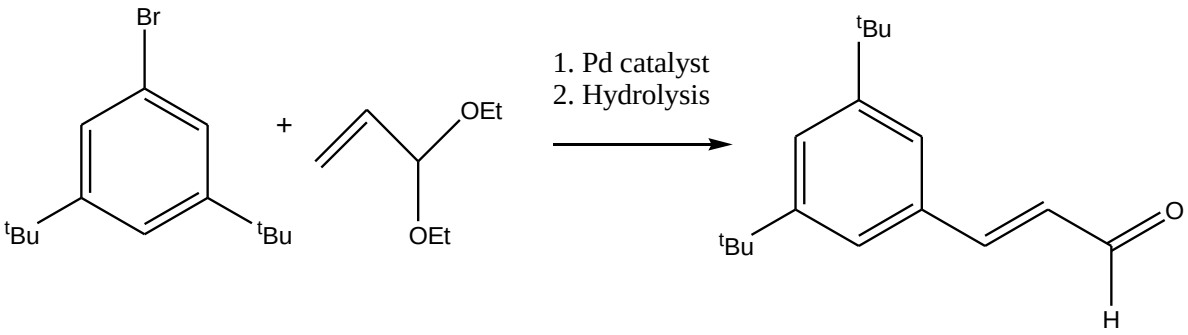

All solid reagents were dried in vacuo for a full day before addition of any liquid reagents. To a dry degassed mixture of tertrabutyl ammonium acetate (2.24 g, 7.42 mmol) was added palladium acetate (0.03 g, 0.11 mmol), potassium chloride (0.28 g, 3.71 mmol), potassium carbonate (0.77 g, 5.37 mmol), 1-bromo-3,5 ditertbutylbenzene (1.00 g, 3.71 mmol) in dry degassed DMF and finally dry degassed acrolein diethyl acetate (1.45 g, 1.70 cm^3, 11.13 mmol) was added. This mixture was then stirred at 90 °C for 18 hours, then it was left to cool to room temperature and a pale yellow solution was observed. Then enough 2M HCl was added to neutralise excess potassium carbonate and then further stirred for another 10 minutes. The resulting mixture was diluted with diethyl ether and washed with water. The organic layer was dried over sodium sulphate and the solvent removed to give 3,5 ditertbutyl *trans* cinnamaldehyde which was then purified in a column with ethyl acetate: hexane in a 1:9 ratio. The product was the final eluted fraction.

NB: The above procedure is that of the published synthetic route to cinnamaldehydes, and it was not possible to purify the compound. [94]

^{1}H NMR 400 MHz (CD_2Cl_2): δ_H 9.73 (d, 1H, $^3J_{HH}$ 7.8 Hz, C*H*O), 7.56 (d, 1H, $^3J_{HH}$ 15 Hz, ArC*H*), 7.46 (s, 2H, Ar*H*), 7.34 (s, 1H, Ar*H*), 6.78 (dd, 1H, $^3J_{HH}$ 7.8 Hz, $^3J_{HH}$ 15 Hz C*H*CHO), 1.35 (s, 18H, ArC(C*H*$_3$)$_3$)

ESI Mass spectrometry : 242.24 m/z = [M^+]

6.4 Ligand synthesis

Cis,*cis*-1,3,5-tris(3,5-ditertbutylphenylpropenylideneimino)cyclohexane

The reported method is taken from unpublished literature, with the ratio of tach to cinnamaldehyde being 1:3. This allows for appropriate scale up.

To a stirred suspension of tach in dry degassed MeOH over activated 3Å molecular sieves, was added a solution of 3,5-di-tert-butylcinnamaldehyde in dry degassed MeOH. The reaction mixture was refluxed with stirring for 3h. The resulting white ppt was filtered off and dried under vacuum to yield 3,5-di-tert-butylprotach.

^{1}H NMR 400 MHz (CD_2Cl_2): δ_H, 8.12 (d, 3H, $^{3}J_{HH}$ 10.1 Hz, N=C*H*), 7.41 (s, 3H, Ar*H*), 7.36 (s, 3H, Ar*H*), 6.97 (m, 6H, ArC*H*C*H*), 6.97 (m, 6H, $^{3}J_{HH}$ 10.1 Hz, C*H*C*H*), 3.39 (m, 3H, C*H*N), 1.77 (m, 6H, CH_2), 1.32 (s, 54H, ArC(CH_3)$_3$)

ESI Mass spectrometry: 808.65 m/z = [M^+]

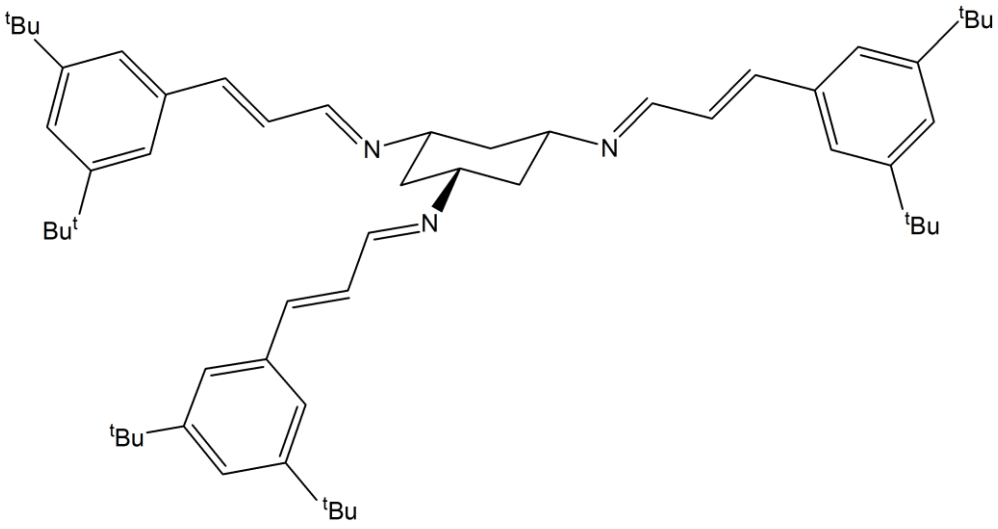

6.5 Complexes

6.5.1 *Cis,cis*-1,3,5-tris(3,5-ditertbutylphenylpropenylideneimino)cyclohexane Zinc hydroxide tetraphenyl borate

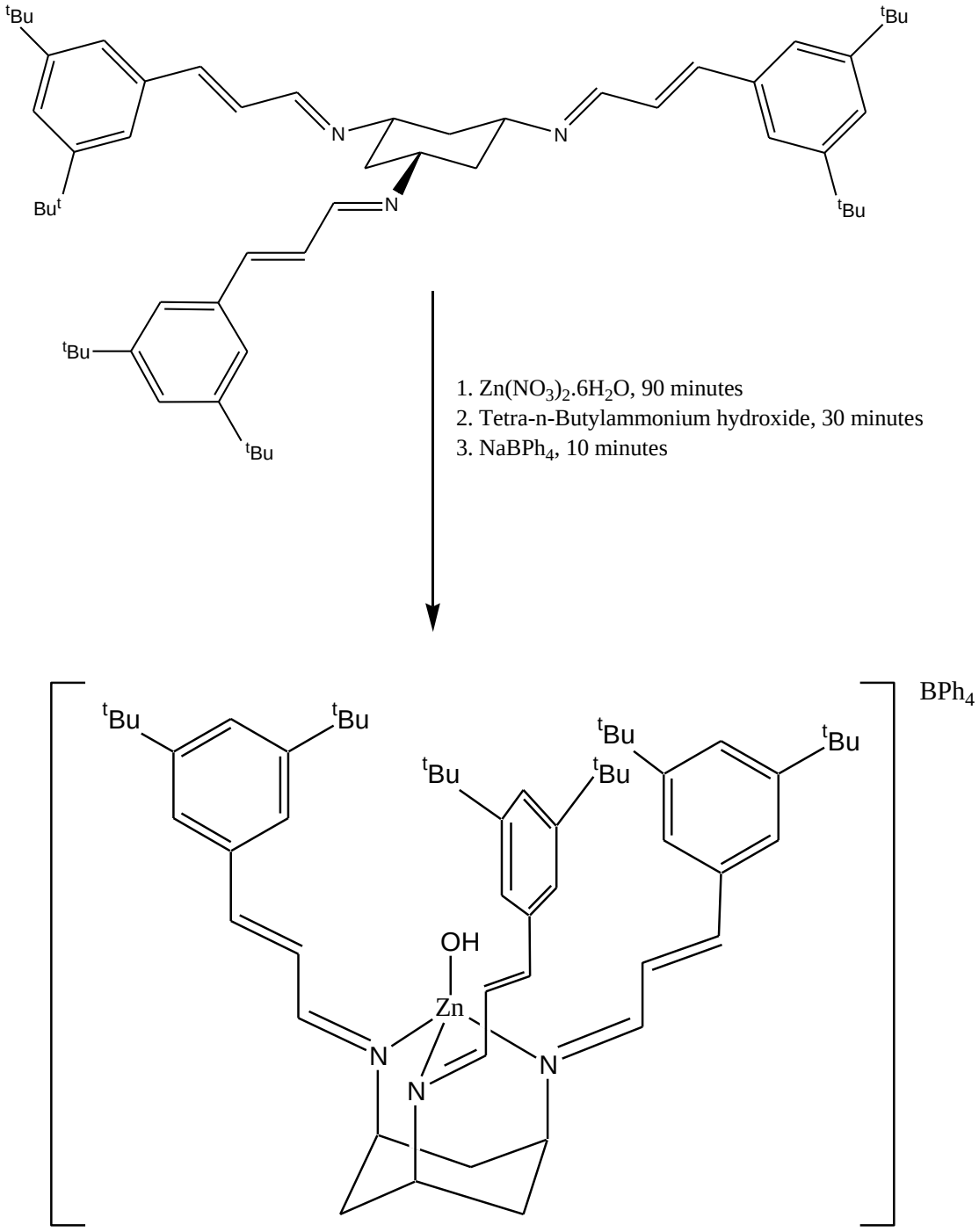

All solid reagents were dried in vacuo for a full day before the addition of any liquid reagents. Firstly, to 3,5 ^{t}BuTCT (25 mg, $3.09x10^{-5}$ mol) was added $Zn(NO_3)_2.6H_2O$ (9 mg, $3.09x10^{-5}$ mol). Toluene was added to dissolve the ligand (ca. 1 ml) and methanol was added to dissolve the zinc salt (minimum amount ca. 0.5 ml), until complete solvation. This was stirred for 90 minutes, at which point tetra-n-butylammonium hydroxide 1M in MeOH was added (0.04 ml, $4x10^{-5}$ mol). This was stirred for a further 30 minutes, at which point a solution of $NaBPh_4$ in methanol was added (11 mg, $3.09x10^{-5}$ mol). This was stirred for ca.10 minutes or until a precipitate was seen, at which point the precipitate was allowed to digest and then filtered via cannulae and dried under N_2. At this point the complex was then allowed to dry for roughly ca. 3 hours under N_2, which yielded the complex as a white solid.

NB: It proved difficult to synthesise *Cis,cis*-1,3,5-tris(3,5-ditertbutylphenylpropenylideneimino)cyclohexane Zinc hydroxide tetraphenyl borate. At times the precipitate did not form altogether, and to produce solid the solution was left to stir with the sodium tetraphenyl borate for a period of ca. 2 hours. This was then left in the fridge overnight to allow precipitation. If a precipitate had still not been observed some of the solution was removed in vacuo until the start of precipitation. On the occasions when a precipitate did not form immediately, or within a minute of addition of sodium tetraphenyl borate, observation of the hydroxide was very unlikely. The solid produced by extra manipulation of the solution often was of poor quality, and often did not dissolve in the deuterated solvent, with deuterated acetone proving particularly problematic.

^{1}H NMR 400 MHz (CD_2Cl_2): δ_H, 7.99 (d, 3H, $^{3}J_{HH}$ 10.1 Hz, N=C*H*), 7.81 (dd, 3H, $^{3}J_{HH}$ 15.7 Hz, $^{3}J_{HH}$ 10.1 Hz NCHC*H*), 7.53 (s, 3H, Ar*H*), 7.48 (s, 6H, Ar*H*), 7.25 (d, 3H, $^{3}J_{HH}$ 15.7 Hz ArC*H*), 3.91 (s, 3H, C*H*N), 2.23 (d, 3H, CH_2), 1.95 (d, 3H, CH_2), 1.35 (s, 54H, ArC(CH_3)$_3$), -0.09 (s, 1H, O*H*)

^{13}C NMR 400 MHz (CD_2Cl_2): δ 151.4 (CH*C*HN), 37.1 (*C*H_2CH), 35.3 (*C*CH_3), 31.8 (*C*H_3)

6.5.2 *Cis,cis*-1,3,5-tris(3,5-ditertbutylphenylpropenylideneimino)cyclohexane Zinc ethoxide

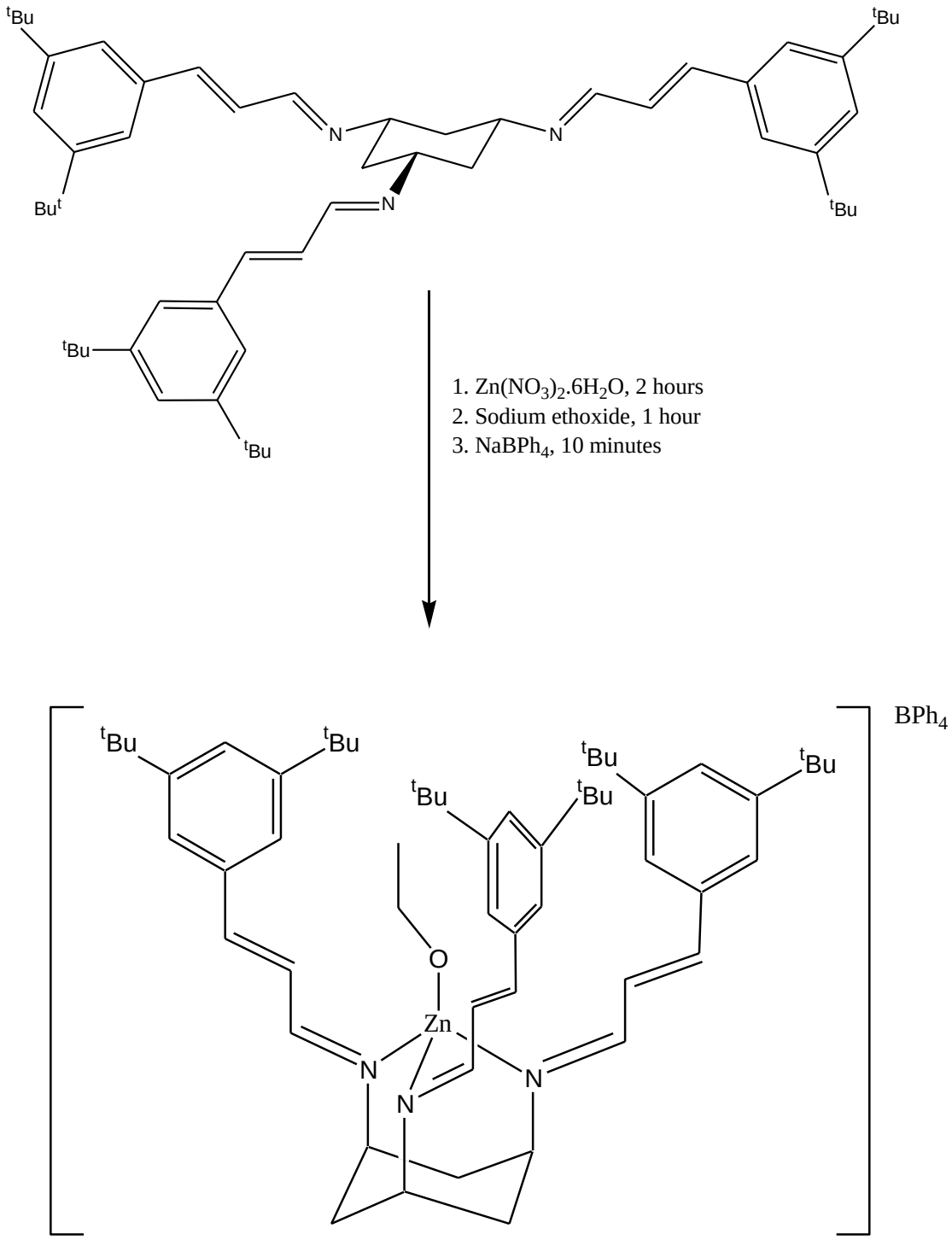

All solid reagents were dried in vacuo for a full day before the addition of any liquid reagents. Firstly, to 3,5 ^{t}BuTCT (10 mg, $1.23x10^{-5}$ mol) was added $Zn(NO_3)_2.6H_2O$ (3.68 mg, $1.23x10^{-5}$ mol). Toluene was added (ca. 0.5 ml) to dissolve the ligand and ethanol was added drop wise until the zinc salt had fully disappeared. This was stirred for 2 hours and NaOEt (1.04 mg, $1.23x10^{-5}$ mol) in minimum amount of ethanol was added. This was then left for 1 hour, and finally $NaBPh_4$ was added (4.23 mg, $1.23x10^{-5}$) again in ethanol and then 10 minutes was given for full precipitation. The solution was removed via canulae and the precipitate was dried under N_2. This was then redissolved in DCM and filtered again to remove any salt left behind from postprecipitation.

^{1}H NMR 400 MHz (CD_2Cl_2): δ_H, 7.99 (d, 3H, $^{3}J_{HH}$ 10.1 Hz, N=C*H*), 7.81 (dd, 3H, $^{3}J_{HH}$ 15.7 Hz, $^{3}J_{HH}$ 10.1 Hz NCHC*H*), 7.53 (s, 3H, Ar*H*), 7.48 (s, 6H, Ar*H*), 7.25 (d, 3H, $^{3}J_{HH}$ 15.7 Hz ArC*H*), 3.91 (s, 3H, C*H*N), 2.23 (d, 3H, CH_2), 1.95 (d, 3H, CH_2), 1.35 (s, 54H, ArC(CH_3)$_3$), 1.30 (m, 3H OCH_2CH_3) 0.97 (t, 2H OCH_2CH_3)

ESI Mass spectrometry : 916.57 m/z = [M^+]

6.6 Crystallographic data

6.6.1 $[Zn^{II}(Cl)\ 3,5\ ^{t}BuTCT]^{+}\ [BPh_4]^{-}$

Identification code	phw1111
Empirical formula	$C_{81.5}H_{102}BCl_2N_3Zn$
Formula weight	1270.74
Temperature/K	110.00(10)
Crystal system	monoclinic
Space group	$P2_1/c$
a/Å	25.5393(8)
b/Å	14.4385(3)
c/Å	25.3063(7)
α/°	90.00
β/°	116.218(4)
γ/°	90.00
Volume/$Å^3$	8371.6(4)
Z	4
$\rho_{calc}mg/mm^3$	1.008
m/mm^{-1}	0.396
F(000)	2724.0
Crystal size/mm^3	0.2628 × 0.2155 × 0.1403
2Θ range for data collection	5.58 to 58.08°
Index ranges	$-34 \leq h \leq 21$, $-11 \leq k \leq 19$, $-32 \leq l \leq 32$
Reflections collected	33644
Independent reflections	18862[R(int) = 0.0250]
Data/restraints/parameters	18862/289/834
Goodness-of-fit on F^2	1.161
Final R indexes [I>=2σ (I)]	$R_1 = 0.0705$, $wR_2 = 0.2103$
Final R indexes [all data]	$R_1 = 0.0944$, $wR_2 = 0.2289$
Largest diff. peak/hole / e $Å^{-3}$	1.33/-0.79

Fractional Atomic Coordinates ($\times 10^4$) and Equivalent Isotropic Displacement Parameters ($Å^2 \times 10^3$) for phw1111. U_{eq} is defined as 1/3 of of the trace of the orthogonalised U_{IJ} tensor.

Atom	*x*	*y*	*z*	U(eq)
Zn1	1533.44(13)	7948.8(2)	4254.62(14)	23.61(12)
Cl1	2498.1(3)	7822.5(6)	4719.5(4)	41.5(2)
N3	1130.3(9)	9193.7(16)	4187.8(10)	23.5(5)
N2	986.2(10)	7240.4(16)	4501.9(10)	23.6(5)
N1	1076.2(10)	7645.1(16)	3376.9(10)	24.3(5)
C70	10322.4(12)	8012.5(19)	5819.1(12)	24.2(6)
C58	9284.1(12)	7159.3(18)	5122.8(12)	22.8(6)
C76	10108.0(11)	6306.9(18)	6081.1(12)	22.3(5)
C74	10638.6(13)	9561(2)	5670.0(13)	29.5(6)
C5	484.7(11)	9126.9(19)	3852.3(12)	23.7(6)
C45	2934.2(14)	12094(2)	5571.3(15)	35.0(7)

C69	9817.9(12)	8392.5(19)	6666.9(12)	25.1(6)
C65	8947.2(14)	7551(2)	6132.0(14)	31.4(6)
C41	1345.4(12)	9991(2)	4396.5(12)	27.2(6)
C2	196.6(12)	7159(2)	3476.9(13)	26.5(6)
C25	1696.4(13)	6540(2)	5386.4(13)	30.3(6)
C63	9189.1(13)	7755(2)	4653.2(13)	28.3(6)
C77	10194.7(12)	5615.1(19)	5738.7(12)	24.1(6)
C8	1854.0(13)	7115(2)	3166.9(14)	31.6(7)
C64	9510.6(12)	7769.3(18)	6204.5(12)	24.6(6)
C66	8711.3(15)	7922(2)	6487.3(16)	38.3(8)
C1	442.0(12)	7798(2)	3154.7(12)	25.9(6)
C71	10908.7(13)	7747(2)	6019.0(14)	29.0(6)
C78	10519.5(12)	4819.8(19)	5978.5(13)	26.2(6)
C24	1109.5(12)	6700(2)	4938.6(12)	27.9(6)
C43	2171.7(13)	10994(2)	4951.9(14)	31.0(6)
C48	3814.8(13)	10887(2)	5614.8(14)	36.0(7)
C6	318.3(11)	8813.5(19)	3220.6(12)	24.1(6)
C26	1798.1(13)	6051(2)	5871.0(14)	32.4(7)
C3	362.3(11)	7435(2)	4117.1(12)	25.0(6)
C4	239.6(11)	8468(2)	4160.9(12)	24.7(6)
C42	1965.9(12)	10162(2)	4726.8(13)	29.3(6)
C59	8877.8(12)	6435.4(19)	4986.4(13)	27.8(6)
C10	2588.3(13)	6350(2)	2916.2(14)	33.2(7)
C49	3232.2(13)	10657(2)	5292.9(13)	31.4(6)
C73	11202.2(13)	9264(2)	5855.2(14)	34.1(7)
C7	1255.1(13)	7347(2)	3008.7(13)	28.8(6)
C80	10685.2(13)	5336(2)	6934.7(13)	30.7(6)
C68	9585.4(13)	8766.2(19)	7022.6(12)	29.3(6)
C46	3523.5(14)	12351(2)	5900.2(16)	39.0(8)
C32	2874.8(14)	6341(2)	6419.2(16)	40.7(8)
C67	9025.5(14)	8529(2)	6931.4(14)	34.1(7)
C60	8412.3(12)	6327(2)	4439.0(13)	29.9(6)
B1	9803.0(14)	7310(2)	5798.8(14)	23.1(6)
C81	10358.2(12)	6126(2)	6687.0(12)	27.3(6)
C9	2006.6(14)	6714(2)	2782.7(14)	36.0(7)
C14	3607.5(13)	6099(3)	3592.5(16)	40.2(8)
C79	10773.0(13)	4672(2)	6582.6(13)	28.1(6)
C44	2789.9(13)	11248(2)	5273.0(14)	31.2(6)
C75	10210.1(13)	8948(2)	5651.8(12)	26.3(6)
C61	8334.3(13)	6946(2)	3983.7(14)	34.7(7)
C72	11337.9(13)	8358(2)	6033.0(14)	33.9(7)
C15	3066.9(13)	6496(2)	3459.4(14)	36.4(7)
C28	2372.6(16)	5502(2)	6886.3(15)	42.2(8)
C27	2362.3(14)	5949(2)	6391.9(14)	35.4(7)
C29	2894.9(17)	5445(2)	7410.5(15)	48.1(9)
C62	8726.4(13)	7647(3)	4094.6(14)	37.2(7)
C47	3946.5(14)	11730(2)	5919.0(16)	38.9(8)
C11	2654.7(14)	5810(2)	2489.9(15)	37.7(7)
C12	3186.9(14)	5395(3)	2604.3(17)	43.4(8)
C30	3386.2(17)	5839(3)	7416.6(17)	54.7(11)

C13	3652.4(14)	5553(3)	3155.9(17)	45.1(9)
C18	3029(2)	5378(4)	1553(2)	73.2(14)
C31	3394.8(15)	6291(2)	6929.5(17)	48.3(9)
C54	4309.4(14)	10229(3)	5663.5(16)	46.2(9)
C50	3681.7(15)	13280(2)	6227.6(18)	47.2(9)
C20	4123.9(15)	6274(3)	4194.4(17)	52.7(10)
C37	3954.9(17)	6751(3)	6981(2)	64.4(13)
C16	3222.8(17)	4792(3)	2121(2)	58.6(11)
C39	4141(2)	7490(3)	7473(3)	94(2)
C17	2818(2)	3973(3)	1985(3)	78.3(15)
C33	2878.2(19)	4970(3)	7947.2(17)	65.0(12)
C57A	4090(3)	9341(4)	5303(3)	51.1(14)
C55A	4666(3)	9961(6)	6302(3)	66.4(18)
C34B	2518(6)	4058(7)	7796(6)	63.7(18)
C22A	3967(4)	5863(7)	4659(4)	75(2)
C19	3843.6(19)	4475(4)	2291(2)	85.9(17)
C40	3877(2)	7215(4)	6414(3)	85.9(18)
C38	4453.4(18)	6039(3)	7160(3)	82.5(16)
C51A	3309(3)	13473(5)	6542(3)	62.0(15)
C53A	4316(3)	13317(5)	6696(3)	57.7(15)
C35B	3529(5)	4776(11)	8398(6)	81(2)
C52A	3584(4)	14035(6)	5785(4)	91(2)
C56A	4709(3)	10743(5)	5447(4)	63.5(16)
C23A	4211(5)	7297(6)	4279(5)	94(3)
C36B	2634(7)	5696(10)	8211(6)	80(2)
C21A	4677(3)	5752(8)	4253(5)	97(4)
Cl3	1212.9(9)	4594.0(16)	2084.2(10)	63.7(6)
Cl2	1826.8(18)	2854(2)	2505.2(16)	107.3(11)
C82	1522(6)	3847(8)	2562(7)	135(6)
C23B	4068(10)	7200(11)	4469(10)	94(3)
C22B	4168(7)	5490(11)	4612(7)	75(2)
C21B	4698(6)	6399(16)	4147(10)	97(4)
C55B	4889(5)	10693(9)	5797(7)	63.5(16)
C54B	4517(7)	9655(11)	6255(6)	66.4(18)
C56B	4122(5)	9591(9)	5140(5)	51.1(14)
C52B	4112(6)	13777(11)	6071(8)	91(2)
C53B	4106(5)	13132(9)	6872(5)	57.7(15)
C51B	3181(5)	13827(9)	6223(6)	62.0(15)
C36A	2414(6)	5420(10)	8124(6)	80(2)
C34A	2673(5)	3978(6)	7771(5)	63.7(18)
C35A	3422(5)	4936(10)	8501(5)	81(2)

Anisotropic Displacement Parameters ($Å^2 \times 10^3$) for phw1111. The Anisotropic displacement factor exponent takes the form: $-2\pi^2[h^2a^{*2}U_{11}+...+2hka \times b \times U_{12}]$

Atom	**U_{11}**	**U_{22}**	**U_{33}**	**U_{23}**	**U_{13}**	**U_{12}**
Zn1	24.19(18)	25.42(19)	20.24(18)	-1.18(13)	8.93(14)	0.03(13)
Cl1	35.0(4)	46.8(5)	40.4(5)	-1.0(4)	14.7(4)	1.8(3)
N3	25.6(11)	25.1(12)	19.5(11)	0.8(9)	9.6(9)	-0.1(10)
N2	26.2(11)	23.4(12)	18.8(11)	-0.9(9)	7.9(9)	1.2(9)
N1	29.1(12)	23.4(11)	20.6(11)	-1.8(10)	11(1)	-1.4(10)
C70	32.2(14)	21.9(13)	19.1(13)	-2.9(11)	12.0(11)	0.9(11)
C58	29.1(13)	21.0(13)	20.1(13)	-2.6(11)	12.5(11)	3.5(11)
C76	26.4(13)	20.2(13)	21.3(13)	0.0(11)	11.3(11)	-1.8(11)
C74	45.0(17)	18.6(13)	25.2(14)	-0.5(11)	15.8(13)	0.3(13)
C5	22.8(12)	24.0(13)	22.5(13)	-1.3(11)	8.4(11)	2.1(11)
C45	35.1(16)	30.1(16)	39.2(18)	-2.4(14)	15.9(15)	-4.1(13)
C69	33.7(14)	22.0(13)	17.1(13)	4.2(11)	8.8(11)	4.9(12)
C65	45.1(17)	22.8(14)	31.6(16)	-6.3(13)	21.7(14)	-5.1(13)
C41	30.3(14)	24.5(14)	25.9(14)	-0.5(12)	11.6(12)	1.9(12)
C2	28.3(14)	25.6(14)	22.5(14)	-0.1(11)	8.4(12)	-2.9(11)
C25	32.6(15)	25.9(14)	28.1(15)	2.9(12)	9.6(12)	0.7(12)
C63	30.3(14)	31.1(15)	23.3(14)	3.5(12)	11.6(12)	-2.3(12)
C77	34.6(14)	21.3(13)	17.2(12)	-1.2(11)	12.2(11)	-0.5(12)
C8	34.2(15)	37.2(17)	23.1(14)	1.2(13)	12.5(13)	4.8(13)
C64	35.6(15)	18.6(13)	19.3(13)	4.6(11)	12.0(12)	4.6(11)
C66	45.7(18)	35.4(17)	45(2)	-3.5(15)	30.4(17)	-1.5(14)
C1	25.8(13)	30.1(15)	19.4(13)	-1.8(11)	7.9(11)	-1.4(12)
C71	32.2(15)	20.1(13)	31.4(16)	-2.7(12)	11.0(13)	0.8(12)
C78	36.1(15)	21.5(13)	26.4(14)	-3.1(11)	18.7(12)	0.2(12)
C24	33.6(15)	25.4(14)	22.7(14)	-1.7(12)	10.8(12)	-3.1(12)
C43	31.6(14)	25.4(15)	33.0(16)	0.3(13)	11.6(13)	-1.2(12)
C48	34.0(15)	47.1(19)	32.2(17)	-7.1(15)	19.5(14)	-4.6(14)
C6	25.4(13)	25.4(14)	18.1(13)	5.2(11)	6.6(11)	1.7(11)
C26	34.4(15)	25.1(15)	29.5(16)	-0.1(13)	6.6(13)	-0.3(13)
C3	23.9(13)	28.2(14)	20.6(13)	2.2(12)	7.8(11)	-2.4(12)
C4	22.7(12)	30.8(15)	20.0(13)	-0.4(12)	8.8(11)	0.0(11)
C42	28.1(14)	26.8(15)	31.0(15)	-1.1(13)	11.3(12)	0.1(12)
C59	35.9(15)	21.2(13)	27.6(15)	-3.1(12)	15.1(12)	0.4(12)
C10	37.4(16)	36.7(17)	29.2(16)	-1.6(13)	18.2(13)	0.0(14)
C49	36.0(15)	30.3(15)	29.6(15)	-3.7(13)	15.8(13)	-5.6(13)
C73	36.2(16)	29.8(16)	35.2(17)	-5.6(14)	14.9(14)	-10.6(13)
C7	34.6(15)	27.0(14)	25.1(14)	-2.0(12)	13.5(12)	-0.4(12)
C80	44.3(17)	28.1(15)	21.9(14)	5.4(12)	16.6(13)	6.9(13)
C68	46.6(17)	19.8(13)	20.8(14)	0.4(11)	14.4(13)	4.1(13)
C46	39.9(17)	35.5(17)	47(2)	-8.3(16)	23.9(16)	-13.2(15)
C32	41.0(17)	28.9(16)	37.7(18)	-1.2(14)	4.3(15)	1.2(14)
C67	53.3(19)	24.4(14)	34.7(17)	-1.4(13)	28.6(15)	5.7(14)
C60	28.1(14)	28.0(15)	32.4(16)	-7.1(13)	12.3(12)	-2.7(12)
B1	31.4(16)	17.5(14)	20.3(15)	-0.8(12)	11.6(13)	0.8(12)
C81	39.8(15)	23.7(14)	21.4(14)	1.2(11)	16.1(12)	4.5(12)
C9	38.2(16)	44.0(18)	24.3(15)	-4.6(14)	12.4(13)	5.2(15)
C14	31.2(15)	48(2)	41.2(19)	0.4(16)	15.3(14)	-4.2(15)

C79	35.8(15)	21.6(13)	28.8(15)	4.3(12)	16.1(13)	3.6(12)
C44	35.0(15)	28.3(15)	31.6(16)	-0.3(13)	15.9(13)	-6.7(13)
C75	36.4(15)	24.6(14)	20.2(13)	1.3(11)	14.5(12)	2.2(12)
C61	27.6(14)	44.5(19)	25.6(15)	-6.2(14)	5.9(12)	1.1(14)
C72	28.5(14)	32.1(16)	36.3(17)	-3.8(14)	10.0(13)	0.1(13)
C15	40.0(17)	39.4(18)	34.2(17)	-2.2(15)	20.4(14)	1.4(15)
C28	50.6(19)	34.0(17)	30.4(17)	1.6(14)	7.2(15)	7.0(15)
C27	43.7(17)	23.2(15)	27.6(16)	1.2(13)	4.9(13)	3.2(13)
C29	64(2)	35.2(18)	24.8(16)	1.1(14)	1.6(16)	13.9(18)
C62	33.4(16)	47.6(19)	26.7(16)	9.3(15)	9.8(13)	0.8(15)
C47	31.0(15)	46.3(19)	42.9(19)	-14.6(16)	19.7(15)	-13.6(15)
C11	35.3(16)	44.9(19)	38.0(18)	-8.0(15)	20.9(15)	-1.1(15)
C12	35.9(17)	51(2)	53(2)	-12.6(18)	28.0(16)	-1.5(16)
C30	52(2)	37.0(19)	38(2)	-7.9(17)	-13.7(17)	7.1(17)
C13	34.0(17)	47(2)	59(2)	-6.6(18)	25.1(17)	2.7(15)
C18	69(3)	107(4)	59(3)	-37(3)	43(2)	-20(3)
C31	42.1(18)	31.5(17)	47(2)	-3.3(16)	-2.2(16)	0.7(15)
C54	33.8(16)	57(2)	53(2)	-17.7(19)	24.3(17)	-4.5(16)
C50	44.9(19)	36.2(18)	64(3)	-12.7(18)	27.3(19)	-13.1(16)
C20	36.1(18)	67(3)	47(2)	-4(2)	10.7(16)	2.9(18)
C37	47(2)	40(2)	70(3)	-8(2)	-6(2)	-12.3(18)
C16	46(2)	72(3)	72(3)	-30(2)	39(2)	-6(2)
C39	75(3)	49(3)	99(4)	-20(3)	-15(3)	-14(2)
C17	92(3)	62(3)	106(4)	-35(3)	66(3)	-9(3)
C33	83(3)	61(3)	29.2(19)	11.4(19)	5.1(19)	20(2)
C22A	61(5)	99(7)	43(3)	-1(4)	2(3)	9(4)
C19	59(3)	119(4)	89(4)	-40(3)	41(3)	19(3)
C40	53(3)	73(3)	104(4)	8(3)	9(3)	-26(2)
C38	45(2)	67(3)	97(4)	-10(3)	-2(2)	-1(2)
C23A	86(5)	74(4)	79(6)	-5(4)	-2(3)	-35(4)
C21A	32(2)	165(12)	76(6)	-29(9)	7(3)	10(6)
Cl3	58.9(11)	61.5(13)	59.7(13)	-3.5(11)	16.1(10)	-26.9(10)
Cl2	162(3)	99(2)	97(2)	25.5(18)	90(2)	16(2)
C82	182(15)	128(12)	168(15)	7(11)	145(14)	-7(11)
C23B	86(5)	74(4)	79(6)	-5(4)	-2(3)	-35(4)
C22B	61(5)	99(7)	43(3)	-1(4)	2(3)	9(4)
C21B	32(2)	165(12)	76(6)	-29(9)	7(3)	10(6)

Bond Lengths for phw1111.

Atom	**Atom**	**Length/Å**	**Atom**	**Atom**	**Length/Å**
Zn1	Cl1	2.2194(9)	C73	C72	1.377(4)
Zn1	N3	2.041(2)	C80	C81	1.388(4)
Zn1	N2	2.041(2)	C80	C79	1.393(4)
Zn1	N1	2.049(2)	C68	C67	1.387(4)
N3	C5	1.487(3)	C46	C47	1.389(5)
N3	C41	1.284(4)	C46	C50	1.533(5)
N2	C24	1.274(4)	C32	C27	1.400(5)
N2	C3	1.481(3)	C32	C31	1.386(5)

N1	C1	1.478(3)	C60	C61	1.401(5)
N1	C7	1.280(4)	C14	C15	1.392(4)
C70	C71	1.406(4)	C14	C13	1.402(5)
C70	B1	1.653(4)	C14	C20	1.533(5)
C70	C75	1.407(4)	C61	C62	1.363(5)
C58	C63	1.398(4)	C28	C27	1.398(5)
C58	C59	1.404(4)	C28	C29	1.408(5)
C58	B1	1.651(4)	C29	C30	1.371(6)
C76	C77	1.403(4)	C29	C33	1.539(6)
C76	B1	1.650(4)	C11	C12	1.394(4)
C76	C81	1.401(4)	C12	C13	1.396(5)
C74	C73	1.371(4)	C12	C16	1.536(5)
C74	C75	1.391(4)	C30	C31	1.403(6)
C5	C6	1.530(4)	C18	C16	1.549(7)
C5	C4	1.530(4)	C31	C37	1.530(6)
C45	C46	1.410(4)	C54	C57A	1.529(7)
C45	C44	1.398(4)	C54	C55A	1.513(8)
C69	C64	1.408(4)	C54	C56A	1.544(7)
C69	C68	1.388(4)	C54	C55B	1.520(10)
C65	C64	1.404(4)	C54	C54B	1.582(11)
C65	C66	1.392(4)	C54	C56B	1.507(10)
C41	C42	1.449(4)	C50	C51A	1.512(7)
C2	C1	1.537(4)	C50	C53A	1.528(7)
C2	C3	1.535(4)	C50	C52A	1.503(8)
C25	C24	1.443(4)	C50	C52B	1.505(11)
C25	C26	1.337(4)	C50	C53B	1.522(10)
C63	C62	1.394(4)	C50	C51B	1.499(10)
C77	C78	1.389(4)	C20	C22A	1.521(8)
C8	C7	1.439(4)	C20	C23A	1.495(9)
C8	C9	1.329(4)	C20	C21A	1.551(8)
C64	B1	1.652(4)	C20	C23B	1.542(13)
C66	C67	1.370(5)	C20	C22B	1.519(12)
C1	C6	1.524(4)	C20	C21B	1.534(12)
C71	C72	1.396(4)	C37	C39	1.547(7)
C78	C79	1.388(4)	C37	C40	1.514(8)
C43	C42	1.333(4)	C37	C38	1.541(6)
C43	C44	1.468(4)	C16	C17	1.508(6)
C48	C49	1.385(4)	C16	C19	1.518(5)
C48	C47	1.399(5)	C33	C34B	1.554(10)
C48	C54	1.542(5)	C33	C35B	1.570(10)
C26	C27	1.469(4)	C33	C36B	1.518(10)
C3	C4	1.538(4)	C33	C36A	1.581(9)
C59	C60	1.379(4)	C33	C34A	1.522(9)
C10	C9	1.468(4)	C33	C35A	1.474(10)
C10	C15	1.394(4)	Cl3	C82	1.551(11)
C10	C11	1.401(4)	Cl2	C82	1.667(10)
C49	C44	1.399(4)			

Bond Angles for phw1111.

Atom	Atom	Atom	Angle/°	Atom	Atom	Atom	Angle/°
N3	Zn1	Cl1	121.17(7)	C13	C12	C16	124.4(3)
N3	Zn1	N1	94.22(9)	C29	C30	C31	123.5(3)
N2	Zn1	Cl1	123.13(7)	C12	C13	C14	123.4(3)
N2	Zn1	N3	94.48(9)	C32	C31	C30	117.6(4)
N2	Zn1	N1	94.91(9)	C32	C31	C37	122.1(4)
N1	Zn1	Cl1	121.64(7)	C30	C31	C37	120.3(3)
C5	N3	Zn1	112.44(16)	C48	C54	C56A	108.7(4)
C41	N3	Zn1	130.29(19)	C48	C54	C54B	108.6(6)
C41	N3	C5	117.3(2)	C57A	C54	C48	113.5(3)
C24	N2	Zn1	129.3(2)	C57A	C54	C56A	108.4(4)
C24	N2	C3	117.9(2)	C57A	C54	C54B	90.4(7)
C3	N2	Zn1	112.77(17)	C55A	C54	C48	109.1(4)
C1	N1	Zn1	112.60(17)	C55A	C54	C57A	108.2(5)
C7	N1	Zn1	130.2(2)	C55A	C54	C56A	108.8(5)
C7	N1	C1	117.2(2)	C55A	C54	C55B	78.9(6)
C71	C70	B1	123.8(2)	C55A	C54	C54B	20.7(6)
C71	C70	C75	114.4(3)	C56A	C54	C54B	126.1(7)
C75	C70	B1	121.7(2)	C55B	C54	C48	115.4(6)
C63	C58	C59	114.6(3)	C55B	C54	C57A	124.5(6)
C63	C58	B1	123.9(2)	C55B	C54	C56A	30.3(5)
C59	C58	B1	121.3(2)	C55B	C54	C54B	97.7(8)
C77	C76	B1	122.0(2)	C56B	C54	C48	112.1(5)
C81	C76	C77	115.0(2)	C56B	C54	C57A	22.0(5)
C81	C76	B1	122.5(2)	C56B	C54	C55A	126.1(7)
C73	C74	C75	120.3(3)	C56B	C54	C56A	89.1(6)
N3	C5	C6	110.0(2)	C56B	C54	C55B	111.4(7)
N3	C5	C4	110.5(2)	C56B	C54	C54B	110.8(8)
C6	C5	C4	111.2(2)	C51A	C50	C46	111.6(4)
C44	C45	C46	120.5(3)	C51A	C50	C53A	106.5(5)
C68	C69	C64	123.1(3)	C51A	C50	C53B	77.2(6)
C66	C65	C64	122.7(3)	C53A	C50	C46	112.7(4)
N3	C41	C42	123.4(3)	C52A	C50	C46	108.3(5)
C3	C2	C1	114.7(2)	C52A	C50	C51A	108.8(5)
C26	C25	C24	121.2(3)	C52A	C50	C53A	108.8(5)
C62	C63	C58	123.0(3)	C52A	C50	C52B	50.1(7)
C78	C77	C76	123.1(3)	C52A	C50	C53B	134.9(7)
C9	C8	C7	121.1(3)	C52B	C50	C46	108.9(7)
C69	C64	B1	122.3(3)	C52B	C50	C51A	138.9(8)
C65	C64	C69	114.5(3)	C52B	C50	C53A	62.6(7)
C65	C64	B1	123.2(2)	C52B	C50	C53B	95.3(9)
C67	C66	C65	120.8(3)	C53B	C50	C46	110.4(6)
N1	C1	C2	110.1(2)	C53B	C50	C53A	33.4(5)
N1	C1	C6	110.3(2)	C51B	C50	C46	115.8(6)
C6	C1	C2	111.5(2)	C51B	C50	C51A	34.3(5)
C72	C71	C70	122.4(3)	C51B	C50	C53A	126.6(6)
C77	C78	C79	120.4(3)	C51B	C50	C52A	75.6(7)
N2	C24	C25	123.5(3)	C51B	C50	C52B	117.8(9)
C42	C43	C44	125.9(3)	C51B	C50	C53B	106.5(8)

C49	C48	C47	117.8(3)	C14	C20	C21A	111.2(5)
C49	C48	C54	121.9(3)	C14	C20	C23B	112.4(9)
C47	C48	C54	120.2(3)	C14	C20	C21B	112.0(9)
C1	C6	C5	115.1(2)	C22A	C20	C14	107.4(4)
C25	C26	C27	126.3(3)	C22A	C20	C21A	106.1(6)
N2	C3	C2	111.1(2)	C22A	C20	C23B	83.2(9)
N2	C3	C4	109.3(2)	C22A	C20	C21B	134.0(10)
C2	C3	C4	110.9(2)	C23A	C20	C14	108.3(5)
C5	C4	C3	115.1(2)	C23A	C20	C22A	110.4(6)
C43	C42	C41	121.6(3)	C23A	C20	C21A	113.3(7)
C60	C59	C58	123.2(3)	C23A	C20	C23B	28.0(9)
C15	C10	C9	122.0(3)	C23A	C20	C22B	132.6(9)
C15	C10	C11	119.5(3)	C23A	C20	C21B	78.9(10)
C11	C10	C9	118.5(3)	C23B	C20	C21A	129.9(10)
C48	C49	C44	121.0(3)	C22B	C20	C14	109.6(7)
C74	C73	C72	118.9(3)	C22B	C20	C22A	30.1(6)
N1	C7	C8	123.6(3)	C22B	C20	C21A	77.6(8)
C81	C80	C79	120.7(3)	C22B	C20	C23B	109.0(11)
C67	C68	C69	120.1(3)	C22B	C20	C21B	111.2(11)
C45	C46	C50	120.4(3)	C21B	C20	C21A	37.1(8)
C47	C46	C45	117.5(3)	C21B	C20	C23B	102.5(12)
C47	C46	C50	122.1(3)	C31	C37	C39	108.1(4)
C31	C32	C27	121.0(4)	C31	C37	C38	110.8(4)
C66	C67	C68	118.8(3)	C40	C37	C31	112.7(3)
C59	C60	C61	120.0(3)	C40	C37	C39	108.8(4)
C58	B1	C70	112.2(2)	C40	C37	C38	108.7(5)
C58	B1	C64	108.7(2)	C38	C37	C39	107.6(4)
C76	B1	C70	107.8(2)	C12	C16	C18	108.8(4)
C76	B1	C58	110.0(2)	C17	C16	C12	110.5(3)
C76	B1	C64	109.9(2)	C17	C16	C18	108.1(4)
C64	B1	C70	108.1(2)	C17	C16	C19	110.7(4)
C80	C81	C76	122.7(3)	C19	C16	C12	111.6(4)
C8	C9	C10	125.6(3)	C19	C16	C18	107.0(4)
C15	C14	C13	117.3(3)	C29	C33	C34B	113.9(6)
C15	C14	C20	119.9(3)	C29	C33	C35B	106.7(7)
C13	C14	C20	122.8(3)	C29	C33	C36A	112.5(6)
C78	C79	C80	118.0(3)	C34B	C33	C35B	110.5(8)
C45	C44	C43	118.7(3)	C34B	C33	C36A	88.9(6)
C45	C44	C49	119.9(3)	C35B	C33	C36A	123.6(7)
C49	C44	C43	121.4(3)	C36B	C33	C29	104.9(6)
C74	C75	C70	123.2(3)	C36B	C33	C34B	112.3(7)
C62	C61	C60	118.7(3)	C36B	C33	C35B	108.2(7)
C73	C72	C71	120.7(3)	C36B	C33	C36A	23.8(6)
C14	C15	C10	121.3(3)	C36B	C33	C34A	128.5(7)
C27	C28	C29	120.3(4)	C34A	C33	C29	107.6(5)
C32	C27	C26	121.9(3)	C34A	C33	C34B	16.5(6)
C28	C27	C26	118.2(3)	C34A	C33	C35B	99.3(7)
C28	C27	C32	119.7(3)	C34A	C33	C36A	105.4(6)
C28	C29	C33	118.2(4)	C35A	C33	C29	118.1(7)
C30	C29	C28	117.9(4)	C35A	C33	C34B	114.4(8)

C30	C29	C33	123.8(3)	C35A	C33	C35B	18.9(7)
C61	C62	C63	120.6(3)	C35A	C33	C36B	90.2(7)
C46	C47	C48	123.3(3)	C35A	C33	C36A	104.7(7)
C12	C11	C10	121.2(3)	C35A	C33	C34A	107.7(7)
C11	C12	C13	117.3(3)	Cl3	C82	Cl2	128.8(10)
C11	C12	C16	118.3(3)				

Hydrogen Atom Coordinates (Å×10^4) and Isotropic Displacement Parameters (Å^2×10^3) for phw1111.

Atom	***x***	***y***	***z***	**U(eq)**
H74	10540	10187	5554	35
H5	315	9756	3838	28
H45	2633	12499	5552	42
H69	10203	8565	6739	30
H65	8717	7132	5828	38
H41	1084	10494	4331	33
H2A	-234	7151	3256	32
H2B	337	6521	3473	32
H25	2016	6787	5336	36
H63	9452	8255	4718	34
H77	10023	5694	5323	29
H8	2145	7251	3552	38
H66	8328	7752	6421	46
H1	248	7638	2726	31
H71	11017	7128	6149	35
H78	10568	4374	5728	31
H24	799	6384	4971	33
H43	1893	11464	4900	37
H6A	-104	8930	2980	29
H6B	533	9200	3058	29
H26	1474	5740	5879	39
H3	120	7062	4260	30
H4A	-188	8558	3990	30
H4B	405	8640	4582	30
H42	2232	9670	4784	35
H59	8926	6000	5286	33
H49	3131	10088	5082	38
H73	11494	9677	5861	41
H7	977	7275	2609	35
H80	10851	5248	7349	37
H68	9810	9185	7329	35
H32	2866	6647	6083	49
H67	8863	8782	7172	41
H60	8145	5832	4371	36
H81	10302	6561	6939	33
H9	1714	6659	2388	43
H79	11000	4133	6751	34
H75	9823	9173	5520	32

H61	8015	6878	3605	42
H72	11728	8147	6167	41
H15	3023	6875	3744	44
H28	2025	5234	6868	51
H62	8684	8065	3789	45
H47	4345	11885	6150	47
H11	2331	5725	2116	45
H30	3740	5804	7769	66
H13	4018	5277	3240	54
H18A	3290	5911	1630	110
H18B	2628	5595	1428	110
H18C	3047	4997	1241	110
H39A	4243	7185	7852	141
H39B	3818	7922	7389	141
H39C	4480	7830	7491	141
H17A	2416	4192	1849	117
H17B	2928	3598	2341	117
H17C	2846	3596	1676	117
H57A	3840	9002	5438	77
H57B	4424	8953	5353	77
H57C	3867	9499	4886	77
H55A	4814	10521	6541	100
H55B	4994	9571	6339	100
H55C	4419	9616	6440	100
H34A	2115	4189	7509	96
H34B	2520	3800	8155	96
H34C	2691	3611	7627	96
H22A	3668	6248	4695	113
H22B	4315	5844	5039	113
H22C	3816	5234	4543	113
H19A	3969	4051	2627	129
H19B	4104	5014	2399	129
H19C	3859	4156	1957	129
H40A	3578	7698	6309	129
H40B	3755	6754	6098	129
H40C	4247	7495	6469	129
H38A	4356	5578	6846	124
H38B	4506	5729	7525	124
H38C	4816	6356	7223	124
H51A	2898	13514	6253	93
H51B	3430	14060	6757	93
H51C	3357	12971	6820	93
H53A	4400	12774	6953	87
H53B	4379	13882	6931	87
H53C	4576	13319	6504	87
H35A	3716	4396	8209	121
H35B	3538	4446	8740	121
H35C	3739	5365	8525	121
H52A	3816	13908	5571	137
H52B	3703	14631	5989	137

H52C	3169	14059	5505	137
H56A	4470	11016	5060	95
H56B	4987	10304	5417	95
H56C	4922	11233	5727	95
H23A	4384	7534	4029	140
H23B	4473	7429	4693	140
H23C	3834	7599	4172	140
H36A	2729	6315	8120	120
H36B	2805	5614	8639	120
H36C	2209	5628	8044	120
H21A	4576	5109	4123	146
H21B	4972	5760	4665	146
H21C	4835	6056	4008	146
H82A	1232	3668	2705	162
H82B	1834	4182	2892	162
H23D	4037	7709	4201	140
H23E	4412	7292	4846	140
H23F	3717	7187	4534	140
H22D	3838	5521	4710	113
H22E	4534	5547	4973	113
H22F	4162	4895	4423	113
H21D	4804	5814	4023	146
H21E	5008	6582	4531	146
H21F	4649	6882	3856	146
H55D	4818	11261	5564	95
H55E	5132	10271	5697	95
H55F	5090	10846	6217	95
H54A	4652	10081	6590	100
H54B	4837	9241	6295	100
H54C	4190	9288	6244	100
H56D	3787	9222	5107	77
H56E	4446	9177	5192	77
H56F	4012	9958	4781	77
H52D	4404	13336	6072	137
H52E	4306	14265	6361	137
H52F	3906	14053	5679	137
H53D	3947	12667	7044	87
H53E	4162	13718	7086	87
H53F	4481	12917	6900	87
H51D	2950	14082	5828	93
H51E	3331	14335	6508	93
H51F	2934	13422	6329	93
H36D	2528	6060	8254	120
H36E	2397	5063	8446	120
H36F	2030	5417	7783	120
H34D	2261	3979	7483	96
H34E	2719	3628	8121	96
H34F	2907	3689	7597	96
H35D	3719	4589	8437	121
H35E	3347	4629	8806	121

H35F	3561	5568	8627	121

6.6.2 $[Zn^{II}(NO_3)\ 3,5\ ^tBuTCT]^+\ [BPh_4]^-$

Identification code	phw1116
Empirical formula	$C_{91}H_{121}BN_4O_{5.5}Zn$
Formula weight	1435.10
Temperature/K	109.95(10)
Crystal system	monoclinic
Space group	C2/c
a/Å	45.5238(13)
b/Å	14.4697(4)
c/Å	25.9797(8)
α/°	90.00
β/°	95.209(2)
γ/°	90.00
Volume/Å^3	17042.5(9)
Z	8
ρ_{calc}mg/mm^3	1.119
m/mm^{-1}	0.340
F(000)	6192.0
Crystal size/mm^3	0.3639 × 0.246 × 0.2113
2Θ range for data collection	5.92 to 59.34°
Index ranges	$-59 \leq h \leq 62$, $-18 \leq k \leq 20$, $-33 \leq l \leq 35$
Reflections collected	42267
Independent reflections	20748[R(int) = 0.0264]
Data/restraints/parameters	20748/27/986
Goodness-of-fit on F^2	1.131
Final R indexes [I>=2σ (I)]	R_1 = 0.0858, wR_2 = 0.2227
Final R indexes [all data]	R_1 = 0.1062, wR_2 = 0.2359
Largest diff. peak/hole / e Å^{-3}	1.29/-0.75

Fractional Atomic Coordinates ($\times 10^4$) and Equivalent Isotropic Displacement Parameters ($Å^2 \times 10^3$) for phw1116. U_{eq} is defined as 1/3 of of the trace of the orthogonalised U_{IJ} tensor.

Atom	*x*	*y*	*z*	U(eq)
B1	2382.7(8)	4823(2)	4099.6(13)	20.5(6)
C58	2124.3(7)	4669(2)	4496.0(12)	22.2(6)
C59	2084.8(8)	5235(2)	4921.0(13)	29.5(7)
C60	1853.9(9)	5122(3)	5230.3(15)	38.8(9)
C61	1647.3(8)	4434(3)	5124.8(15)	37.1(8)
C62	1682.2(7)	3842(3)	4714.8(14)	31.6(7)
C63	1915.9(7)	3959(2)	4411.2(13)	25.8(6)
C64	2236.3(7)	5295(2)	3554.5(12)	23.4(6)
C65	1944.4(8)	5155(3)	3354.2(15)	37.3(8)
C66	1830.5(10)	5538(3)	2884.8(18)	52.8(12)
C67	2004.5(10)	6082(3)	2596.7(15)	41.8(9)
C68	2295.6(9)	6232(2)	2779.9(13)	30.9(7)
C69	2406.0(8)	5849(2)	3248.3(12)	25.9(6)
C70	2647.1(7)	5509(2)	4344.2(11)	20.3(6)
C71	2591.2(7)	6444(2)	4452.0(12)	23.4(6)
C72	2807.2(8)	7047(2)	4660.6(12)	26.7(7)
C73	3094.5(8)	6748(2)	4772.6(13)	29.8(7)
C74	3162.4(7)	5835(2)	4662.9(15)	31.6(7)
C75	2940.9(7)	5239(2)	4453.0(13)	26.2(7)
C76	2529.4(7)	3812(2)	3970.5(11)	20.7(6)
C77	2629.6(7)	3594(2)	3493.2(12)	26.3(6)
C78	2783.6(8)	2777(2)	3410.9(14)	30.6(7)
C79	2840.8(7)	2146(2)	3804.6(13)	26.2(7)
C80	2739.0(7)	2326(2)	4282.7(13)	24.2(6)
C81	2586.2(7)	3145(2)	4363.4(12)	22.3(6)
C1	2699.9(7)	4948(2)	6065.4(12)	24.8(6)
C2	2645.0(7)	5978(2)	5957.7(12)	25.8(6)
C3	2780.7(7)	6632(2)	6379.0(13)	26.3(6)
C4	2693.8(8)	6343(2)	6912.8(13)	29.1(7)
C5	2743.8(7)	5322(2)	7044.7(12)	26.9(7)
C6	2615.1(7)	4694(2)	6606.4(13)	28.0(7)
C7	3063.3(7)	4198(2)	5621.7(12)	25.4(6)
C8	3352.7(7)	3992(2)	5470.8(13)	25.8(6)
C9	3384.4(7)	3504(2)	5041.3(13)	26.4(7)
C10	3658.1(7)	3367(2)	4793.6(13)	26.1(6)
C11	3641.8(7)	2922(2)	4316.8(13)	29.1(7)
C12	3889.1(8)	2819(3)	4038.9(14)	33.1(8)

C13	4154.6(8)	3175(3)	4262.3(15)	34.4(8)
C14	4181.6(7)	3618(2)	4746.9(14)	29.1(7)
C15	3930.5(7)	3711(2)	5006.7(13)	26.6(7)
C16	3855.7(9)	2354(3)	3505.8(16)	42.7(10)
C17	3633.9(13)	2922(4)	3135.6(19)	61.6(13)
C18	3727.1(11)	1386(3)	3553.6(19)	53.4(11)
C19	4141.2(12)	2302(5)	3257(2)	72.5(18)
C20	4480.3(8)	4032(3)	4950.5(16)	35.6(8)
C21	4724.9(8)	3302(3)	4958(2)	48.6(11)
C22	4477.2(9)	4415(4)	5498.4(18)	50.1(11)
C23	4551.9(11)	4828(3)	4589(2)	57.6(13)
C24	3217.6(8)	7452(2)	6274.0(14)	30.7(7)
C25	3529.6(8)	7623(2)	6271.1(15)	33.8(8)
C26	3633.5(8)	8450(3)	6140.6(16)	35.4(8)
C27	3946.0(8)	8701(3)	6139.9(15)	34.5(8)
C28	4024.3(9)	9548(3)	5935.3(19)	45.7(10)
C29	4318.0(9)	9798(3)	5923(2)	49.1(11)
C30	4534.5(9)	9184(3)	6116.8(18)	44(1)
C31	4465.9(8)	8327(3)	6323.5(14)	34.5(8)
C32	4170.1(8)	8096(3)	6332.9(14)	32.1(7)
C33	4404.7(11)	10728(4)	5687(3)	65.1(15)
C34	4736(3)	10888(10)	5734(7)	100(4)
C34A	4601(4)	11257(9)	6107(7)	83(3)
C35	4274(3)	11507(8)	6010(6)	91(3)
C35A	4168(3)	11261(12)	5462(9)	100(4)
C36	4262(3)	10788(8)	5120(6)	83(3)
C36A	4630(4)	10543(9)	5282(7)	91(3)
C37	4702.7(8)	7621(3)	6517.1(15)	39.6(9)
C38	5014.6(9)	8027(4)	6542(2)	61.3(14)
C39	4647.3(9)	7282(4)	7056.1(16)	47.5(10)
C40	4689.5(10)	6799(4)	6143.1(19)	54.3(12)
C41	3147.8(8)	4887(2)	7625.4(13)	30.6(7)
C42	3445.5(9)	4630(3)	7801.1(13)	33.3(8)
C43	3513.4(9)	4319(3)	8285.3(14)	38.1(8)
C44	3800.5(8)	3961(3)	8486.5(13)	36.7(8)
C45	3818.0(8)	3423(3)	8931.2(13)	35.9(8)
C46	4082.3(8)	3006(3)	9122.1(14)	38.6(9)
C47	4329.6(9)	3163(4)	8857.8(15)	48.5(11)
C48	4321.6(9)	3727(4)	8418.2(15)	55.0(13)
C49	4055.5(9)	4112(4)	8238.1(15)	48.3(11)
C50	4089.7(9)	2423(3)	9619.6(16)	44.7(10)

C51	4397.7(11)	2034(4)	9779(2)	62.1(14)
C52	3998.4(10)	3041(4)	10059.6(15)	49.5(11)
C53	3869.3(11)	1615(4)	9540.3(19)	55.5(12)
C54	4597.2(11)	3893(6)	8131.3(19)	84(2)
C55	4878.9(12)	3697(8)	8463(2)	116(4)
C56	4618.3(18)	4926(9)	7994(4)	151(5)
C57	4556.6(15)	3358(9)	7629(2)	138(4)
N1	3011.9(6)	4723.9(19)	6004.1(10)	24.3(5)
N2	3107.8(6)	6665.5(19)	6378.5(11)	25.6(6)
N3	3063.8(6)	5137.6(19)	7162.2(11)	26.4(6)
N4	3884.3(15)	5559(5)	6533(5)	39.5(19)
N4A	3873(5)	5454(15)	6747(11)	39.5(19)
O1	3737.1(10)	5454(3)	6108.5(19)	51.0(11)
O1A	3681(3)	5054(8)	6431(5)	51.0(11)
O2	3725.7(13)	5668(5)	6925(3)	55.2(17)
O2A	3817(4)	5926(14)	7050(8)	55.2(17)
O3	4151.0(11)	5596(4)	6584(3)	57.5(15)
O3A	4133(3)	5187(11)	6730(7)	57.5(15)
Zn1	3299.83(9)	5373.0(3)	6534.76(14)	26.15(11)
C82	3328.8(15)	2924(4)	6705(3)	75.5(17)
C83	3529.2(17)	2152(5)	6735(3)	92(2)
C84	3801(2)	2523(4)	6986(3)	113(3)
C85	3812.5(13)	3458(4)	6720(3)	70.8(15)
C86	3068.2(18)	2199(5)	8463(3)	44(2)
C87	3190(3)	2099(7)	7947(3)	106(6)
C88	3406(3)	1352(8)	8107(4)	84(4)
C89	3235(2)	711(6)	8415(4)	72(3)
O4	3506.3(8)	3755(3)	6664.2(14)	63.7(9)
O5	3033.6(12)	1289(4)	8650(2)	47.1(14)
C90A	4604(4)	274(15)	7521(6)	118(6)
C90B	4094(4)	5(13)	7273(6)	108(5)
C91A	4276(4)	273(15)	7544(6)	115(6)
C91B	4409(4)	110(20)	7487(9)	143(8)
C92A	4254(4)	639(14)	8081(6)	98(5)
C92B	4420(6)	400(20)	8044(9)	197(13)
C93A	4534(3)	444(15)	8412(6)	124(6)
C93B	4129(5)	877(18)	8063(9)	152(10)
O6A	4738(3)	402(10)	8031(5)	145(5)
O6B	3946(4)	475(11)	7650(6)	163(6)

Anisotropic Displacement Parameters ($Å^2 \times 10^3$) for phw1116. The Anisotropic displacement factor exponent takes the form: $-2\pi^2[h^2a^{*2}U_{11}+...+2hka \times b \times U_{12}]$

Atom	U_{11}	U_{22}	U_{33}	U_{23}	U_{13}	U_{12}
B1	24.7(16)	18.8(15)	17.8(15)	-0.6(13)	1.9(12)	1.6(12)
C58	22.2(14)	23.0(14)	21.1(14)	2.5(12)	0.2(11)	2.2(12)
C59	28.3(16)	32.1(17)	28.4(16)	-4.7(14)	4.2(13)	-3.8(13)
C60	38(2)	47(2)	33.5(19)	-9.9(17)	14.2(16)	-2.2(17)
C61	24.6(16)	47(2)	41(2)	5.7(18)	12.1(15)	0.3(15)
C62	25.6(16)	31.5(17)	37.4(18)	6.5(15)	0.9(14)	-2.7(13)
C63	26.2(15)	24.2(15)	26.9(15)	0.2(13)	1.3(12)	-0.9(12)
C64	30.0(16)	18.6(14)	21.3(14)	-0.3(12)	0.9(12)	4.7(12)
C65	32.8(18)	42(2)	35.8(19)	13.8(17)	-6.0(15)	-5.9(16)
C66	44(2)	63(3)	47(2)	23(2)	-20.0(19)	-10(2)
C67	55(2)	38(2)	30.3(18)	13.5(16)	-8.7(17)	3.1(18)
C68	51(2)	21.7(15)	20.6(15)	0.8(13)	6.6(14)	4.5(14)
C69	33.6(17)	22.1(15)	22.4(15)	-1.3(12)	4.4(12)	4.6(13)
C70	24.2(14)	20.8(14)	16.4(13)	2.6(11)	4.9(11)	-0.4(11)
C71	25.9(15)	24.7(15)	19.7(14)	0.6(12)	3.6(11)	2.3(12)
C72	36.8(18)	20.3(14)	23.7(15)	-1.0(12)	5.6(13)	-0.5(13)
C73	31.5(17)	27.4(16)	30.3(17)	-0.5(14)	2.2(13)	-9.5(14)
C74	23.5(15)	29.2(17)	42.1(19)	1.5(15)	3.3(14)	-1.5(13)
C75	23.5(15)	22.5(15)	33.1(17)	2.2(13)	4.5(13)	-0.3(12)
C76	21.6(14)	19.3(14)	20.6(14)	-1.1(11)	-1.4(11)	-0.8(11)
C77	33.5(17)	25.3(15)	20.1(14)	0.7(13)	2.6(12)	0.4(13)
C78	34.5(18)	29.6(17)	27.9(16)	-7.1(14)	4.0(14)	4.0(14)
C79	23.5(15)	20.7(14)	34.5(17)	-4.8(13)	2.5(13)	0.4(12)
C80	21.6(14)	22.3(14)	28.0(15)	2.7(13)	-1.3(12)	-0.7(12)
C81	22.5(14)	23.9(15)	20.6(14)	-0.8(12)	2.4(11)	-1.2(12)
C1	21.6(14)	29.9(16)	23.0(15)	-2.4(13)	3.0(12)	-2.8(12)
C2	21.9(14)	33.3(17)	22.3(14)	1.0(13)	2.4(12)	-1.1(13)
C3	26.7(15)	24.0(15)	27.9(16)	2.4(13)	1.4(12)	-0.1(12)
C4	31.0(17)	27.8(16)	28.7(16)	-2.8(14)	3.9(13)	0.7(13)
C5	29.2(16)	30.0(17)	21.7(14)	0.8(13)	4.7(12)	-4.1(13)
C6	28.1(16)	28.6(16)	27.8(16)	-0.9(14)	5.7(13)	-4.3(13)
C7	23.1(15)	28.2(16)	24.5(15)	-2.2(13)	0.9(12)	-4.7(12)
C8	20.8(14)	27.3(16)	29.1(16)	-1.9(13)	0.5(12)	-1.2(12)
C9	22.5(15)	24.8(15)	31.6(16)	-3.5(13)	0.0(12)	-2.6(12)
C10	25.1(15)	23.7(15)	29.4(16)	-1.8(13)	2.8(12)	-0.5(12)
C11	25.4(15)	31.6(17)	30.7(17)	-6.2(14)	5.3(13)	-5.7(13)
C12	32.3(18)	34.1(18)	34.2(18)	-9.3(15)	10.7(14)	-7.3(14)
C13	27.8(17)	31.5(18)	46(2)	-5.5(16)	14.1(15)	-4.1(14)

C14	24.1(15)	23.3(15)	40.1(19)	-1.4(14)	3.8(13)	-4.7(12)
C15	24.9(15)	25.0(15)	29.9(16)	-4.0(13)	2.6(12)	-3.2(12)
C16	44(2)	47(2)	40(2)	-16.7(18)	17.8(17)	-13.6(18)
C17	77(4)	68(3)	40(2)	-7(2)	8(2)	-1(3)
C18	61(3)	50(3)	51(3)	-20(2)	13(2)	-13(2)
C19	55(3)	103(5)	64(3)	-39(3)	28(2)	-30(3)
C20	24.4(16)	31.8(18)	51(2)	-4.5(17)	4.5(15)	-8.3(14)
C21	23.7(17)	46(2)	76(3)	-7(2)	4.4(18)	-5.1(16)
C22	28.6(19)	63(3)	57(3)	-19(2)	-2.3(18)	-10.5(19)
C23	46(3)	44(2)	82(4)	6(2)	3(2)	-23(2)
C24	27.8(16)	26.4(16)	36.5(18)	2.2(14)	-4.7(14)	-0.7(13)
C25	28.6(17)	26.5(17)	45(2)	2.0(16)	-3.0(15)	0.9(14)
C26	26.7(17)	27.9(17)	50(2)	4.0(16)	-6.0(15)	-0.5(14)
C27	28.4(17)	31.1(18)	44(2)	1.3(16)	-0.3(15)	-4.5(14)
C28	30.8(19)	32(2)	72(3)	8(2)	-4.7(19)	-4.4(15)
C29	33(2)	38(2)	75(3)	12(2)	-3(2)	-10.6(17)
C30	27.0(18)	46(2)	58(3)	-1(2)	-2.4(17)	-10.6(16)
C31	26.5(16)	43(2)	33.4(18)	-5.0(16)	-3.0(14)	-2.3(15)
C32	28.1(17)	33.6(18)	33.5(18)	-2.0(15)	-2.8(14)	-1.9(14)
C33	45(3)	45(3)	105(4)	20(3)	5(3)	-15(2)
C34	67(5)	77(6)	151(9)	52(6)	-8(6)	-31(5)
C34A	95(7)	48(5)	105(8)	22(5)	-2(6)	-26(5)
C35	105(8)	52(5)	117(8)	19(5)	20(7)	-23(5)
C35A	67(5)	77(6)	151(9)	52(6)	-8(6)	-31(5)
C36	95(7)	48(5)	105(8)	22(5)	-2(6)	-26(5)
C36A	105(8)	52(5)	117(8)	19(5)	20(7)	-23(5)
C37	25.8(17)	58(3)	33.6(19)	1.1(18)	-4.3(14)	3.1(17)
C38	30(2)	89(4)	63(3)	13(3)	-7(2)	-2(2)
C39	36(2)	66(3)	38(2)	2(2)	-11.0(17)	-1(2)
C40	45(2)	66(3)	50(3)	-9(2)	-6.9(19)	21(2)
C41	39.6(19)	30.1(17)	22.3(15)	-0.2(14)	4.8(14)	0.7(14)
C42	40.1(19)	35.3(18)	24.8(16)	1.2(15)	4.3(14)	-1.6(15)
C43	38(2)	50(2)	26.1(17)	4.5(16)	1.5(15)	0.8(17)
C44	34.1(18)	53(2)	23.0(16)	5.0(16)	1.8(14)	-3.0(17)
C45	30.7(17)	52(2)	24.4(16)	3.7(16)	1.7(13)	-2.3(16)
C46	33.5(18)	55(2)	27.0(17)	-0.4(17)	-1.0(14)	-0.9(17)
C47	27.7(18)	87(3)	30.3(19)	0(2)	0.0(15)	1(2)
C48	30.2(19)	108(4)	26.5(18)	3(2)	3.5(15)	-9(2)
C49	38(2)	79(3)	27.3(18)	10(2)	3.4(15)	-8(2)
C50	41(2)	57(3)	35(2)	10.2(19)	-7.3(16)	1.8(19)

C51	51(3)	83(4)	49(3)	14(3)	-10(2)	15(3)
C52	53(3)	66(3)	28.9(19)	10(2)	-1.9(17)	-4(2)
C53	61(3)	55(3)	48(3)	8(2)	-9(2)	-7(2)
C54	37(2)	181(8)	35(2)	4(3)	6.9(19)	-21(3)
C55	35(3)	265(11)	51(3)	3(5)	13(2)	-2(4)
C56	74(5)	259(13)	124(7)	63(8)	36(5)	-62(7)
C57	57(4)	307(14)	56(4)	-29(6)	33(3)	-21(6)
N1	22.7(13)	27.2(14)	22.9(12)	1.4(11)	0.7(10)	-0.6(10)
N2	23.3(13)	26.6(13)	26.2(13)	-0.7(11)	-1.7(10)	-2.2(11)
N3	32.2(14)	22.5(13)	24.0(13)	-1.5(11)	0.0(11)	-2.1(11)
N4	27.8(18)	36(3)	55(6)	-4(4)	3(3)	-3.2(17)
N4A	27.8(18)	36(3)	55(6)	-4(4)	3(3)	-3.2(17)
O1	53(2)	37(2)	58(3)	-11.0(18)	-19(2)	2.8(18)
O1A	53(2)	37(2)	58(3)	-11.0(18)	-19(2)	2.8(18)
O2	36(4)	66(4)	66(4)	28(3)	16(3)	7(3)
O2A	36(4)	66(4)	66(4)	28(3)	16(3)	7(3)
O3	23.5(16)	56(4)	92(4)	-7(3)	0(2)	-3(2)
O3A	23.5(16)	56(4)	92(4)	-7(3)	0(2)	-3(2)
Zn1	28.1(2)	27.3(2)	22.17(19)	0.45(15)	-2.40(14)	-4.74(15)
C82	92(4)	63(4)	72(4)	-8(3)	10(3)	-20(3)
C83	107(6)	77(4)	88(5)	8(4)	-13(4)	-11(4)
C84	148(7)	52(4)	124(6)	-1(4)	-66(6)	9(4)
C85	64(3)	68(4)	79(4)	6(3)	2(3)	14(3)
C86	43(4)	61(5)	29(4)	-21(4)	9(3)	-30(4)
C87	120(12)	46(6)	140(13)	24(7)	-57(10)	-54(7)
C88	103(10)	106(10)	45(6)	-7(6)	8(6)	-27(8)
C89	71(7)	93(8)	58(6)	-29(6)	44(5)	-11(6)
O4	67(2)	58(2)	64(2)	-4.4(18)	-4.1(18)	5.3(18)
O5	39(3)	54(4)	51(3)	5(3)	17(3)	7(3)

Bond Lengths for phw1116.

Atom	Atom	Length/Å	Atom	Atom	Length/Å
B1	C58	1.648(5)	C29	C33	1.544(6)
B1	C64	1.657(4)	C30	C31	1.397(6)
B1	C70	1.643(5)	C31	C32	1.390(5)
B1	C76	1.655(4)	C31	C37	1.536(5)
C58	C59	1.399(5)	C33	C34	1.522(12)
C58	C63	1.402(4)	C33	C34A	1.548(16)

C59	C60	1.389(5)	C33	C35	1.555(15)
C60	C61	1.380(6)	C33	C35A	1.409(16)
C61	C62	1.387(5)	C33	C36	1.558(14)
C62	C63	1.391(5)	C33	C36A	1.557(18)
C64	C65	1.397(5)	C37	C38	1.532(6)
C64	C69	1.408(5)	C37	C39	1.526(6)
C65	C66	1.396(5)	C37	C40	1.534(6)
C66	C67	1.384(6)	C41	C42	1.439(5)
C67	C68	1.384(6)	C41	N3	1.282(4)
C68	C69	1.389(5)	C42	C43	1.345(5)
C70	C71	1.410(4)	C43	C44	1.458(5)
C70	C75	1.397(4)	C44	C45	1.389(5)
C71	C72	1.388(5)	C44	C49	1.396(5)
C72	C73	1.383(5)	C45	C46	1.396(5)
C73	C74	1.391(5)	C46	C47	1.389(6)
C74	C75	1.400(5)	C46	C50	1.542(6)
C76	C77	1.396(4)	C47	C48	1.401(6)
C76	C81	1.412(4)	C48	C49	1.376(6)
C77	C78	1.401(5)	C48	C54	1.535(6)
C78	C79	1.378(5)	C50	C51	1.532(6)
C79	C80	1.389(5)	C50	C52	1.538(6)
C80	C81	1.399(4)	C50	C53	1.542(6)
C1	C2	1.533(5)	C54	C55	1.505(8)
C1	C6	1.535(4)	C54	C56	1.542(14)
C1	N1	1.480(4)	C54	C57	1.515(10)
C2	C3	1.534(5)	N1	Zn1	2.043(3)
C3	C4	1.534(5)	N2	Zn1	2.089(3)
C3	N2	1.490(4)	N3	Zn1	2.061(3)
C4	C5	1.530(5)	N4	O1	1.246(12)
C5	C6	1.531(5)	N4	O2	1.312(14)
C5	N3	1.485(4)	N4	O3	1.211(8)
C7	C8	1.439(4)	N4A	O1A	1.28(2)
C7	N1	1.290(4)	N4A	O2A	1.09(3)
C8	C9	1.339(5)	N4A	O3A	1.25(3)
C9	C10	1.467(4)	O1	Zn1	2.367(5)
C10	C11	1.392(5)	O1A	Zn1	1.838(12)
C10	C15	1.403(4)	O2	Zn1	2.148(6)
C11	C12	1.399(5)	C82	C83	1.439(9)
C12	C13	1.391(5)	C82	O4	1.459(7)
C12	C16	1.534(5)	C83	C84	1.447(10)
C13	C14	1.409(5)	C84	C85	1.523(9)

C14	C15	1.386(5)	C85	O4	1.454(6)
C14	C20	1.535(5)	C86	C87	1.505(5)
C16	C17	1.563(7)	C86	O5	1.417(5)
C16	C18	1.528(6)	C87	C88	1.495(5)
C16	C19	1.504(6)	C88	C89	1.491(5)
C20	C21	1.533(5)	C89	O5	1.418(5)
C20	C22	1.529(6)	C90A	C91A	1.501(5)
C20	C23	1.540(6)	C90A	O6A	1.420(5)
C24	C25	1.442(5)	C90B	C91B	1.496(5)
C24	N2	1.281(4)	C90B	O6B	1.413(5)
C25	C26	1.341(5)	C91A	C92A	1.504(5)
C26	C27	1.469(5)	C91B	C92B	1.502(5)
C27	C28	1.395(5)	C92A	C93A	1.497(5)
C27	C32	1.402(5)	C92B	C93B	1.499(5)
C28	C29	1.388(6)	C93A	O6A	1.421(5)
C29	C30	1.387(6)	C93B	O6B	1.420(5)

Bond Angles for phw1116.

Atom	**Atom**	**Atom**	**Angle/°**	**Atom**	**Atom**	**Atom**	**Angle/°**
C58	B1	C64	109.6(2)	C34	C33	C36A	51.0(9)
C58	B1	C76	109.4(2)	C34A	C33	C35	59.1(9)
C70	B1	C58	112.3(2)	C34A	C33	C36	143.4(7)
C70	B1	C64	107.7(2)	C34A	C33	C36A	100.8(10)
C70	B1	C76	108.5(2)	C35	C33	C36	108.7(8)
C76	B1	C64	109.3(2)	C35	C33	C36A	142.7(7)
C59	C58	B1	124.4(3)	C35A	C33	C29	115.4(6)
C59	C58	C63	114.8(3)	C35A	C33	C34	131.7(8)
C63	C58	B1	120.8(3)	C35A	C33	C34A	113.1(11)
C60	C59	C58	123.1(3)	C35A	C33	C35	60.7(11)
C61	C60	C59	120.5(3)	C35A	C33	C36	48.5(10)
C60	C61	C62	118.3(3)	C35A	C33	C36A	109.8(12)
C61	C62	C63	120.5(3)	C36A	C33	C36	67.4(9)
C62	C63	C58	122.8(3)	C38	C37	C31	112.3(4)
C65	C64	B1	123.6(3)	C38	C37	C40	107.8(4)
C65	C64	C69	115.1(3)	C39	C37	C31	110.2(3)
C69	C64	B1	121.3(3)	C39	C37	C38	108.3(3)
C66	C65	C64	122.2(4)	C39	C37	C40	109.4(4)
C67	C66	C65	120.9(4)	C40	C37	C31	108.8(3)
C68	C67	C66	118.7(3)	N3	C41	C42	124.3(3)

C67	C68	C69	119.8(3)	C43	C42	C41	120.9(3)
C68	C69	C64	123.3(3)	C42	C43	C44	125.2(4)
C71	C70	B1	121.2(3)	C45	C44	C43	118.6(3)
C75	C70	B1	124.3(3)	C45	C44	C49	119.0(4)
C75	C70	C71	114.5(3)	C49	C44	C43	122.3(4)
C72	C71	C70	123.2(3)	C44	C45	C46	121.4(4)
C73	C72	C71	120.5(3)	C45	C46	C50	119.1(3)
C72	C73	C74	118.5(3)	C47	C46	C45	117.6(4)
C73	C74	C75	119.9(3)	C47	C46	C50	123.2(4)
C70	C75	C74	123.3(3)	C46	C47	C48	122.4(4)
C77	C76	B1	123.4(3)	C47	C48	C54	121.6(4)
C77	C76	C81	115.8(3)	C49	C48	C47	118.0(4)
C81	C76	B1	120.6(3)	C49	C48	C54	120.3(4)
C76	C77	C78	122.3(3)	C48	C49	C44	121.6(4)
C79	C78	C77	120.6(3)	C46	C50	C53	109.8(3)
C78	C79	C80	118.9(3)	C51	C50	C46	112.2(4)
C79	C80	C81	120.2(3)	C51	C50	C52	108.3(4)
C80	C81	C76	122.1(3)	C51	C50	C53	109.0(4)
C2	C1	C6	110.5(3)	C52	C50	C46	108.5(4)
N1	C1	C2	109.6(3)	C52	C50	C53	108.9(4)
N1	C1	C6	111.7(3)	C48	C54	C56	109.6(6)
C1	C2	C3	114.9(3)	C55	C54	C48	112.6(4)
C2	C3	C4	110.9(3)	C55	C54	C56	104.3(7)
N2	C3	C2	110.9(3)	C55	C54	C57	115.4(7)
N2	C3	C4	110.4(3)	C57	C54	C48	107.3(5)
C5	C4	C3	114.9(3)	C57	C54	C56	107.5(7)
C4	C5	C6	111.6(3)	C1	N1	Zn1	113.0(2)
N3	C5	C4	110.0(3)	C7	N1	C1	117.1(3)
N3	C5	C6	110.4(3)	C7	N1	Zn1	129.9(2)
C5	C6	C1	115.3(3)	C3	N2	Zn1	111.8(2)
N1	C7	C8	124.5(3)	C24	N2	C3	116.0(3)
C9	C8	C7	120.4(3)	C24	N2	Zn1	132.2(2)
C8	C9	C10	126.6(3)	C5	N3	Zn1	112.3(2)
C11	C10	C9	118.3(3)	C41	N3	C5	116.6(3)
C11	C10	C15	119.3(3)	C41	N3	Zn1	131.1(3)
C15	C10	C9	122.3(3)	O1	N4	O2	114.4(6)
C10	C11	C12	121.9(3)	O3	N4	O1	123.8(11)
C11	C12	C16	119.6(3)	O3	N4	O2	121.8(10)
C13	C12	C11	117.0(3)	O2A	N4A	O1A	124(2)
C13	C12	C16	123.3(3)	O2A	N4A	O3A	120(2)
C12	C13	C14	122.9(3)	O3A	N4A	O1A	116(2)

C13	C14	C20	119.2(3)	N4	O1	Zn1	90.0(5)
C15	C14	C13	118.1(3)	N4A	O1A	Zn1	113.0(13)
C15	C14	C20	122.6(3)	N4	O2	Zn1	98.4(5)
C14	C15	C10	120.8(3)	N1	Zn1	N2	92.80(11)
C12	C16	C17	109.3(4)	N1	Zn1	N3	96.26(11)
C18	C16	C12	109.6(3)	N1	Zn1	O1	102.85(13)
C18	C16	C17	107.5(4)	N1	Zn1	O2	155.0(2)
C19	C16	C12	113.0(4)	N2	Zn1	O1	102.69(13)
C19	C16	C17	107.3(4)	N2	Zn1	O2	104.9(2)
C19	C16	C18	109.9(4)	N3	Zn1	N2	93.59(11)
C14	C20	C23	108.2(3)	N3	Zn1	O1	154.08(14)
C21	C20	C14	110.8(3)	N3	Zn1	O2	99.9(2)
C21	C20	C23	109.2(4)	O1A	Zn1	N1	110.0(3)
C22	C20	C14	112.3(3)	O1A	Zn1	N2	125.4(4)
C22	C20	C21	107.8(4)	O1A	Zn1	N3	129.9(4)
C22	C20	C23	108.4(4)	O1A	Zn1	O1	25.7(4)
N2	C24	C25	123.9(3)	O1A	Zn1	O2	45.2(4)
C26	C25	C24	121.7(3)	O2	Zn1	O1	56.6(2)
C25	C26	C27	125.8(3)	C83	C82	O4	106.9(5)
C28	C27	C26	120.0(3)	C82	C83	C84	104.4(6)
C28	C27	C32	118.8(3)	C83	C84	C85	100.9(5)
C32	C27	C26	121.2(3)	O4	C85	C84	103.6(6)
C29	C28	C27	121.2(4)	O5	C86	C87	106.1(6)
C28	C29	C33	121.2(4)	C88	C87	C86	96.2(8)
C30	C29	C28	118.6(4)	C89	C88	C87	103.7(9)
C30	C29	C33	120.2(4)	O5	C89	C88	104.7(8)
C29	C30	C31	122.1(4)	C85	O4	C82	106.3(4)
C30	C31	C37	122.8(3)	C86	O5	C89	107.8(6)
C32	C31	C30	118.1(4)	O6A	C90A	C91A	108.1(14)
C32	C31	C37	119.1(4)	O6B	C90B	C91B	101.1(17)
C31	C32	C27	121.2(4)	C90A	C91A	C92A	100.7(14)
C29	C33	C34A	107.7(6)	C90B	C91B	C92B	110(2)
C29	C33	C35	107.1(6)	C93A	C92A	C91A	110.0(15)
C29	C33	C36	108.9(5)	C93B	C92B	C91B	102(2)
C29	C33	C36A	109.0(6)	O6A	C93A	C92A	100.7(14)
C34	C33	C29	112.9(6)	O6B	C93B	C92B	104.2(19)
C34	C33	C34A	50.5(8)	C90A	O6A	C93A	113.6(14)
C34	C33	C35	105.8(9)	C90B	O6B	C93B	115.9(17)
C34	C33	C36	113.2(9)				

Torsion Angles for phw1116.

A	**B**	**C**	**D**	**Angle/°**
B1	C58	C59	C60	176.0(3)
B1	C58	C63	C62	-175.5(3)
B1	C64	C65	C66	-177.8(4)
B1	C64	C69	C68	177.6(3)
B1	C70	C71	C72	179.7(3)
B1	C70	C75	C74	-179.8(3)
B1	C76	C77	C78	172.4(3)
B1	C76	C81	C80	-172.8(3)
C58	B1	C64	C65	-29.8(4)
C58	B1	C64	C69	152.7(3)
C58	B1	C70	C71	-64.3(4)
C58	B1	C70	C75	117.0(3)
C58	B1	C76	C77	145.9(3)
C58	B1	C76	C81	-40.4(4)
C58	C59	C60	C61	-0.6(6)
C59	C58	C63	C62	2.0(5)
C59	C60	C61	C62	2.2(6)
C60	C61	C62	C63	-1.7(6)
C61	C62	C63	C58	-0.5(5)
C63	C58	C59	C60	-1.5(5)
C64	B1	C58	C59	-102.9(3)
C64	B1	C58	C63	74.4(3)
C64	B1	C70	C71	56.5(4)
C64	B1	C70	C75	-122.3(3)
C64	B1	C76	C77	25.9(4)
C64	B1	C76	C81	-160.3(3)
C64	C65	C66	C67	-0.3(8)
C65	C64	C69	C68	-0.1(5)
C65	C66	C67	C68	0.7(7)
C66	C67	C68	C69	-0.9(6)
C67	C68	C69	C64	0.6(5)
C69	C64	C65	C66	-0.1(6)
C70	B1	C58	C59	16.8(4)
C70	B1	C58	C63	-165.9(3)
C70	B1	C64	C65	-152.2(3)
C70	B1	C64	C69	30.2(4)
C70	B1	C76	C77	-91.3(3)
C70	B1	C76	C81	82.4(3)
C70	C71	C72	C73	0.3(5)

C71	C70	C75	C74	1.4(5)
C71	C72	C73	C74	1.1(5)
C72	C73	C74	C75	-1.2(5)
C73	C74	C75	C70	-0.1(5)
C75	C70	C71	C72	-1.5(4)
C76	B1	C58	C59	137.4(3)
C76	B1	C58	C63	-45.3(4)
C76	B1	C64	C65	90.1(4)
C76	B1	C64	C69	-87.5(3)
C76	B1	C70	C71	174.7(3)
C76	B1	C70	C75	-4.0(4)
C76	C77	C78	C79	0.4(5)
C77	C76	C81	C80	1.3(4)
C77	C78	C79	C80	1.0(5)
C78	C79	C80	C81	-1.2(5)
C79	C80	C81	C76	0.0(5)
C81	C76	C77	C78	-1.6(5)
C1	C2	C3	C4	-51.3(4)
C1	C2	C3	N2	71.8(3)
C1	N1	Zn1	N2	-50.6(2)
C1	N1	Zn1	N3	43.3(2)
C1	N1	Zn1	O1	-154.3(2)
C1	N1	Zn1	O1A	179.9(5)
C1	N1	Zn1	O2	173.6(4)
C2	C1	C6	C5	-49.9(4)
C2	C1	N1	C7	-112.3(3)
C2	C1	N1	Zn1	64.7(3)
C2	C3	C4	C5	50.0(4)
C2	C3	N2	C24	116.9(3)
C2	C3	N2	Zn1	-61.6(3)
C3	C4	C5	C6	-49.1(4)
C3	C4	C5	N3	73.8(3)
C3	N2	Zn1	N1	48.7(2)
C3	N2	Zn1	N3	-47.8(2)
C3	N2	Zn1	O1	152.5(2)
C3	N2	Zn1	O1A	165.7(5)
C3	N2	Zn1	O2	-149.1(3)
C4	C3	N2	C24	-119.8(3)
C4	C3	N2	Zn1	61.7(3)
C4	C5	C6	C1	49.2(4)
C4	C5	N3	C41	115.1(3)

C4	C5	N3	Zn1	-63.4(3)
C5	N3	Zn1	N1	-44.6(2)
C5	N3	Zn1	N2	48.6(2)
C5	N3	Zn1	O1	177.9(3)
C5	N3	Zn1	O1A	-167.3(5)
C5	N3	Zn1	O2	154.5(3)
C6	C1	C2	C3	51.0(4)
C6	C1	N1	C7	124.9(3)
C6	C1	N1	Zn1	-58.0(3)
C6	C5	N3	C41	-121.4(3)
C6	C5	N3	Zn1	60.2(3)
C7	C8	C9	C10	169.4(3)
C7	N1	Zn1	N2	125.9(3)
C7	N1	Zn1	N3	-140.2(3)
C7	N1	Zn1	O1	22.2(3)
C7	N1	Zn1	O1A	-3.6(5)
C7	N1	Zn1	O2	-9.8(6)
C8	C7	N1	C1	172.9(3)
C8	C7	N1	Zn1	-3.5(5)
C8	C9	C10	C11	-173.0(3)
C8	C9	C10	C15	3.6(6)
C9	C10	C11	C12	175.7(3)
C9	C10	C15	C14	-176.1(3)
C10	C11	C12	C13	0.6(6)
C10	C11	C12	C16	-177.7(4)
C11	C10	C15	C14	0.5(5)
C11	C12	C13	C14	0.4(6)
C11	C12	C16	C17	60.3(5)
C11	C12	C16	C18	-57.4(5)
C11	C12	C16	C19	179.7(4)
C12	C13	C14	C15	-0.8(6)
C12	C13	C14	C20	-177.0(4)
C13	C12	C16	C17	-117.9(4)
C13	C12	C16	C18	124.5(4)
C13	C12	C16	C19	1.5(6)
C13	C14	C15	C10	0.4(5)
C13	C14	C20	C21	-54.7(5)
C13	C14	C20	C22	-175.3(4)
C13	C14	C20	C23	65.0(5)
C15	C10	C11	C12	-1.0(5)
C15	C14	C20	C21	129.4(4)

C15	C14	C20	C22	8.7(5)
C15	C14	C20	C23	-110.9(4)
C16	C12	C13	C14	178.5(4)
C20	C14	C15	C10	176.4(3)
C24	C25	C26	C27	178.1(4)
C24	N2	Zn1	N1	-129.5(3)
C24	N2	Zn1	N3	134.0(3)
C24	N2	Zn1	O1	-25.7(3)
C24	N2	Zn1	O1A	-12.5(6)
C24	N2	Zn1	O2	32.7(4)
C25	C24	N2	C3	178.0(3)
C25	C24	N2	Zn1	-3.8(6)
C25	C26	C27	C28	172.1(4)
C25	C26	C27	C32	-6.6(6)
C26	C27	C28	C29	-179.1(4)
C26	C27	C32	C31	178.8(4)
C27	C28	C29	C30	0.3(8)
C27	C28	C29	C33	178.9(5)
C28	C27	C32	C31	0.1(6)
C28	C29	C30	C31	-0.1(7)
C28	C29	C33	C34	177.4(10)
C28	C29	C33	C34A	123.6(9)
C28	C29	C33	C35	61.3(9)
C28	C29	C33	C35A	-3.8(14)
C28	C29	C33	C36	-56.1(9)
C28	C29	C33	C36A	-127.9(9)
C29	C30	C31	C32	-0.2(6)
C29	C30	C31	C37	177.1(4)
C30	C29	C33	C34	-4.1(11)
C30	C29	C33	C34A	-57.9(10)
C30	C29	C33	C35	-120.1(8)
C30	C29	C33	C35A	174.7(12)
C30	C29	C33	C36	122.4(8)
C30	C29	C33	C36A	50.6(10)
C30	C31	C32	C27	0.1(6)
C30	C31	C37	C38	9.7(6)
C30	C31	C37	C39	130.5(4)
C30	C31	C37	C40	-109.6(5)
C32	C27	C28	C29	-0.3(7)
C32	C31	C37	C38	-173.1(4)
C32	C31	C37	C39	-52.2(5)

C32	C31	C37	C40	67.6(5)
C33	C29	C30	C31	-178.6(5)
C37	C31	C32	C27	-177.3(3)
C41	C42	C43	C44	174.0(4)
C41	N3	Zn1	N1	137.3(3)
C41	N3	Zn1	N2	-129.5(3)
C41	N3	Zn1	O1	-0.3(5)
C41	N3	Zn1	O1A	14.6(6)
C41	N3	Zn1	O2	-23.7(4)
C42	C41	N3	C5	176.3(3)
C42	C41	N3	Zn1	-5.6(5)
C42	C43	C44	C45	-161.4(4)
C42	C43	C44	C49	16.3(7)
C43	C44	C45	C46	175.4(4)
C43	C44	C49	C48	-176.5(5)
C44	C45	C46	C47	1.4(6)
C44	C45	C46	C50	179.5(4)
C45	C44	C49	C48	1.2(7)
C45	C46	C47	C48	0.8(7)
C45	C46	C50	C51	-178.8(4)
C45	C46	C50	C52	-59.2(5)
C45	C46	C50	C53	59.8(5)
C46	C47	C48	C49	-1.9(8)
C46	C47	C48	C54	180.0(5)
C47	C46	C50	C51	-0.8(6)
C47	C46	C50	C52	118.9(5)
C47	C46	C50	C53	-122.2(5)
C47	C48	C49	C44	0.9(8)
C47	C48	C54	C55	-20.7(10)
C47	C48	C54	C56	-136.3(6)
C47	C48	C54	C57	107.3(7)
C49	C44	C45	C46	-2.4(6)
C49	C48	C54	C55	161.3(7)
C49	C48	C54	C56	45.7(8)
C49	C48	C54	C57	-70.7(9)
C50	C46	C47	C48	-177.3(5)
C54	C48	C49	C44	179.0(5)
N1	C1	C2	C3	-72.5(3)
N1	C1	C6	C5	72.4(4)
N1	C7	C8	C9	-174.2(3)
N2	C3	C4	C5	-73.3(4)

N2	C24	C25	C26	177.5(4)
N3	C5	C6	C1	-73.4(4)
N3	C41	C42	C43	-175.9(4)
N4	O1	Zn1	N1	-159.6(4)
N4	O1	Zn1	N2	104.5(4)
N4	O1	Zn1	N3	-23.1(6)
N4	O1	Zn1	O1A	-50.0(9)
N4	O1	Zn1	O2	4.9(5)
N4	O2	Zn1	N1	33.6(8)
N4	O2	Zn1	N2	-100.2(5)
N4	O2	Zn1	N3	163.3(5)
N4	O2	Zn1	O1	-4.7(5)
N4	O2	Zn1	O1A	25.3(7)
N4A	O1A	Zn1	N1	178.8(15)
N4A	O1A	Zn1	N2	70.0(16)
N4A	O1A	Zn1	N3	-64.1(16)
N4A	O1A	Zn1	O1	101.0(18)
N4A	O1A	Zn1	O2	-4.9(14)
O1	N4	O2	Zn1	8.2(8)
O2	N4	O1	Zn1	-7.3(7)
O2A	N4A	O1A	Zn1	1(3)
O3	N4	O1	Zn1	175.5(8)
O3	N4	O2	Zn1	-174.6(7)
O3A	N4A	O1A	Zn1	172.6(17)
C82	C83	C84	C85	-41.5(8)
C83	C82	O4	C85	-5.3(7)
C83	C84	C85	O4	38.0(8)
C84	C85	O4	C82	-20.2(6)
C86	C87	C88	C89	43.7(10)
C87	C86	O5	C89	25.0(10)
C87	C88	C89	O5	-31.4(12)
C88	C89	O5	C86	3.9(11)
O4	C82	C83	C84	30.2(8)
O5	C86	C87	C88	-42.3(9)
C90A	C91A	C92A	C93A	-25(2)
C90B	C91B	C92B	C93B	-26(3)
C91A	C90A	O6A	C93A	3(2)
C91A	C92A	C93A	O6A	26(2)
C91B	C90B	O6B	C93B	2(3)
C91B	C92B	C93B	O6B	25(3)
C92A	C93A	O6A	C90A	-18(2)

C92B	C93B	O6B	C90B	-18(3)
O6A	C90A	C91A	C92A	13(2)
O6B	C90B	C91B	C92B	16(3)

Hydrogen Atom Coordinates ($Å \times 10^4$) and Isotropic Displacement Parameters ($Å^2 \times 10^3$) for phw1116.

Atom	***x***	***y***	***z***	**U(eq)**
H59	2222	5719	5002	35
H60	1838	5522	5517	47
H61	1485	4368	5328	45
H62	1546	3353	4641	38
H63	1935	3540	4135	31
H65	1819	4787	3544	45
H66	1631	5424	2762	63
H67	1926	6348	2279	50
H68	2420	6596	2586	37
H69	2606	5966	3368	31
H71	2396	6673	4378	28
H72	2757	7671	4727	32
H73	3242	7156	4921	36
H74	3359	5617	4730	38
H75	2993	4619	4381	31
H77	2592	4015	3214	32
H78	2849	2657	3081	37
H79	2948	1597	3750	31
H80	2773	1892	4556	29
H81	2519	3255	4693	27
H1	2573	4583	5805	30
H2A	2429	6085	5913	31
H2B	2725	6137	5627	31
H3	2702	7267	6303	32
H4A	2808	6720	7179	35
H4B	2482	6487	6931	35
H5	2642	5179	7361	32
H6A	2397	4706	6601	34
H6B	2680	4052	6685	34
H7	2899	3928	5426	30
H8	3522	4204	5677	31
H9	3212	3217	4881	32
H11	3458	2681	4176	35

H13	4325	3116	4080	41
H15	3943	4012	5333	32
H17A	3443	2951	3280	92
H17B	3610	2622	2796	92
H17C	3710	3550	3098	92
H18A	3861	1013	3785	80
H18B	3703	1095	3212	80
H18C	3535	1429	3694	80
H19A	4213	2929	3201	109
H19B	4108	1980	2925	109
H19C	4288	1964	3485	109
H21A	4682	2799	5192	73
H21B	4914	3585	5078	73
H21C	4735	3056	4609	73
H22A	4316	4861	5508	75
H22B	4665	4724	5600	75
H22C	4449	3908	5738	75
H23A	4578	4581	4245	86
H23B	4734	5135	4728	86
H23C	4389	5275	4564	86
H24	3086	7951	6194	37
H25	3665	7138	6364	41
H26	3492	8914	6040	43
H28	3874	9961	5802	55
H30	4736	9351	6109	53
H32	4119	7517	6473	38
H34A	4818	10748	6087	149
H34B	4777	11535	5654	149
H34C	4828	10484	5491	149
H34D	4490	11363	6408	125
H34E	4659	11852	5968	125
H34F	4778	10891	6211	125
H35A	4066	11374	6049	136
H35B	4289	12100	5832	136
H35C	4384	11540	6351	136
H35D	4055	10897	5195	149
H35E	4245	11817	5305	149
H35F	4040	11441	5728	149
H36A	4341	10296	4914	125
H36B	4307	11390	4974	125
H36C	4047	10716	5117	125

H36D	4797	10190	5444	136
H36E	4700	11133	5155	136
H36F	4534	10189	4993	136
H38A	5058	8222	6196	92
H38B	5158	7557	6671	92
H38C	5028	8561	6775	92
H39A	4656	7807	7296	71
H39B	4798	6828	7174	71
H39C	4452	6994	7044	71
H40A	4500	6481	6152	81
H40B	4851	6369	6246	81
H40C	4709	7022	5792	81
H41	3004	4870	7869	37
H42	3596	4680	7572	40
H43	3362	4335	8514	46
H45	3647	3338	9109	43
H47	4511	2878	8980	58
H49	4045	4489	7938	58
H51A	4536	2545	9858	93
H51B	4464	1665	9495	93
H51C	4390	1644	10086	93
H52A	4137	3557	10113	74
H52B	4000	2677	10378	74
H52C	3799	3282	9968	74
H53A	3871	1257	9861	83
H53B	3926	1215	9262	83
H53C	3671	1859	9448	83
H55A	4866	3955	8809	174
H55B	5045	3981	8307	174
H55C	4909	3028	8489	174
H56A	4449	5098	7752	226
H56B	4802	5039	7833	226
H56C	4617	5298	8309	226
H57A	4599	2703	7696	208
H57B	4692	3600	7388	208
H57C	4353	3426	7476	208
H82A	3220	2951	7018	91
H82B	3184	2863	6399	91
H83A	3559	1918	6386	110
H83B	3454	1643	6941	110
H84A	3972	2133	6922	135

H84B	3790	2590	7363	135
H85A	3937	3899	6935	85
H85B	3891	3398	6379	85
H86A	3206	2555	8705	53
H86B	2876	2524	8425	53
H87A	3039	1897	7672	128
H87B	3288	2671	7839	128
H88A	3474	1034	7802	101
H88B	3579	1604	8319	101
H89A	3128	246	8189	86
H89B	3367	387	8681	86
H90C	4668	-320	7379	142
H90D	4661	779	7294	142
H90A	4058	301	6929	130
H90B	4035	-653	7246	130
H91C	4192	-358	7503	139
H91D	4175	684	7279	139
H91A	4507	580	7286	171
H91B	4514	-484	7459	171
H92C	4218	1314	8066	118
H92D	4086	343	8234	118
H92A	4437	-142	8278	236
H92B	4587	826	8135	236
H93C	4583	948	8663	149
H93D	4523	-149	8599	149
H93A	4048	767	8398	183
H93B	4150	1551	8011	183

Abbreviations

3,5 ^{t}BuTCT	*Cis,cis* - 1,3,5 – *tris* (3,5- ditertbutylphenylpropenylideneimino) cyclohexane
Å	Angstrom
^{t}Bu	tertiary butyl
C	Celsius
CA	carbonic anhydrase
cm	centimetres
d	doublet
Da	Dalton
DCM	dichloromethane
DMF	dimethyl formamide
Et	ethyl
EtOH	ethanol
HCAII	human carbonic anhydrase II
HCO_3^-	bicarbonate
IR	Infra red (spectroscopy)
J	coupling constant
L	ligand, 3,5 ^{t}BuTCT
LADH	liver alcohol dehydrogenase
LIFDI	Liquid Injection Field Desorption Ionisation
m	multiplet
Me	Methyl
MeOH	methanol

mg	milligrams
MHz	megahertz
mL	millilitres
mmol	millimoles
MS	mass spectroscopy
NO_3	nitrate
NMR	nuclear magnetic resonance (spectroscopy)
OAc	acetate
Ph	phenyl
ppm	parts per million
q	quartet
s	singlet
tach	*cis*, *cis* - 1,3,5 – triaminocyclohexane
TBAH	n-tetrabutyl ammonium hydroxide
TBT	*cis*, *cis* – 1,3,5 - *tris*[(E,E) - benzylideneamino] cyclohexane
TCT	*cis*, *cis* – 1,3,5 - *tris*[(E,E) - phenylpropylideneamino] cyclohexane
THF	tetrahydrofuran
UV	ultraviolet
Vis	visible

Amino acids

Ala	Alanine
Asn	Asparagine
Asp	Aspartic acid
Gln	Glutamine
Glu	Glutamic acid
His	Histidine
Leu	Leucine
Thr	Threonine
Phe	Phenylalanine
Trp	Tryptophan
Val	Valine

Chapter 7: *References*

1

1. P. O. Nyman and S. Lindskog, *Biochimica Et Biophysica Acta*, 1964, **85**, 141-&.
2. J. F. Domsic, B. S. Avvaru, C. U. Kim, S. M. Gruner, M. Agbandje-McKenna, D. N. Silverman and R. McKenna, *Journal of Biological Chemistry*, 2008, **283**, 30766-30771.
3. C. Bergquist, T. Fillebeen, M. M. Morlok and G. Parkin, *Journal of the American Chemical Society*, 2003, **125**, 6189-6199.
4. C. Kimblin and G. Parkin, *Inorganic Chemistry*, 1996, **35**, 6912-&.
5. R. Alsfasser, S. Trofimenko, A. Looney, G. Parkin and H. Vahrenkamp, *Inorganic Chemistry*, 1991, **30**, 4098-4100.
6. C. Bergquist and G. Parkin, *Journal of the American Chemical Society*, 1999, **121**, 6322-6323.
7. R. Han, A. Looney, K. McNeill, G. Parkin, A. L. Rheingold and B. S. Haggerty, *Journal of Inorganic Biochemistry*, 1993, **49**, 105-121.
8. C. Kimblin, W. E. Allen and G. Parkin, *Journal of the Chemical Society-Chemical Communications*, 1995, 1813-1815.
9. A. Looney, R. Han, K. McNeill and G. Parkin, *Journal of the American Chemical Society*, 1993, **115**, 4690-4697.
10. A. Looney, A. Saleh, Y. H. Zhang and G. Parkin, *Inorganic Chemistry*, 1994, **33**, 1158-1164.
11. G. Parkin, *Chemical Reviews*, 2004, **104**, 699-767.
12. J. A. Ibers and R. H. Holm, *Science*, 1980, **209**, 223-235.
13. H. Vahrenkamp, *Dalton Transactions*, 2007, 4751-4759.
14. H. Vahrenkamp, *Accounts of Chemical Research*, 1999, **32**, 589-596.
15. M. Rombach, C. Maurer, K. Weis, E. Keller and H. Vahrenkamp, *Chemistry-a European Journal*, 1999, **5**, 1013-1027.
16. A. Peter and H. Vahrenkamp, *Zeitschrift Fur Anorganische Und Allgemeine Chemie*, 2005, **631**, 2347-2351.
17. C. P. Olmo, K. Bohmerle and H. Vahrenkamp, *Inorganica Chimica Acta*, 2007, **360**, 1510-1516.
18. P. Chaudhuri, C. Stockheim, K. Wieghardt, W. Deck, R. Gregorzik, H. Vahrenkamp, B. Nuber and J. Weiss, *Inorganic Chemistry*, 1992, **31**, 1451-1457.
19. L. Cronin, S. P. Foxon, P. J. Lusby and P. H. Walton, *Journal of Biological Inorganic Chemistry*, 2001, **6**, 367-377.
20. L. Cronin and P. H. Walton, *Chemical Communications*, 2003, 1572-1573.
21. P. J. Lusby, *Synthetic models of human carbonic anhydrase II*, [York],, 2000.
22. S. P. Foxon, *Small molecule models of carbonic anhydrase*, [s.n.], [York], 2000.
23. J. A. Hammond, *Modelling the secondary coordination sphere of human carbonic anhydrase II*, [s.n.], [York], 2007.
24. B. Greener, *A small molecule model for carbonic anhydrase*, [York],, 1997.
25. N. U. Meldrum and F. J. W. Roughton, *Nature*, 1933, **131**, 874-875.

26. N. U. Meldrum and F. J. Roughton, *The Journal of physiology*, 1933, **80**, 113-142.
27. R. Bauer, P. Limkilde and J. T. Johansen, *Biochemistry*, 1976, **15**, 334-342.
28. P. J. Stein, S. P. Merrill and R. W. Henkens, *Journal of the American Chemical Society*, 1977, **99**, 3194-3196.
29. A. M. Register, M. K. Koester and E. A. Noltmann, *Journal of Biological Chemistry*, 1978, **253**, 4143-4152.
30. J. J. Led, E. Neesgaard and J. T. Johansen, *Febs Letters*, 1982, **147**, 74-80.
31. S. Lindskog, P. Engberg, C. Forsman, S. A. Ibrahim, B.-H. Jonsson, I. Simonsson and L. Tibell, *Annals of the New York Academy of Sciences*, 1984, **429**, 61-75.
32. T. J. Williams and R. W. Henkens, *Biochemistry*, 1985, **24**, 2459-2462.
33. J. J. Led and E. Neesgaard, *Biochemistry*, 1987, **26**, 183-192.
34. P. Paneth and M. H. Oleary, *Biochemistry*, 1987, **26**, 1728-1731.
35. A. E. Eriksson, T. A. Jones and A. Liljas, *Proteins: Structure, Function, and Bioinformatics*, 1988, **4**, 274-282.
36. D. N. Silverman and S. Lindskog, *Accounts of Chemical Research*, 1988, **21**, 30-36.
37. C. K. Tu, D. N. Silverman, C. Forsman, B. H. Jonsson and S. Lindskog, *Biochemistry*, 1989, **28**, 7913-7918.
38. M. Kenneth M, Jr., *Journal of Molecular Biology*, 1990, **214**, 799-802.
39. J. Y. Liang and W. N. Lipscomb, *Proceedings of the National Academy of Sciences*, 1990, **87**, 3675-3679.
40. K. M. Merz, *Journal of Molecular Biology*, 1990, **214**, 799-802.
41. K. M. Merz, *Journal of the American Chemical Society*, 1991, **113**, 406-411.
42. K. M. Merz, *Journal of the American Chemical Society*, 1991, **113**, 3572-3575.
43. K. Håkansson and A. Wehnert, *Journal of Molecular Biology*, 1992, **228**, 1212-1218.
44. Y. J. Zheng and K. M. Merz, *Journal of the American Chemical Society*, 1992, **114**, 10498-10507.
45. N. Kitajima, S. Hikichi, M. Tanaka and Y. Morooka, *Journal of the American Chemical Society*, 1993, **115**, 5496-5508.
46. Z. W. Liang, Y. F. Xue, G. Behravan, B. H. Jonsson and S. Lindskog, *European Journal of Biochemistry*, 1993, **211**, 821-827.
47. Z. W. Liang, B. H. Jonsson and S. Lindskog, *Biochimica Et Biophysica Acta*, 1993, **1203**, 142-146.
48. S. Lindskog and A. Liljas, *Current Opinion in Structural Biology*, 1993, **3**, 915-920.
49. Y. F. Xue, J. Vidgren, L. A. Svensson, A. Liljas, B. H. Jonsson and S. Lindskog, *Proteins-Structure Function and Genetics*, 1993, **15**, 80-87.
50. Y. F. Xue, A. Liljas, B. H. Jonsson and S. Lindskog, *Proteins-Structure Function and Genetics*, 1993, **17**, 93-106.
51. M. Sakurai, T. Furuki and Y. Inoue, *The Journal of Physical Chemistry*, 1995, **99**, 17789-17794.
52. B. Greener, M. H. Moore and P. H. Walton, *Chemical Communications*, 1996, 27-28.
53. L. Cronin, *Ligand design: new small molecule models for carbonic anhydrase*, [York],, 1997.

54. E. SoltesRak, M. E. Mulligan and J. R. Coleman, *Journal of Bacteriology*, 1997, **179**, 769-774.
55. L. Sven, *Pharmacology & Therapeutics*, 1997, **74**, 1-20.
56. C. J. Boxwell and P. H. Walton, *Chemical Communications*, 1999, 1647-1648.
57. W. R. Chegwidden, N. D. Carter and Y. H. Edwards, *The carbonic anhydrases: new horizons*, Birkhäuser, 2000.
58. C. Kimblin, V. J. Murphy, T. Hascall, B. M. Bridgewater, J. B. Bonanno and G. Parkin, *Inorganic Chemistry*, 2000, **39**, 967-974.
59. C. T. Supuran and A. Scozzafava, *Expert Opinion on Therapeutic Patents*, 2000, **10**, 575-600.
60. T. Marino, N. Russo and M. Toscano, *Journal of the American Chemical Society*, 2005, **127**, 4242-4253.
61. K. Okrasa and R. J. Kazlauskas, *Chemistry – A European Journal*, 2006, **12**, 1587-1596.
62. J. Chen, E. Lecuona, A. Briva, L. C. Welch and J. I. Sznajder, *Am. J. Respir. Cell Mol. Biol.*, 2008, **38**, 32-37.
63. F. J. Ferreira, C. Guo and J. R. Coleman, *Plant Physiology*, 2008, **147**, 585-594.
64. Y. Xu, L. Feng, P. D. Jeffrey, Y. Shi and F. M. M. Morel, *Nature*, 2008, **452**, 56-U53.
65. B. S. Avvaru, S. A. Busby, M. J. Chalmers, P. R. Griffin, B. Venkatakrishnan, M. Agbandje-McKenna, D. N. Silverman and R. McKenna, *Biochemistry*, 2009, **48**, 7365-7372.
66. C. M. Maupin, R. McKenna, D. N. Silverman and G. A. Voth, *Journal of the American Chemical Society*, 2009, **131**, 7598-7608.
67. B. Sjoeblom, M. Polentarutti and K. Djinovic-Carugo, unpublished work.
68. B. S. Avvaru, C. U. Kim, K. H. Sippel, S. M. Gruner, M. Agbandje-McKenna, D. N. Silverman and R. McKenna, *Biochemistry*, 2010, **49**, 249-251.
69. B. S. Avvaru, J. M. Wagner, A. Maresca, A. Scozzafava, A. H. Robbins, C. T. Supuran and R. McKenna, *Bioorganic & Medicinal Chemistry Letters*, 2010, **20**, 4376-4381.
70. R. Silaghi-Dumitrescu, M.-M. Uta, A. Kallay and J. Bodis, *Journal of Molecular Structure-Theochem*, 2010, **942**, 15-18.
71. M. M. Ibrahim, M. A. Amin and K. Ichikawa, *Journal of Molecular Structure*, 2011, **985**, 191-201.
72. R. Kannappan, M. Matsumoto, J. Hallren and K. M. Nicholas, *Journal of Molecular Catalysis a-Chemical*, 2011, **339**, 72-78.
73. M. L. Zastrow, F. A. PeacockAnna, J. A. Stuckey and V. L. Pecoraro, *Nat Chem*, 2011, **advance online publication**.
74. J. M. Berg, J. L. Tymoczko and L. Stryer, *Biochemistry*, W. H. Freeman, 2007.
75. J. C. Mareque-Rivas, R. Prabaharan and S. Parsons, *Dalton Transactions*, 2004, 1648-1655.
76. R. Vilar, *Annual Reports Section "A" (Inorganic Chemistry)*, 2009, **105**, 477-504.
77. N. M. Price and F. M. M. Morel, *Nature*, 1990, **344**, 658-660.
78. T. W. Lane, M. A. Saito, G. N. George, I. J. Pickering, R. C. Prince and F. M. M. Morel, *Nature*, 2005, **435**, 42-42.
79. K. D. Karlin, *Science*, 1993, **261**, 701-708.

80. M. M. Ibrahim, K. Ichikawa and M. Shiro, *Inorganic Chemistry Communications*, 2003, **6**, 1030-1034.
81. M. M. Ibrahim, S. Y. Shaban and K. Ichikawa, *Tetrahedron Letters*, 2008, **49**, 7303-7306.
82. Trofimen.S, *Journal of the American Chemical Society*, 1966, **88**, 1842-&.
83. S. Karabocek, S. Guner and N. Karabocek, *Transition Metal Chemistry*, 1998, **23**, 159-163.
84. C. J. Boxwell, R. Bhalla, L. Cronin, S. S. Turner and P. H. Walton, *Journal of the Chemical Society-Dalton Transactions*, 1998, 2449-2450.
85. B. Clive Julian and C. J. Boxwell, York, York], 2000.
86. L. Cronin, B. Greener, M. H. Moore and P. H. Walton, *Journal of the Chemical Society-Dalton Transactions*, 1996, 3337-3339.
87. L. Cronin, B. Greener, S. P. Foxon, S. L. Heath and P. H. Walton, *Inorganic Chemistry*, 1997, **36**, 2594-2600.
88. B. Greener, S. P. Foxon and P. H. Walton, *New Journal of Chemistry*, 2000, **24**, 269-273.
89. J. D. Freeman, B. Greener, R. N. Perutz and P. H. Walton, *Journal of Inorganic Biochemistry*, 1999, **74**, 131-131.
90. T. Itoh, Y. Fujii, T. Tada, Y. Yoshikawa and H. Hisada, *Bulletin of the Chemical Society of Japan*, 1996, **69**, 1265-1274.
91. B. Greener, L. Cronin, G. D. Wilson and P. H. Walton, *Journal of the Chemical Society-Dalton Transactions*, 1996, 401-403.
92. A. K. Nairn, S. J. Archibald, R. Bhalla, C. J. Boxwell, A. C. Whitwood and P. H. Walton, *Dalton Transactions*, 2006, 1790-1795.
93. T. Bowen, R. P. Planalp and M. W. Brechbiel, *Bioorganic & Medicinal Chemistry Letters*, 1996, **6**, 807-810.
94. G. Battistuzzi, S. Cacchi and G. Fabrizi, *Organic Letters*, 2003, **5**, 777-780.
95. H. E. Gottlieb, V. Kotlyar and A. Nudelman, *The Journal of Organic Chemistry*, 1997, **62**, 7512-7515.
96. G. R. Fulmer, A. J. M. Miller, N. H. Sherden, H. E. Gottlieb, A. Nudelman, B. M. Stoltz, J. E. Bercaw and K. I. Goldberg, *Organometallics*, 2010, **29**, 2176-2179.
97. G. B. Deacon and R. J. Phillips, *Coordination Chemistry Reviews*, 1980, **33**, 227-250.
98. Z.-W. Mao, F. W. Heinemann, G. Liehr and R. v. Eldik, *Journal of the Chemical Society, Dalton Transactions*, 2001, 3652-3662.
99. K. L. Pang, Y. Rong and G. Parkin, *Polyhedron*, 2010, **29**, 1881-1890.
100. T. Welton, *Chemical Reviews*, 1999, **99**, 2071-2083.
101. I. Krossing and I. Raabe, *Angewandte Chemie-International Edition*, 2004, **43**, 2066-2090.